MOLECULAR MECHANISMS UNDERLYING REGULATION AND FUNCTION OF NEURONAL GAP JUNCTION PROTEINS: CONNEXIN 36 AND CONNEXIN 27.5

Anna Kotova

A DISSERTATION SUBMITTED TO

THE FACULTY OF GRADUATE STUDIES

IN PARTIAL FULFILLMENT OF THE REQUIREMENTS FOR THE DEGREE OF

DOCTOR OF PHILOSOPHY

GRADUATE PROGRAM IN BIOLOGY

YORK UNIVERSITY

TORONTO, ONTARIO

September 2022

ABSTRACT

Electrical synapses, known as gap junctions, are critical to neuronal synchronization and signal transmission. Gap junctions are composed of two docked hemichannels, each consisting of single protein subunits called connexins. Regulation and function of connexins are vital for the plasticity of the electrical synapses. Connexin regulation is dependent on their interacting partners as they affect turnover and channel properties. Here we explored the functional relevance of the interaction between mouse Connexin 36 (Cx36), major neuronal connexin, and mouse Caveolin-1 (Cav-1) in the Neuro 2a cell line. Cav-1 is known to mediate the endocytosis of membrane proteins, therefore its role in trafficking of Cx36 was explored. Together results showed that Cx36/Cav-1 interaction selects for the rapid calcium and caveolin dependent endocytosis and is critical for the internalization of Cx36.

Another means for regulating connexin function is through their ability to oligomerize with different connexin isoforms to form heteromeric and heterotypic channels. The oligomerization capabilities between zebrafish Cx35b, an orthologue of mouse Cx36, and a novel zebrafish connexin, Cx27.5, were explored in Neuro 2a cells. The co-localization of Cx36/35b and Cx27.5 was also investigated in the zebrafish retina, as its high organization allows to study the gap junction connections between different cell types. Data showed that oligomerization of Cx35b and Cx27.5 led to a formation of distinct channels which potentially allow for specialized intercellular connection between different cell types.

Cx27.5 is a novel connexin, and its functional relevance remains unknown. Previously reported expression in the zebrafish retina and co-localization with Cx36/35b further reinforced the hypothesis that the Cx27.5 function could be critical for visual processing. The protein and mRNA expression profile of Cx27.5 showed high expression in the brain and retina, specifically, the inner plexiform layer. By employing a Cx27.5 knock-out zebrafish line, the role of Cx27.5 in visual processing was investigated. The results proved Cx27.5 to be an essential player in the signal transmission and network connectivity of the zebrafish retina, as well as the perception of directional motion. In summary, the findings in this thesis describe the multifaced molecular mechanisms that underlie the function and regulation of neuronal connexins.

DEDICATION

I would like to dedicate this dissertation to my loving and supportive family and partner.

ACKNOWLEDGEMENTS

First and foremost, I would like to thank my thesis supervisor, Dr. Georg Zoidl. I could not imagine going through my graduate studies under somebody else's guidance. You have been instrumental in developing my critical thinking skills and becoming an independent scientist. Thanks to you, I have never seen negative results as failures but rather as learning opportunities. Thank you for ensuring an inviting atmosphere in the lab and always having "your door open". Lastly, I am thankful to you for simply being a great person, always sympathetic and understanding.

Thank you to my committee members, Dr. Mark Bayfield and Dr. Logan Donaldson, for making me a better scientist. Your insights and constructive criticism allowed me to improve the quality of my work.

Another whole-hearted thank you is extended to our lab manager Christiane. Your tips and tricks helped me refine my molecular biology skills. Also, your organization skills are something I admire and try to follow both in the lab and in life. Lastly, your famous waffles are one of the biggest highlights of any celebration and make any gathering feel extra special. Thank you for always being there for us, always ready to lend a hand.

Special gratitude is extended to my lab twin and best friend, Ksenia. Going through this, at times, uneasy process together with you made it truly memorable. Having someone to brainstorm with and discuss my findings made this journey extra special. I am grateful to have you by my side throughout all the important aspects of my life.

Thanks to all members of Zoidl lab, past, and present, for all the support and encouragement. It was great working by your side all these years.

Lastly, I am grateful to my family and partner for always being there for me through this process. Your support allowed me to keep going during the most challenging times. I am incredibly blessed to have all of you by my side.

STATEMENT OF CONTRIBUTIONS

Manuscripts included in this dissertation:

Kotova, A., Timonina, K., & Zoidl, G. R. (2020). Endocytosis of connexin 36 is mediated by interaction with caveolin-1. *International Journal of Molecular Sciences*, *21*(15), 5401. doi.org/10.3390/ijms21155401 (Chapter 3)

Kotova, A., Timonina, K., Zoidl C., & Zoidl, G. R. Chapter 5. Connexin 27.5 is critical for visual perception and processing in zebrafish. Manuscript in preparation. (Chapter 5)

Several co-authors have contributed directly by performing experiments or collecting data and assisting in manuscript preparation and editing:

Dr. Georg Zoidl provided mentorship in conceptualizing experiments and manuscript preparation.

Christiane Zoidl performed immunohistochemistry experiments depicted in Figure 4.6 (Chapter 4) and Figure 5.4 (Chapter 5).

Ksenia Timonina aided with data collection and analysis for the co-localization assays in Figure 3.3 (Chapter 3) and survival rates and body length measurements for Cx27.5$^{-/-}$ larvae in Figure 5.2 (Chapter 5).

Elena Hernandez Gerez established the F0 of the Cx27.5 knock-out zebrafish line used in Chapter 5.

All other experiments were performed by me. I was responsible for writing this thesis, the first author manuscripts, and generating all figures.

Manuscripts not included in this dissertation:

Timonina, K., **Kotova, A**., & Zoidl, G. (2020). Role of an aromatic–aromatic interaction in the assembly and trafficking of the zebrafish panx1a membrane channel. *Biomolecules*, *10*(2), 272. doi.org/10.3390/biom10020272

Siu, R. C., **Kotova, A**., Timonina, K., Zoidl, C., & Zoidl, G. R. (2021). Convergent NMDA receptor—Pannexin1 signaling pathways regulate the interaction of CaMKII with Connexin-36. *Communications biology*, *4*(1), 1-14. doi.org/10.1038/s42003-021-02230-x

Tetenborg, S., Liss V*., Breitsprecher, L.*, Timonina, K.*, **Kotova, A**.*, Acevedo Harnecker, AJ., Yuan, C., Shihabeddin, E., Dedek, K., Zoidl, G.R., Hensel, M., and O`Brien, J. Intralumenal docking of Cx36 channels in the ER isolates mis-trafficked protein. *BioRxiv*. https://doi.org/https://doi.org/10.1101/2022.07.15.500247

*Authors contributed equally

Timonina, K., **Kotova, A**., Zoidl C., & Zoidl, G. R. CaMKII regulates the function of panx1a membrane channel. Manuscript in preparation.

TABLE OF CONTENTS

LIST OF FIGURES

LIST OF SUPPLEMENTARY FIGURES

LIST OF TABLES

LIST OF ABBREVIATIONS

Symbol	Definition
ATP	Adenosine-5’-triphosphate
BAPTA	1,2-bis(o-aminophenoxy) ethane-N,N,N',N'-tetraacetic acid
BSA	Bovine serum albumin
$Ca2^{+}$	Calcium ion
CaM	Calmodulin
CaMKII	Calmodulin-dependent kinase II
Cav-1	Caveolin-1
CL	Cytoplasmic loop
CT	Carboxy terminus
CNS	Central nervous system
CoIP	Co-immunoprecipitation
Cx	Connexin
DMEM	Dulbecco’s modified eagle medium
dpf	Days post-fertilization
EGFP	Enhanced cyan fluorescent protein
EGFP	Enhanced green fluorescent protein
EL	Extracellular loop
ER	Endoplasmic reticulum
EtBr	Ethidium bromide
FRAP	Fluorescence Recovery After Photobleaching
FRET	Förster Resonance Energy Transfer Analysis
gapFRAP	Gap junction fluorescence recovery after photobleaching
GJC	Gap junction channel
GJIC	Gap junction intercellular communication
GJP	Gap junction plaque
hr	Hour
Iono	Ionomycin
IHC	Immunohistochemistry
INL	Inner nuclear layer
IPL	Inner plexiform layer
kDa	Kilodaltons
KO -/-	Knock-out
min	Minute
mL	Milliliter

mM	Millimolar
Neuro 2a	Neuroblastoma 2a
NGS	Normal goat serum
OMR	Opto-motor response
ONL	Outer nuclear layer
OPL	Outer plexiform layer
PBS	Phosphate buffered saline
PCR	Polymerase chain reaction
PKA	Protein kinase A or cAMP-dependent protein kinase
PKC	Protein kinase C
RGC	Retinal ganglion cell
ROI	Region of interest
RT	Room temperature
s	Second
SEM	Standard error of the mean
TALEN	Transcription activator-like effector technology
TIRF	Total Internal Reflection Fluorescence
VMR	Visual-motor response
TL	Tupfel longfin
WT	Wild-type
µL	Microliter
µM	Micromolar
µm	Micrometer

Chapter 1. Introduction

1.1. Communications in the Nervous System

Communication between two neurons occurs at specialized cellular regions called a synapse. Electrical and chemical transmission represent the two modes of synaptic transmission and are known to co-exist within the same networks (**Figure 1.1**). Both types of transmission are critical for neuronal synchronization. While chemical synaptic transmission is a more common mode behind neuronal signaling, electrical coupling of neighbouring neurons has been demonstrated as much as 50 years back (Mastronarde, 1983; A. Watanabe, 1958).

Chemical synapses operate by transferring information through the neurotransmitter release from one cell and further detection by the adjacent cell (Gibson et al., 1999). While electrical synapses also allow for the passage of small molecules through the gap junction channels, they are unable to amplify and transform presynaptic signals. This feature is reserved for the chemical synapses. However, unlike chemical synapses, electrical synapses are bidirectional, which allows for activity coordination of large networks of coupled neurons (M. V. L. Bennett & Zukin, 2004).

In the case of electrical synapses, adjacent cells are connected through the intercellular channels known as gap junctions. Each channel comprises of six protein subunits called connexins (M. V. L. Bennett & Zukin, 2004). While the connexin family accounts for over 20 different isoforms (Goodenough & Paul, 2009), only a few connexins are expressed in neurons. These include connexin 36 (Cx36), connexin 45 (Cx45), connexin 50 (Cx50), connexin 30.2 (Cx32) and connexin 31.1 (Cx31.1) (Pereda et al., 2013; Shimizu & Stopfer, 2013; Söhl et al., 2005). The diversity of the neuronal connexins

has been most investigated in the retina due to its high organization and interconnection between different cell types (Bloomfield & Volgyi, 2009). Because of its ubiquitous expression, Cx36 is considered the main neuronal connexin (Condorelli et al., 2000). However, while the electrical transmission is significantly reduced in Cx36 knock-out mice, low coupling levels can still be detected, suggesting that other connexin isoforms might also be vital for the neuronal connections (Curti et al., 2012; S. C. Lee et al., 2010).

Understanding the details of gap junction regulation remains an important aim for future research. Future studies can help to further explain the crucial role of gap junctions in neuronal interconnection and signal processing, with the retina remaining a vital resource for this venture.

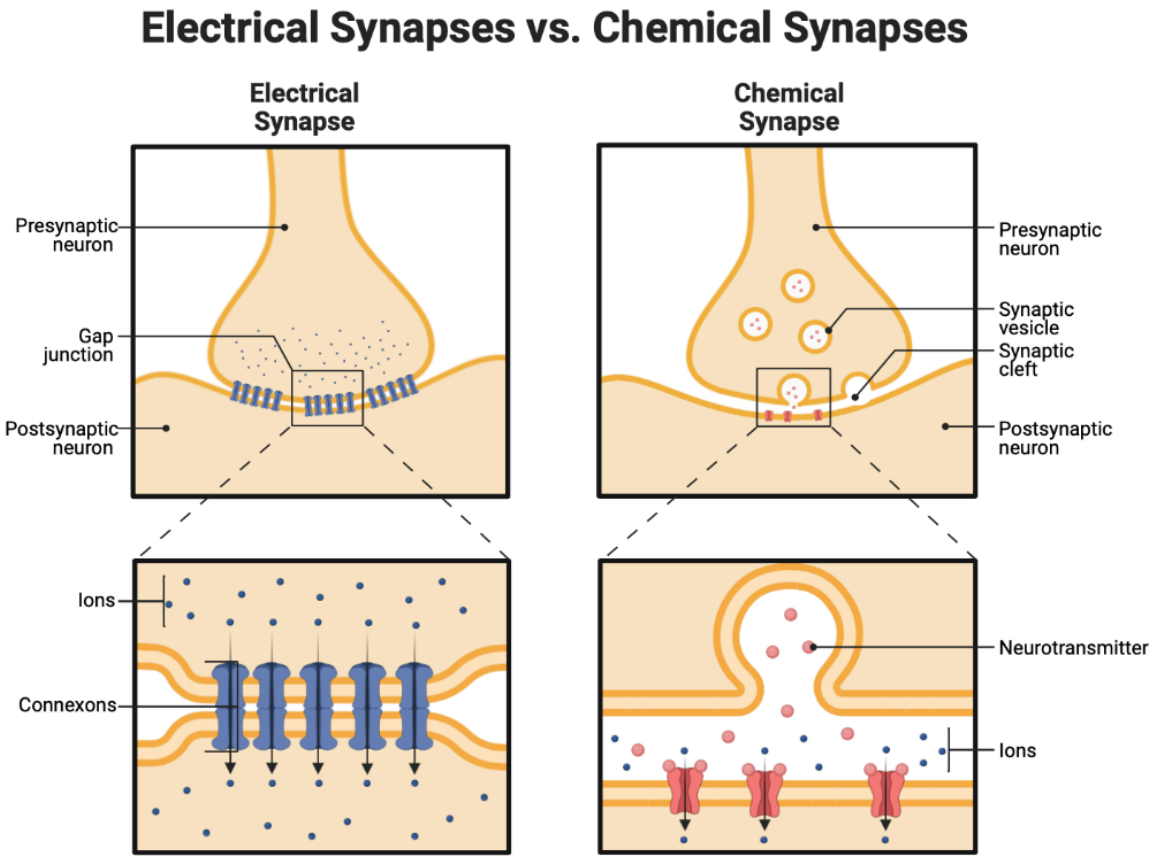

Figure 1.1. Comparison between electric and chemical synapses. Electrical transmission (right) is mediated by intercellular channels called gap junctions. Gap junctions connect presynaptic and postsynaptic neurons allowing the bidirectional

transfer of electrical currents (ions). Chemical transmission (left) relies on the neurotransmitter release from the presynaptic neuron, which is up taken by the channels in the postsynaptic neuron. The image was created with BioRender.com.

1.2. Gap Junctions/Connexins

1.2.1. Structure

Connexins are the building blocks of the intercellular channels known as gap junctions. Oligomerization of six connexins results in a formation of a hemichannel which is referred to as a connexon. Two of these connexons on the adjacent cells dock to each other forming gap junction channels. These channels allow for the passage of ions, second messengers, metabolites, and nucleotides up to 1 kDa in size (Evans & Martin, 2002). Some connexins also function as hemichannels and allow for the exchange of molecules between the extracellular space and cell interior (Paul et al., 1991; Windoffer et al., 2000). Hemichannels also allow for the passage of small molecules into the cell and are often gates by the cations (De Vuyst et al., 2006; Verselis & Srinivas, 2008).

Each connexin protein contains four transmembrane domains, amino and carboxy termini, and an intracellular loop localized on the cytosolic side of the membrane, and two extracellular loops (Verselis & Srinivas, 2008) (**Figure 1.2**). The amino acid makeup and length of the carboxy terminus and intracellular loop define the extensive variability between different connexin isoforms. On the contrary, the four transmembrane regions, the two extracellular loops, and the amino terminus are often considerably conserved between different connexin proteins.

Thus far, 21 different connexin isoforms have been identified in humans (Söhl & Willecke, 2004). While some connexins show a ubiquitous expression pattern, others are

restricted to specific tissues or cell types. The connexin channels composed of different connexins often exhibit vast differences in electrophysiological capabilities.

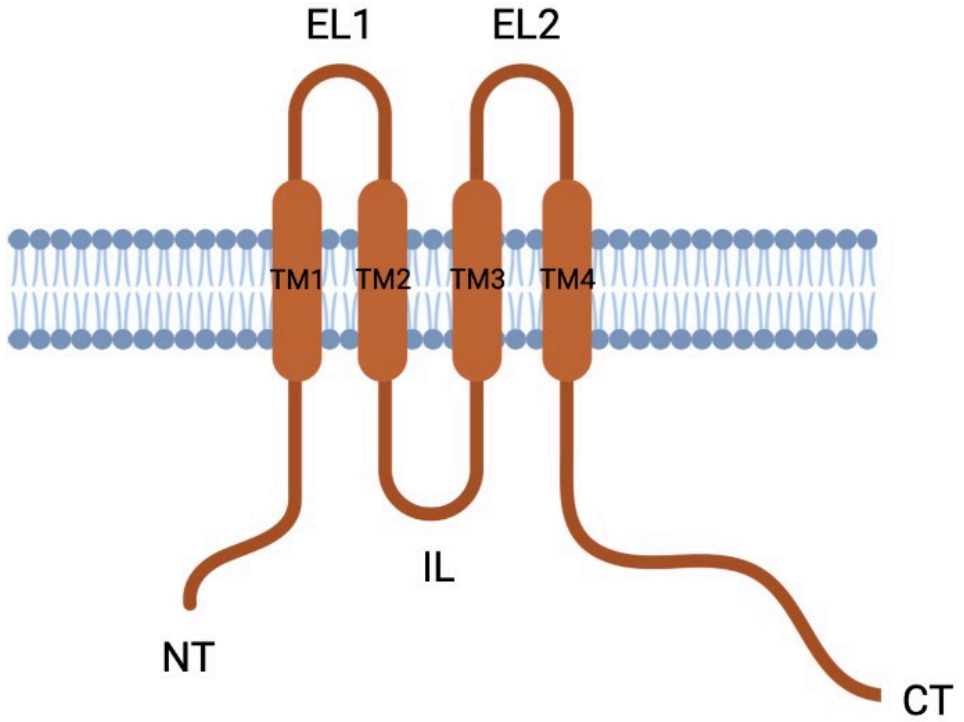

Figure 1.2. Transmembrane topology of a single connexin subunit. Each connexin possesses the following conserved regions: four transmembrane domains (TM), two extracellular loops (EL), one intracellular loop (IL), carboxy terminus (CT), and amino terminus (NT). The image was created with BioRender.com.

1.2.2. Trafficking and Oligomerization

1.2.2.1. Synthesis

The majority of connexin isoforms are co-translationally inserted into the endoplasmic reticulum. However, some connexin isoforms, specifically Cx26, is inserted into the endoplasmic reticulum membrane post-translationally or even directly into the plasma membrane (Ahmad et al., 1999; J. T. Zhang et al., 1996).

Once connexins are checked for the proper conformation, they are transported into the Golgi apparatus (Koval et al., 1997; Laird et al., 1995; Thomas et al., 2005). After the Golgi apparatus, connexins are transported via the trans-Golgi network to the plasma membrane. Cx26, however, follows an alternative route that entirely bypasses the Golgi apparatus (Diez et al., 1999; P. E. M. Martin et al., 2001).

On their route between the endoplasmic reticulum and Golgi, connexins oligomerize into hexameric structures, called connexons. The oligomerization site is believed to be isoform-specific. Cx43 has been shown to oligomerize in the trans-Golgi network, which is distinct from most other multisubunit integral membrane proteins which oligomerize in the Golgi apparatus (Koval et al., 1997; Musil & Goodenough, 1993). Alternatively, Cx32 has been shown to oligomerize at the earlier stage of its trafficking in the endoplasmic reticulum (Koval, 2006; Sarma et al., 2002).

Depending on their oligomerization patterns, connexins are classified into different categories. If six identical subunit isoforms oligomerize, they are referred to as homomeric connexon (Sosinsky & Nicholson, 2005). If six different isoforms oligomerize, the connexon is referred to as heteromeric (**Figure 1.3**).

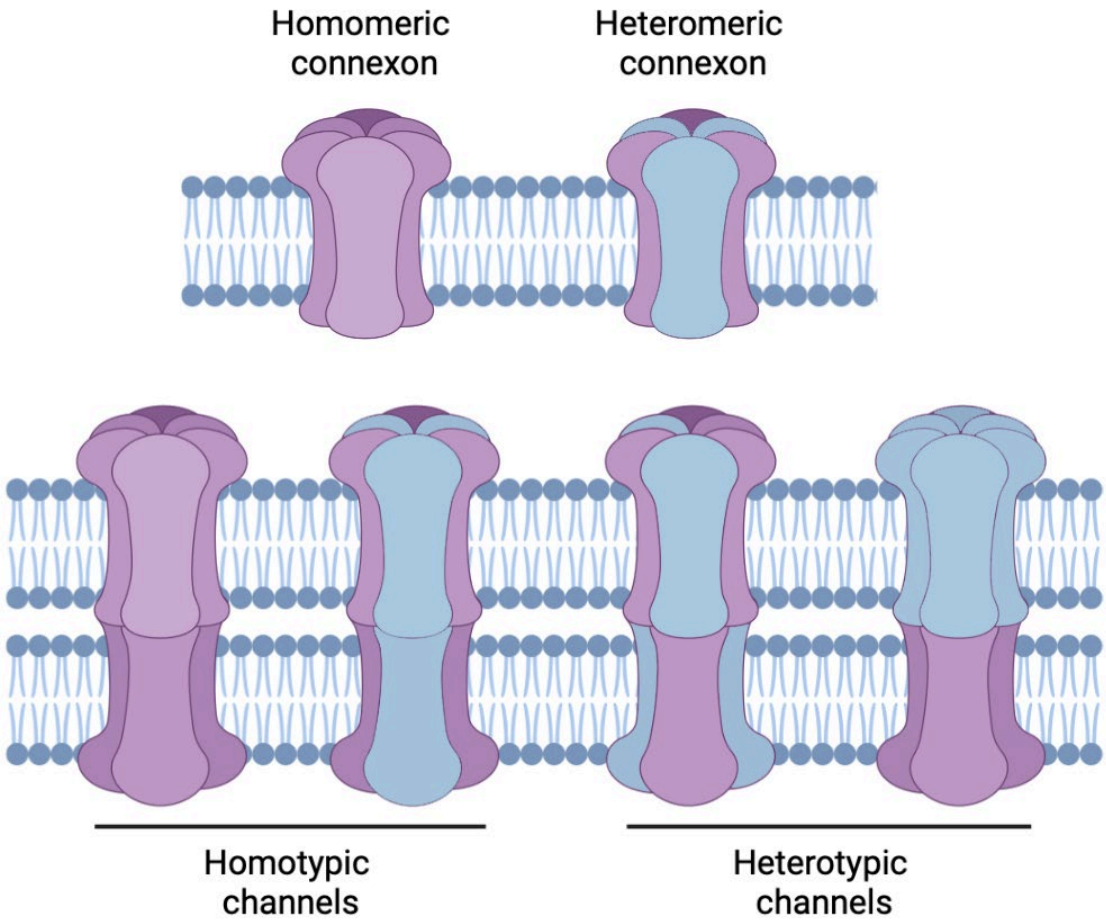

Figure 1.3. Different oligomerization arrangements of gap junction channels. Connexins form hexameric hemichannels called connexons. Connexins subunits can oligomerize with either the same or different isoforms resulting in homomeric or heteromeric connexons. Channels are formed by the docking of two connexons. When two identical connexons dock with each other, it is referred to as a homotypic channel. When different connexons dock, it is referred to as a heterotypic channel. The image was created with BioRender.com.

1.2.2.2. Assembly

After their assembly in the Golgi apparatus, connexons are delivered to the plasma membrane, where they laterally diffuse to the periphery of the existing gap junction plaques. At the membrane, connexons dock with other connexons on the adjacent cell to form the gap junction channels (Lauf et al., 2002; Maza et al., 2005; Thomas et al., 2005). The docking is achieved by a so-called “lock and key” mechanism (Perkins et al., 1998;

Sosinsky & Nicholson, 2005; Unger et al., 1999). The membranes of the two adjacent cells are separated by an extracellular gap of 2-4 nm, giving rise to the name “gap junctions” (Goodenough & Revel, 1970; Revel & Karnovsky, 1967).

If two identical connexons oligomerize together, they are referred to as homotypic channels. Oligomerization of two district connexons leads to the formation of heterotypic channels (Sáez et al., 2003) (**Figure 1.3**). Multiple different connexin isoforms can oligomerize to give rise to an endless number of varying isoform combinations. Moreover, connexin composition highly affects the conductance properties of the channel. This makes a multitude of diverse gap junction channels available for specific cell types. The ability of connexins to form heterotypic and heteromeric channels might also allow for a compensating mechanism; when one connexin isoform is lost due to a mutation, another isoform can form gap junctions in its place.

1.2.2.3. Endocytosis

Unlike many other membrane proteins, connexins possess high turnover rates, with half-lives ranging between 1 and 5 hours (Fallon & Goodenough, 1981; Hervé et al., 2007; Laird et al., 1991). The high turnover suggests the importance and tight regulation of the degradation mechanisms in the life cycle of connexins (Berthoud et al., 2004). The degradation rate of connexins is controlled during endocytosis and at the level of post-endocytic sorting of connexins to lysosomes. Under normal conditions, old connexins are removed from the center of the gap junction via endocytosis, and new connexins are added laterally to the edges of the existing gap junction plaques (Gaietta et al., 2002; Lauf et al., 2002). There is also evidence of internalization of the entire gap junction plaques

(Larsen & Hai-Nan, 1978). In this case, both membranes of the adjacent cells are internalized, leading to a formation of a double membrane vesicle called a connexosome (Archard & Denys, 1979; Jordan et al., 2001; Kitson et al., 1978; Larsen & Hai-Nan, 1978; Nickel et al., 2008; Piehl et al., 2007; Severs et al., 1989; F. H. White et al., 1984).

Like with other membrane proteins, clathrin is recruited to the membrane to initialize the endocytosis of connexins (Gumpert et al., 2008; Nickel et al., 2008; Piehl et al., 2007). It is usually distributed in patches and does not cover the entire gap junction plaque. Clathrin's recruitment is often mediated by clathrin-adaptors AP-2 and Disabled-2 (Dab2). Dynamin is also a key player in the initiation of endocytosis of connexins, as it mediates scission of the vesicle by forming a collar around it (Gilleron et al., 2011; Gumpert et al., 2008; Piehl et al., 2007). The internalized gap junctions are coated with actin filaments (Larsen et al., 1979). Other than actin filaments, endocytosis of gap junctions is also dependent on the actin motor myosin-VI (Piehl et al., 2007).

Following their internalization, connexins are then degraded in lysosomes (Laing et al., 1997; Leithet & Rivedal, 2004; VanSlyke et al., 2000). However, connexins can also follow an alternative endocytic pathway, where connexosomes are able to fuse with lysosomes directly (Murray et al., 1981; Risinger & Larsen, 1983). In the case of Cx43, it is able to enter lysosomes directly from early secretory compartments (Qin et al., 2003). Connexin hemichannels are also endocytosed and degraded in the lysosomal compartments (VanSlyke & Musil, 2005).

High dynamic properties of connexins suggest that endocytosis and post-endocytic trafficking are fundamental mechanisms regulating the number of functional gap junctions available at the membrane.

1.2.3. Interacting Partners

Interactions with many regulatory and structural proteins most likely govern the transport of connexins, their assembly at the plasma membrane as well as channel properties. Work related to connexin interacting partners has been primarily focused on Cx43; therefore, this protein has the most comprehensive network of interaction partners established, which will be discussed below.

1.2.3.1. Cytoskeleton

Like a most connexins, Cx43 has a short half-life of only a few hours (Fallon & Goodenough, 1981), suggesting that it relies on microfilaments and microtubules for fast delivery to and from the cell membrane.

Co-immunoprecipitation confirmed the interaction of Cx43 and microtubules, specifically with α- and β-tubulin (Giepmans, Verlaan, Hengeveld, et al., 2001). The C-terminal tail was found to be necessary for this interaction with ^{234}KGVKDRVKGL^{243} amino acids identified as a binding site. This binding site is also conserved in other connexins such as connexin 46 and connexin 41 (Yoshizaki & Patiño, 1995). Cx36 also binds tubulin; however, the binding occurs through a conserved binding motif, which is distinct from the motif of Cx43 (Brown et al., 2019). This interaction was shown to be critical for tubulin-dependent transport of Cx36 and potentiation of synaptic strength by delivering channels to gap junction plaques.

Cx43 was also shown to co-localize with actin in various cell types (Wall et al., 2007). However, a direct interaction has been demonstrated between Cx43 and an actin-

binding protein called drebrin (Butkevich et al., 2004). Drebrin plays a crucial role in stabilizing Cx43 gap junctions at the membrane and might also serve as a mediator for the Cx43 and actin interaction.

1.2.3.2. Tight Junctions

Multiple connexins have been shown to interact with zonula occludens-1 (ZO-1) protein suggesting a tight interplay between the tight junctions and gap junctions. In the case of Cx43, ZO-1 regulates Cx43-mediated gap junctional communication by altering its membrane localization (Giepmans, Verlaan, & Moolenaar, 2001; Toyofuku et al., 2001). Direct interaction has also been shown between the carboxyl-terminal of Cx45 and ZO-1 (Laing et al., 2001). These studies suggest that ZO-1 interaction with Cx45 and Cx43 may play a role in gap junction composition and may regulate connexin-connexin interactions. Cx36 has also been shown to interact with ZO-1, and unlike other connexins that bind the second of the three PDZ domains in ZO-1, Cx36 interacts with the first PDZ domain of ZO-1 (Li et al., 2000). Cx36 also associates with zonula occludens-2 and zonula occludens-3 proteins through their first PDZ domains (Li et al., 2009). Like Cx36, Cx32 also co-localizes with both ZO-1 and ZO-2 proteins in rat hepatocytes and is involved in forming functional tight junctions and actin organization (Kojima et al., 2002). Cx30 and Cx43 also associate with ZO-2, and this interplay is crucial for mammary epithelial cell differentiation (Talhouk et al., 2008).

Another member of a tight junction protein family called occludin was shown to interact with Cx32 and Cx26 (Duffy et al., 2002; Nusrat et al., 2000). Cx32 and occludin co-localize near tight junctional strands and co-immunoprecipitate together. Along with

an association with occludin, Cx32 also interacts with claudin-1 in hepatocytes (Kojima et al., 2001), while Cx26 (Go et al., 2006) co-localizes with claudin-14 in epithelial cell lines.

1.2.3.3. Adherens Junctions

As we mentioned a multitude of interactions between gap junctions and tight junction complexes, it is not surprising that adherens junctions are also tightly interconnected with gap junctions.

The most reported are the interactions of connexins with cadherin proteins. Wei and colleagues (Wei et al., 2005) reported the interaction of Cx43 protein with N-cadherin, p120, and other N-cadherin associated proteins at regions of cell-cell contact. Another group also showed an association between Cx43 and N-cadherin through Rac1 and RhoA-mediated signaling (Matsuda et al., 2006). The interaction proved to be crucial for the connexin delivery and insertion at the membrane. An upregulation of another cadherin protein, called E-cadherin, leads to an increase in gap junction communications suggesting an functional interplay between these two complexes (Jongen et al., 1991). Moreover, the knock-out of N-cadherin has been shown to lead to inhibition in gap junction dye coupling (Xu et al., 2000).

Cx43 has also been shown to interact with *β*-catenin, mainly at the cell membrane (Ai et al., 2000). *β*-catenin protein possesses both adhesive and transcriptional functions, and its interaction with Cx43 suggests that connexins might be involved in regulating cell growth. In turn, Cx26 co-localizes with both E-cadherin and α-catenin at the gap junction sites (Fujimoto et al., 1997). Connexins 30, 32, and 43 have also been shown to interact with both α-catenin and *β*-catenin proteins. This interaction affects *β*-catenin's localization

by sequestering it away from the nucleus (Talhouk et al., 2008). Additional studies on Cx43 and *β*-catenin show the importance of this interaction for the trafficking of gap junction proteins to the membrane (Govindarajan et al., 2002).

1.2.3.4. Other Membrane Partners

Some other proteins that have been discovered as connexin interacting partners at the membrane include aquaporin-0 and acetylcholine receptors (Chanson et al., 2007). Many connexin isoforms have been shown to interact with caveolin-1 (Cav-1), which likely targets connexins to the lipid rafts (A. L. Schubert et al., 2002). All three members of the caveolin protein family have been shown to interact with Cx43 (Langlois et al., 2008; L. Liu et al., 2010; A. L. Schubert et al., 2002). Caveolin-1 and caveolin-2 interact with Cx43 in the Golgi apparatus, and the complex is also observed at the plasma membrane in lipid rafts. Moreover, caveolins were also shown to regulate gap junctional intercellular communication of Cx43. The role of caveolin-3 in the targeting of connexins to lipid rafts and caveolae remains uncertain for now. Because of the above interaction, it comes as no surprise that connexins also interact with cholesterol (Biswas & Lo, 2007), as lipid rafts, called caveolae, are rich in both cholesterol and caveolin proteins (Murata et al., 1995).

1.2.3.5. Kinases

Post-translational modifications are critical for gap junction regulation. Phosphorylation, being the most abundant modification, has been shown to be essential for the assembly and channel regulation of most connexins (Laird, 2005). While Cx43 has

been shown to be phosphorylated by a multitude of kinases such as protein kinase C, casein kinase 1, mitogen-activated protein kinase (MAPK), Src kinase, and $p34^{cdc2}$ (Lampe & Lau, 2004; Lau et al., 1996), Cx26 is not phosphorylated at all (Traub et al., 1989).

Many connexins have been shown to interact with calmodulin, which has been shown to control channel gating properties (Mesnil et al., 2005; Peracchia et al., 2000). Both calmodulin and calcium/calmodulin-dependant kinase II (CaMKII) share an overlapping binding site in the carboxy-terminus of Cx36 (Siu et al., 2016). CaMKII, which is activated by calmodulin, has been shown to interact and phosphorylate Cx36, which in turn mediates its channel gating function (Mesnil et al., 2005). CaMKII has also been shown to mediate gap junctional coupling of Cx43 (De Pina-Benabou et al., 2001) upon an increase in extracellular K+. CaMKII has been established as a critical player in chemical synaptic transmission; thus, its role in electrical coupling comes as no surprise (De Pina-Benabou et al., 2001; Pereda et al., 2004).

Cx43 has also been shown to function as a v-Src substrate (Swenson et al., 1990) (Crow et al., 1990). Mutations in the putative v-Src phosphorylation site have been shown to abolish gap junction closure (Swenson et al., 1990). This closure is believed to be mediated through initial phosphorylation at Tyrosine 265, followed by the docking of the SH2 domain of Src to Cx43 and subsequent phosphorylation of Tyrosine 247, which leads to channel closure (R. Lin et al., 2001). Interestingly, Tyrosine 265 phosphorylation by c-Src has been shown to mediate the interaction between Cx43 and ZO-1 (Giepmans, Hengeveld, et al., 2001; Toyofuku et al., 2001).

Serine/threonine kinases have also been shown to act as essential players in gap junction regulation. Phosphorylation of Serine 368 in Cx43 by protein kinase C (PKC) leads to the inhibition of gap junction communication (Lampe & Lau, 2000). Cx43 has also been reported to interact with PKCε, and this interaction also has been shown to inhibit the gap junction intercellular communication (GJIC) (Doble et al., 2000). Similar results were reported by the PKCγ isotype (D. Lin et al., 2003). On the contrary, the PKCα isotype was implicated in the upregulation of GJIC (Weng et al., 2002). Protein kinase A (PKA) activation has been shown to cause uncoupling of Cx36 gap junctions (Ouyang et al., 2005). MAP kinase has also been shown to regulate multiple connexins, including Cx26, Cx32, and Cx43 (D. Lin et al., 2003). The opposing regulatory mechanisms that different kinases exhibit prove them as key interactors for the life cycle of connexins.

1.2.4. Neuronal Connexins

1.2.4.1. Connexin 36 (Cx36)

Connexin 36 (Cx36) is the major connexin of the central nervous system, where it forms electrical synapses (gap junctions) (Pereda et al., 2013). Other than the central nervous system (Belluardo et al., 2000; Blatow et al., 2003; De Zeeuw et al., 2003; Deans et al., 2001; Long et al., 2002; J. O'Brien et al., 1998), Cx36 is also expressed in the retina (Deans et al., 2002; Mills et al., 2001; J. O'Brien et al., 2004), olfactory bulb (Christie et al., 2005), neuroendocrine cells of the pancreas (Serre-Beinier et al., 2000), pituitary and pineal organs (Belluardo et al., 2000), and is found in adrenal chromaffin cells (A. O. Martin et al., 2001). In pancreatic beta cells, Cx36 plays a vital role in insulin secretion and glycaemic control (Farnsworth & Benninger, 2014).

Because of its expression patterns, Cx36 is involved in critical brain functions such as learning and memory (Allen et al., 2011; Y. Wang & Belousov, 2011), retina visual processing (Kovács-Öller et al., 2017), and sensorimotor reflexes in the zebrafish (A. C. Miller et al., 2017). It is worth mentioning that Cx36 has four orthologues in zebrafish: Cx35.1(Cx35b), Cx34.7, Cx34.1, and Cx35.5 (A. C. Miller et al., 2017). Cx36-containing electrical synapses also play an essential role in the synchronous activity of neuronal networks, which underlie various cognitive processes (B. C. Bennett et al., 2016; Connors & Long, 2004; Hormuzdi et al., 2004; Saraga et al., 2006). As Cx36 is the critical component of the electrical synapses, its involvement in diseases that entail deficiencies in fast communication and aberrant synchronous firing, such as seizures, has been suggested. However, no consensus on whether Cx36 increases or decreases seizure susceptibility has been reached (Gajda et al., 2005; Jacobson et al., 2010; Shin, 2013; Voss et al., 2010). The turnover rate of Cx36 is exceptionally high, with a half-life of 3.1 hours (H. Y. Wang et al., 2015). High turnover and changes in abundance of Cx36 have been proposed to contribute to synaptic plasticity (Katti et al., 2013).

Cx36 channels possess distinct regulatory properties. Most notably, Cx36 exhibits low sensitivity to the transjunctional voltage and low unitary conductance (Srinivas et al., 1999; Teubner et al., 2000). This feature is believed to be vital for fine-tuning of electrical coupling. Like other connexins, its channel properties can be regulated by intracellular pH and free cytosolic Mg^{2+} ion concentration. However, unlike other connexins, the conductance of Cx36 junctions is upregulated under low pH and Mg^{2+} (González-Nieto et al., 2008; Palacios-Prado et al., 2013). Additionally, Mg^{2+} has been shown to affect the transjunctional voltage sensitivity of Cx36. This is believed to be achieved by an

electrostatic interaction through a Mg^{2+} binding site within the Cx36 pore (Palacios-Prado et al., 2013).

Another means of Cx36 channel regulation is achieved through its phosphorylation. Perhaps the most notable regulation Cx36 undergoes is through its interaction with CaMKII (Alev et al., 2008). Upon phosphorylation, Cx36 exhibit a unique property referred to as the “run-up” phenomenon, in which Cx36 conduction increases 10-fold (Del Corsso et al., 2012). Once the CaMKII binding and phosphorylation regions are deleted, the “run-up” property is lost. The CaMKII modulation of Cx36 channel properties suggests that this interaction is essential for the functional plasticity of the Cx36 containing electrical synapses. As CaMKII is activated by calmodulin, it is not unexpected that calmodulin interacts with Cx36 as well (Burr et al., 2005; Siu et al., 2016). CaMKII and CaM share a Cx36 binding site at which they interact competitively.

Protein kinase A (PKA) activation has been shown to cause uncoupling of Cx36 gap junctions, while PKA inhibition leads to increased coupling in inferior olive and Cx36 transfected HeLa cells (Bazzigaluppi et al., 2017; Ouyang et al., 2005). Cx36 phosphorylation by PKA is also critical for the coupling strength of AII amacrine cells (Urschel et al., 2006). Two critical phosphorylation sites, Ser110 in the intracellular loop and Ser276 in the carboxyl-terminal tail, undergo phosphorylation leading to the uncoupling of Cx36 gap junctions. These sites also undergo phosphorylation by cGMP-dependent protein kinase (PKG), suggesting a convergence of PKA and PKG signalling pathways (Patel et al., 2006). Interestingly, mutations in the major phosphorylation sites of Cx36 did not affect trafficking or gap junction formation (Zoidl et al., 2002). This

suggests that phosphorylation of Cx36 is most likely vital for regulating channel properties rather than trafficking and assembly mechanism.

Aside from kinases, Cx36 also interacts with other protein members. Cx36 has been shown to interact with AF6 and MUPP1 scaffolding proteins (Li et al., 2012). Authors suggest that AF6 may be a target for the cAMP/Epac/Rap1 pathway at electrical synapses, while MUPP1 may be implicated in anchoring CaMKII at these synapses. Cx36 also interacts with the proteins of the zonula occludens family (Li et al., 2000, 2009). The possible roles for the interaction of Cx36 with ZO-1 include recruitment of signaling molecules to gap junctions, as PKC co-localizes with ZO-1, or involvement in the gap junction assembly (Li et al., 2000). ZO-2 and ZO-3 have been proposed to anchor regulatory proteins at the Cx36 gap junctions (Li et al., 2009). In turn, Cx36 interaction with tubulin was shown to mediate delivery of Cx36 channels to the gap junction plaques and potentiate synaptic strength of Cx36 (Brown et al., 2019).

1.2.4.2. Connexin 27.5 (Cx27.5)

Connexin 27.5 (Cx27.5) is a novel neuronal connexin that was first discovered in the zebrafish retina by Dermietzel and colleagues in 2000 (Dermietzel et al., 2000). Cx27.5 is located on chromosome 5, contains two open reading frames, and thus codes for two isoforms, 254 or 240 amino acids long. It shares structural topology with other connexin family members and contains four transmembrane domains, two extracellular loops, one cytoplasmic loop, and amino and carboxy termini facing intracellularly. It also contains three conserved cysteine residues on the extracellular loop like other connexins.

Previous expression analysis via RT-PCR showed vast expression of Cx27.5 in the brain and more limited expression in the eye and inner ear (Chang-Chien et al., 2014; Dermietzel et al., 2000; Zoidl et al., 2008). In-situ hybridization showed Cx27.5-specific expression in the subpopulations of neurons in the retina's inner nuclear and the ganglion cell layers (Dermietzel et al., 2000) and in the otic vesicle (Chang-Chien et al., 2014).

Cx27.5 was first believed to be a homologue of mammalian Cx26 as it shares 80.6% of overall homology with Cx26 (Dermietzel et al., 2000). However, this homology is most apparent within the transmembrane domains, while the cytoplasmic loop and C terminus show notable differences. Moreover, Cx27.5 exhibits a consensus sequence for casein kinase II phosphorylation which is found in all connexins but is absent in Cx26. Channel functionality data further support the differences between Cx27.5 and Cx26. Cx26 channels comprise weak voltage sensitivity (Barrio et al., 1991) and large conductance (Bukauskas et al., 1995) channels, while Cx27.5 form moderate voltage-dependent channels (Dermietzel et al., 2000). The above properties suggest that Cx27.5 is more similar to the mammalian Cx32. The phylogenetic analysis (Dermietzel et al., 2000; Eastman et al., 2006) places Cx27.5 into the beta group of connexins, next to Cx32. Like other connexins, Cx27.5 has a paralogue which is Connexin 31.7, and these two zebrafish connexins are co-orthologues of human Cx32.

It is worth mentioning that mutations in Cx32 lead to the X-linked Charcot-Marie-Tooth neuropathy X type 1 (CMTX1) syndrome (Janssen et al., 1997). The syndrome manifests in motor and sensory neuropathy in males and mild symptoms in the carrier females. Both central and peripheral nervous systems are affected by this disease as

cases of sensory (Stojkovic et al., 1999) and central nervous system deficits (Hu et al., 2019; Wen et al., 2018) have been reported.

Like many connexins, Cx27.5 is also able to form heterotypic channels, specifically with Cx44.1 and Cx55.5 (Dermietzel et al., 2000). While junctional currents in homotypic Cx27.5 channels show symmetrical and slow closure, Cx27.5/Cx44.1 channels showed an apparent asymmetry, with currents closing faster and with a lower threshold. Increased conductance and reduced sensitivity to voltage were also observed in both Cx27.5/Cx44.1 and Cx27.5/Cx55.5 channels.

1.3. Zebrafish as a Model for Visual Processing

The ideal tissue to study gap junction regulation is the retina, as every class of retinal neurons is coupled by gap junctions that express different connexin proteins (Cook & Becker, 1995). This extensive distribution and distinct regulatory pathways suggest that gap junctions maintain reconfigurable circuits and thus play critical roles in visual transmission and processing. This makes the retina the best model for the study of gap junction function and regulation in the central nervous system (CNS).

Compared to the CNS, the retina contains a relatively small number of neuronal cell types. These cell types are usually characterized by fixed positions within a specific layer as well as distinct morphology (Cameron & Carney, 2000) (**Figure 1.4**). The high organization allows for easy identification during immunohistological studies. Moreover, the tissue remains physiologically intact when isolated. Additionally, the eye is fully separated from the CNS early in development, allowing for a more straightforward

interpretation of the developmental processes (Burrill & Easter, 1995; T. Watanabe & Raff, 1988).

Zebrafish are also an ideal model for studying visual system due to their ability to produce transparent embryos. These embryos develop rapidly, allowing for early morphological and behavioural screening. The teleost retina is well studied and characterized (Dowling, 1987; Malicki, 2000; Rodieck RW, 1973). The development rate of the zebrafish retina makes it a perfect model for genetic and developmental research. Retinal neurogenesis has been shown to be complete by 60 hours post fertilization (hpf), and behavioral responses to the visual stimulus can be detected early as 3.5 days post fertilization (dpf) (Easter Jr & Nicola, 1996). Other benefits of the zebrafish model include high fecundity, easy and relatively low-cost maintenance, rapid life cycle, and the immediate separation of the embryo from the maternal organism. Also, the vertebrate retina remained exceptionally conserved throughout evolution. Mammals and teleosts display highly similar retinal organization (Hitchcock & Raymond, 2004). Both retinae are organized in the same layered pattern and contain the same major cell classes.

A most common way to examine the function of a specific gene in zebrafish is by employing a variety of genome-editing techniques. To date, the most commonly used methods employ the use of zinc finger nucleases (ZFNs) (J. C. Miller et al., 2007; Porteus & Baltimore, 2003), transcription activator-like effector nucleases (TALENs) (Cade et al., 2012; Christian et al., 2010; Wood et al., 2011) or clustered regularly interspaced short palindromic repeats (CRISPR) (Deveau et al., 2010; Hwang et al., 2013) These approaches can be used to knock-out the gene of interest which allows to study the molecular and behavioural consequences of the gene absence.

Mutant analysis can provide valuable insights into the regulation of retinal formation and connectivity. Lastly, due to its evolutionary conservation, the zebrafish retina can be employed to model vision defects in humans. Rapid development, high organization, and relative simplicity of the zebrafish retina are only a few of the advantages that make zebrafish a vital organism for the studies of neuronal function and visual processing.

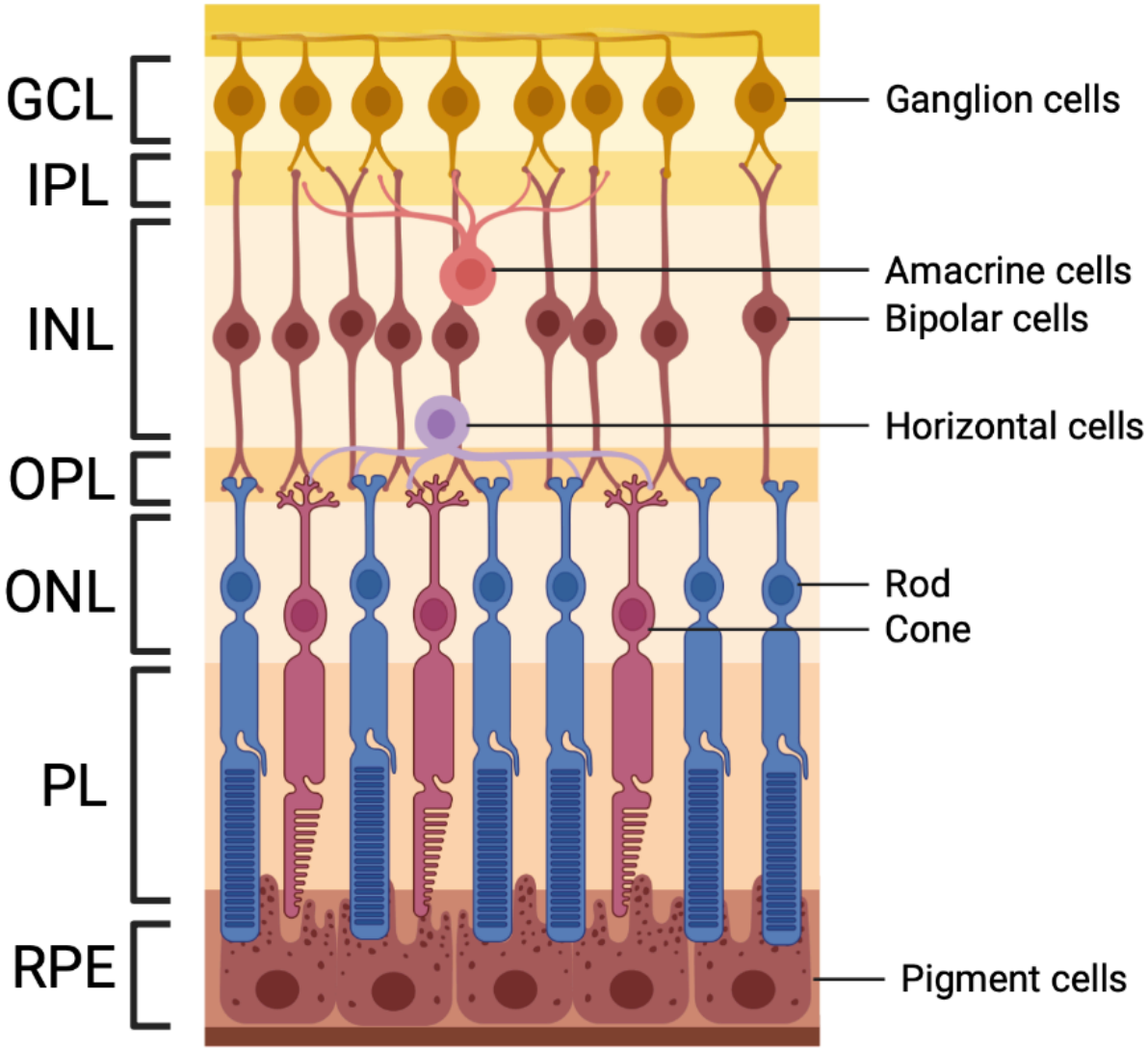

Figure 1.4. Representative illustration of the retinal anatomy. The illustration shows key layers of the retina on the left. On the right, different cell types contained within each

layer are identified. The image was created with BioRender.com. GCL: ganglion cell layer; IPL: inner plexiform layer; INL: inner nuclear layer; OPL: outer plexiform layer; ONL: outer nuclear layer; PL: photoreceptor layer; RPE: retinal photoreceptor layer.

1.4. Hypothesis and Research Objectives

The overarching aim of this thesis is to address the molecular mechanisms underlying the regulation and function of neuronal gap junction proteins, specifically Cx36 and Cx27.5. The objectives and hypotheses pertaining to each study are outlined below.

1.4.1. Determine the functional relevance Cx36 and Cav-1 interaction (Chapter 3)

The binding partners of the gap junction proteins are expected to provide valuable insight into the regulation of electrical synapses in the central nervous system. Our group has previously identified a critical involvement of tubulin (Brown et al., 2019), CamKII (Siu et al., 2021), and CaM (Siu et al., 2016) in the regulation of transport and synaptic strength and outputs of the major neuronal connexin called Cx36. Previously, an interaction between multiple members of the connexin family, including Cx36, with Cav-1 protein has been demonstrated, but its functional relevance remained unknown (A. L. Schubert et al., 2002). The purpose of this study was to uncover the functional relevance behind the mouse Cx36 and mouse Cav-1 interaction in the Neuro 2a cell line. Because of the key role of Cav-1 in the endocytosis of membrane proteins (Kiss & Botos, 2009), we hypothesized that the interaction between these two proteins regulates the trafficking dynamics of Cx36. Specific research aims that were addressed in this project are outlined below:

- Prove the interaction between Cx36 and Cav-1 and determine areas of co-localization

- Explore co-localization patterns with Golgi and ER markers to narrow down the points of contact between the two proteins
- Determine the involvement of Cav-1 in the vesicular and membrane transport of Cx36
- Assess the involvement of Cav-1 in the regulation of Cx36 endocytosis

The data in this chapter suggested that Cx36/Cav-1 interaction may be the key mechanism underlying the caveolin-dependent endocytosis of Cx36.

1.4.2. Uncover the oligomerization capabilities of Cx36 and Cx27.5 (Chapter 4)

As mentioned above, the identification of the interacting partners of gap junction proteins can aid in the discovery of the regulation mechanisms of the electrical synapses. The interactions between different connexin isoforms and their oligomerization are critical in providing means to achieve specialized channel activity in selected cells. In the retina specifically, multiple different connexin isoforms interact to allow for the formation of specialized electrical synapse channels between different cell types. Up to date, Cx36 hasn't been shown to form heteromeric or heterotypic channels. Here, we explore the potential ability of mouse Cx36 or zebrafish Cx35b to form heteromeric or heterotypic channels with a novel zebrafish connexin Cx27.5. Due to their abundant expression in the retina, we hypothesize that the above connexins might interact and form heteromeric or heterotypic channels. Specific research aims that were addressed in this project are outlined below:

- Prove the interaction between mouse Cx36 and Cx35b (zebrafish orthologue of Cx36) with zebrafish Cx27.5 in Neuro 2a cells

- Determine whether the oligomerized Cx35b/Cx27.5 channels possess distinct vesicular and membrane trafficking dynamics
- Explore the functionality of the Cx35b/Cx27.5 channels
- Assess the co-localization patterns of Cx35b and Cx27.5 in the zebrafish retina

The data in this chapter pointed to an oligomerization between Cx35b and Cx27.5 in the zebrafish retina to allow for specialized gap junctions between the different cell types.

1.4.3. Explore the molecular and functional characteristics of Cx27.5 (Chapter 5)

As Cx27.5 is a newly discovered connexin, its functional relevance is not well studied yet. The isoform was first identified in the zebrafish retina (Dermietzel et al., 2000). The retina is known to express a multitude of different connexins that establish specialized networks between different cell types and are crucial for visual processing (J. O'Brien & Bloomfield, 2018). Here, we explore the role of zebrafish Cx27.5 by employing a knock-out zebrafish line. Due to its previously identified expression in the brain and sensory organs, we hypothesize that zebrafish lacking Cx27.5 would display sensory deficits, specifically in visual processing. Specific research aims that were addressed in this project are outlined below:

- Assess the phenotypic and molecular characteristics of Cx27.5 knock-out zebrafish larvae
- Determine temporal and spatial Cx27.5 mRNA expression patterns
- Discover the expression pattern of Cx27.5 protein, specifically in the retina

- Evaluate the effect of the genetic loss of Cx27.5 on visual processing in zebrafish

The data in this chapter uncovered the functional relevance of a newly discovered Cx27.5 and identified it as one of the critical players in visual processing.

Chapter 2. Materials and Methods

2.1. Experimental Methods

2.1.1. Plasmid Construction

The full-length *Rattus norvegicus* Cx36 [NM_019281.2, amino acids (aa) 1–321], isoform 2 of *Mus musculus* Cav-1 [NM_001243064.1, (aa) 1–147], *Danio rerio* Cx27.5 [NM_131811.3, (aa) 1–240], and *Danio rerio* Cx35b [NM_194420.1, (aa) 1–304] were cloned into pEGFP-N1, pEGFP-N3, pECFP-N1, pDsRed-monomer, HA-N1 and HIS-N1 expression vectors (Clontech Laboratories Inc., Mountain View, CA, USA). Organelle markers for ER and Golgi apparatus were tagged with DsRed2 and generated as previously described (Siu et al., 2016). All plasmid constructs used in this study were sequence verified (Eurofins, MWG Operon LLC, Huntsville, AL, USA).

2.1.2. Cell Culture and Transient Transfection

Mouse neuroblastoma 2a (Neuro 2a) cells (ATCC®, CCL-131, Manassas, VA, USA) were cultivated in Dulbecco's Modified Eagle Medium (DMEM) supplemented with 10% fetal bovine serum (FBS), 1% penicillin and streptomycin, and 1% non-essential amino acids (Thermo Fisher Scientific, Rockford, IL, USA) at 37 °C in a humidified atmosphere with 5% CO2. For the co-immunoprecipitation assay, ~3,000,000 cells were seeded in one 100 mM plate. For the cell surface biotinylation assay, ~800,000 cells were seeded in 60 mM plates. For the live and fixed cell imaging, including FRET, ~25,000 cells were seeded in 35 mM glass-bottom dishes (MatTek Corporation, Ashland, MA, USA) or 24-well plates. Half an hour prior to the live microscopy assays, cells were transferred into DMEM lacking phenyl red.

Neuro 2a cells were transiently transfected with Effectene™ Transfection Reagent Kit (Qiagen Inc., Valencia, CA, USA) according to the manufacturer's guidelines. Cells were double transfected with a total of 4000 ng or 1200 ng of DNA for each 100 mM or 60 mM plate, respectively. For 35 mM glass-bottom dishes and 24-well plates, cells were transfected with 200 ng for single transfections and 400 ng for double transfections. All of the experiments were performed 48 h post-transfection.

2.1.3. Pharmacology

Prior to imaging, transfected cells were treated with the 2 μM Ionomycin (Sigma-Aldrich Chemie GmbH, Munich, Germany) and 24 μM of Ca^{2+} chelator BAPTA-AM (Thermo Fisher Scientific, Rockford, IL, USA), for 10 min. Cells were incubated with Brefeldin A (BFA) (Sigma-Aldrich Chemie GmbH, Munich, Germany) at the concentration of 5 μg/mL for 6 h. Dynasore (Sigma-Aldrich Chemie GmbH, Munich, Germany) was used as an endocytosis inhibitor for 1 hr at 50 μM concentration.

2.1.4. Western Blot

For western blot, cell protein lysates were prepared 48 h after transfection. Proteins were separated with 10% sodium dodecyl sulfate polyacrylamide gel electrophoresis (SDS-PAGE) at 150 V for 1.5 h. The gel was transferred to a nitrocellulose membrane using the Trans-Blot Turbo Transfer System (Bio-Rad Inc., Mississauga, ON,Canada) at 1.3 A and 2.5 V for 7 min. The membrane was washed in PBS buffer and blocked with Odyssey Blocking Buffer (LI-COR Biosciences, Lincoln, NE, USA) for 1 hr at room temperature (RT). The membrane was then incubated with the primary antibody

solution overnight at 4 ºC. The following primary antibodies were used for the western blot: rabbit anti-HIS (Bethyl Laboratories Inc., Montgomery, TX, USA) at 1:1000, mouse anti-HA (Roche Holding AG, Basel, Switzerland) at 1:500, mouse-anti-GFP (Santa Cruz Biotechnologies, Dallas, TX, USA) at 1:250, and mouse anti-β-actin (Sigma-Aldrich Chemie GmbH, Munich, Germany) at 1:1500 concentrations. The secondary antibodies, anti-mouse iRDye 800 and anti-rabbit iRDye 680 (LI-COR Biosciences, Lincoln, NE, USA), were used at 1:15,000 concentration. Imaging was performed using the Odyssey® CLx Infrared Imaging System (LI-COR Biosciences, Lincoln, NE, USA).

2.1.5. Co-immunoprecipitation (CoIP) with Protein A-Sepharose (Chapter 3)

Neuro 2a cells were double transfected with HIS tagged constructs as the bait and HA tagged constructs as the prey on 10cm plates. Cells were lysed in IP Lysis buffer (Thermo Fisher Scientific, Rockford, IL, USA) supplemented with a protease inhibitor cocktail kit (Thermo Fisher Scientific, Rockford, IL, USA). Lysates were centrifuged at 20,000×*g* for 10 min at 4 °C to remove the cell pellet. Cell lysates were precleared for 1h at 4 °C with protein A-Sepharose (GE Healthcare, Chicago, IL, USA). The lysate was then transferred to a fresh tube and incubated with 10µg of anti-HIS antibody overnight at 4 °C. Next day, the lysate was combined with 100 µL of a 1:1 slurry of protein A-Sepharose beads and PBS containing 2% bovine serum albumin (BSA). Following a 2-h incubation at 4 °C, the mixture was centrifuged, washed two times with 1 mL of IP lysis buffer, and three times with 1 mL of PBS. The proteins were eluted in a 1×Laemmli sample buffer for 5 min at 95 °C and subjected to western blot analysis.

2.1.6. Co-immunoprecipitation (CoIP) with Dynabead™ Protein A (Chapter 4)

Neuro 2a cells were cultured on 10cm plates and double transfected with HIS tagged constructs as the bait and EGFP tagged constructs as the prey. Cells were lysed using IP Lysis buffer (Thermo Fisher Scientific, Rockford, IL, USA) supplemented with a protease inhibitor cocktail kit (Thermo Fisher Scientific, Rockford, IL, USA) for 5mins at 4°C. Lysates were centrifuged at 20,000×*g* for 10 min at 4°C to collect the supernatant. 50uL of Dynabead™ Protein A (ThermoFisher) were incubated with 10µg of anti-HIS antibody for 15 min at RT. The lysates were then incubated with the antibody conjugated Dynabeads for 1h at RT. Samples were washed three times with PBS. The proteins were eluted in 1X Laemmli sample buffer at 95°C for 5mins and were subjected to western blot analysis.

2.1.7. Cell Surface Biotinylation Assay and Co-immunoprecipitation

Neuro 2a cells were seeded on 60 mM plates and transfected with HIS and HA or HIS and EGFP tagged constructs. Biotinylation assay was performed 48 hr post-transfection. Cells were washed once with PBS containing both calcium and magnesium and labeled with 0.3 mg of membrane-impermeable EZ-linkTM Sulfo-NHS-Biotin (Thermo Fisher Scientific, Rockford, IL, USA) per plate for 30 min at room temperature. Plates were washed three times, 5 min each, with 50 mM glycine buffer to quench the reaction. Cells were then washed with PBS lacking calcium and magnesium and lysed with IP Lysis buffer (Thermo Fisher Scientific, Rockford, IL, USA) supplemented with a protease inhibitor cocktail kit (Thermo Fisher Scientific, Rockford, IL, USA). Cell lysates were either incubated overnight with 90 µl of Dynabeads^{Tm} MyONE^{Tm} Streptavidin C1 (Invitrogen,

Carlsbad, CA, USA) on a shaker at 4 ºC or first subjected to immunoprecipitation using HIS antibody. After immunoprecipitation, the Protein A Dynabeads were washed three times with PBS, and proteins were collected in 2% SDS at 55°C for 5 min. Immunoprecipitated proteins were diluted with IP lysis buffer 5:1 and incubated with 90 µl of Dynabeads^{Tm} MyONE^{Tm} Streptavidin C1 overnight. The next day beads were collected on a magnet and washed using the following buffers: twice with buffer 1 (2% SDS in dH20), once with buffer 2 (0.1% deoxycholate, 1% Triton X-100, 500 mM NaCl, 1 mM EDTA, 50 mM Hepes pH 7.5), once with buffer 3 (250 mM LiCl, 0.5% NP-40, 0.5% deoxycholate, 1 mM EDTA, 10 mM Tris; pH 8.1), and twice with buffer 4 (50 mM Tris, 50 mM NaCl pH 7.4). Beads were boiled for 5 min in 60 µL of 1X Laemmli buffer to disrupt the bead-protein complex and elute proteins. Proteins were analyzed using western blotting.

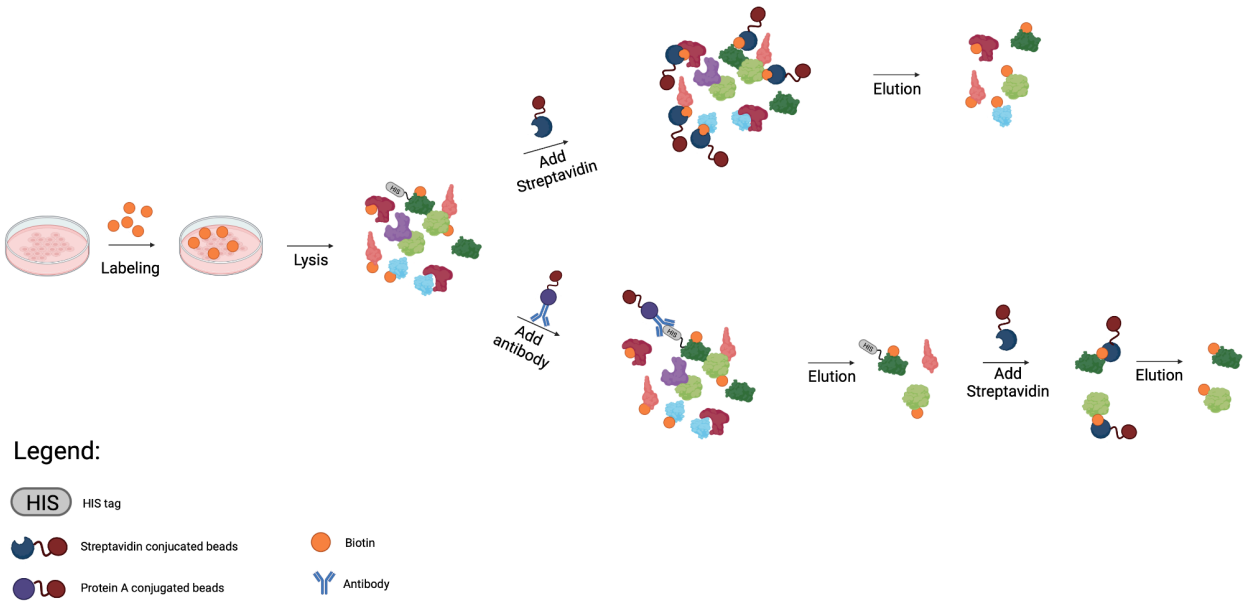

Figure 2.1. Illustration depicting key steps of the cell surface biotinylation assay followed by co-immunoprecipitation. The image depicts critical steps for the two routes for assaying biotinylated proteins. Above is the biotinylation assay to determine the entire pool of membrane proteins. Below is a biotinylation labeling followed by co-

immunoprecipitation, which identifies the interacting membrane proteins of the bait protein. The bait protein is labelled with a HIS tag. The image was created with BioRender.com.

2.1.8. Confocal Microscopy, Co-Localization, and Immunofluorescence

Transfected cells were fixed with 4% paraformaldehyde for 20 min at RT, washed with PBS, and mounted with ProLong Antifade Mountant (Thermo Fisher Scientific, Rockford, IL, USA) for imaging. Samples were visualized using a Zeiss LSM 700 confocal microscope using a Plan-Apochromat 63x/1.4 Oil DIC M27 objective. Zeiss ZEN 2010 program was used to control imaging specifications. The gap junction area was determined using ImageJ by tracing the gap junction area with a free hand tool followed by quantification using the measure tool. ImageJ software was also used to analyze co-localization data.

In the case of immunofluorescence, transfected cells were fixed with ice-cold 100% methanol for 10 min at RT. Cells were blocked using PBS supplemented with 2% BSA for 1 hr at RT. The primary antibodies, rabbit anti-HIS (Bethyl Laboratories Inc., Montgomery, TX, USA) at 1:1000 concentration and mouse anti-HA (Roche Holding AG, Basel, Switzerland) at 1:500, were diluted in PBS with 0.1% BSA and applied to cells for 1 hr at RT. Cells were then incubated in the secondary antibody solution containing 2 µg/mL of Alexa Fluor 568 goat anti-mouse (Thermo Fisher Scientific, Rockford, IL, USA) and 2 µg/mL of Alexa Fluor 488 donkey anti-rabbit (Thermo Fisher Scientific, Rockford, IL, USA) in PBS with 0.1% BSA for 1 hr at RT. Cells were washed in PBS and mounted with FluoroshieldTm (Sigma-Aldrich Chemie GmbH, Munich, Germany).

2.1.9. Förster Resonance Energy Transfer Analysis (FRET)

Neuro 2a cells were double transfected with DsRed tagged constructs as the acceptor fluorophores, and ECFP or EGFP tagged constructs as the donor fluorophores. Cells were fixed with 4% paraformaldehyde and mounted on coverslips. Zeiss LSM 700 confocal microscope was used under a previously established acceptor bleach protocol (Kotova et al., 2020). Baseline readings were recorded prior to the acceptor bleach protocol. DsRed tagged proteins were bleached using the 555 nm laser line (set to 100% intensity), and the resulting intensity change of CFP tagged proteins was measured using the 405 nm laser line. The experiment was conducted until the acceptor channel reached 10% of the initial intensity. FRET efficiency was calculated using the following FRET efficiency formula:

$$FRETeff = (Dpost - Dpre)/Dpost \quad (1)$$

where Dpost is the average intensity after the bleach, and Dpre is the average intensity before the bleach. The threshold value of 10nm distance was converted into FRET efficiency and was calculated to be 1.7% for DsRed and ECFP pair and 1.07% for DsRed and EGFP pair based on the reference distance between the two fluorescent tags (5.1nm and 4.7nm respectively) (Müller et al., 2013).

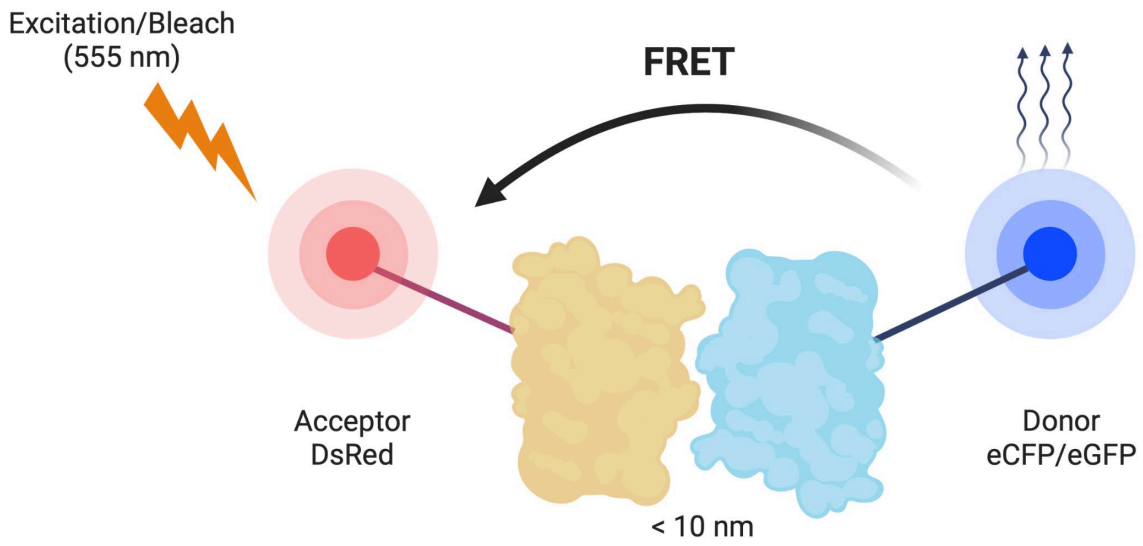

Figure 2.2. Schematic representation of the FRET constructs. Upon excitation with photobleaching, donor fluorophore (DsRed) transfers energy to the acceptor fluorophore (ECFP or EGFP) if both proteins are in proximity of under 10nm. The image was created with BioRender.com.

2.1.10. Fluorescence Recovery After Photobleaching (FRAP)

Neuro 2a cells were seeded on 35 mM glass-bottom dishes and transfected and transfected with EGFP and HA or EGFP and DsRed tagged constructs. Live-cell imaging was performed at 37 °C in a live-cell imaging chamber using a Zeiss 700 confocal microscope. Cx36-EGFP or Cx27.5-EGFP expressing cell pairs containing gap junctions were selected, and a time-lapse baseline image was recorded. The gap junction plaques were selected and bleached using the 488nm laser line with the intensity set to 100% laser power. Images were taken every 1 s for 55 s post bleaching. The fluorescence recovery was calculated using the formula:

$$F = (Ft - F0)/(Fi - F0) \quad (2)$$

where F is the normalized fluorescence at a given time point, Ft is the fluorescence intensity at t seconds, Fi is the fluorescence intensity immediately before bleaching, and F0 is the fluorescence intensity upon bleaching.

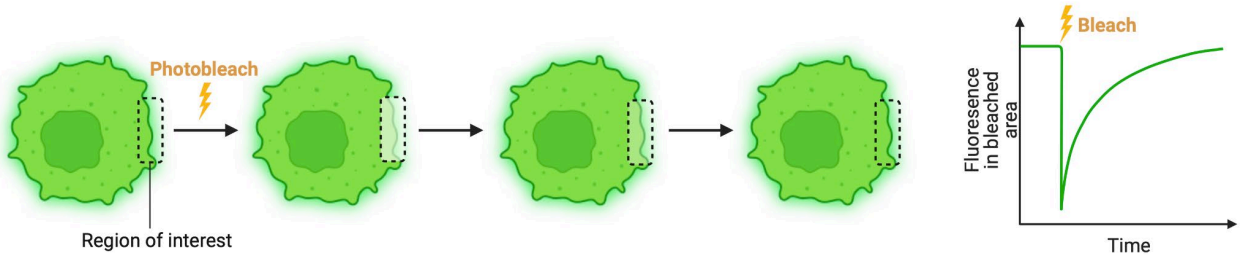

Figure 2.3. Representative illustration of the FRAP assay. Critical steps during FRAP assay are displayed in the image above. The region of interest at the cell membrane is photobleached, and recovery is recorded over time. The image was created with BioRender.com.

2.1.11. Total Internal Reflection Fluorescence (TIRF)

Neuro 2a cells were seeded on 35 mM glass-bottom dishes and transfected with EGFP and HA or EGFP and DsRed tagged constructs. A Zeiss Observer Z1 spinning-disk microscope with Zeiss 100X (Plan-Apochromat, DIC, M27, 1.46) oil immersion lens and Photometrics Evolve™512 camera was used to perform time-lapse TIRF microscopy. Zen 2 (2014) software was used to control imaging specifications under a previously established protocol (Brown et al., 2019). A live cell incubation chamber was used to maintain the temperature at 37 °C and CO2 levels at 5%. Images were acquired at a 512 × 512 pixel resolution in 1-s intervals for 60 s. Imaris (Zurich, Switzerland) program was used to track and analyze single particles expressing EGFP.

2.1.12. Dye Uptake Assay

Neuro 2a cells were cultured on 35mm glass-bottom dishes and transfected with EGFP and ECFP tagged constructs to assess the functionality of connexin hemichannels. Dye uptake analysis was performed as previously described (Timonina et al., 2020). Briefly, cells were incubated in DMEM lacking Phenyl red for 15 minutes prior to imaging. Cells were treated with 10uM EtBr immediately prior to recording. The recording was performed using Zeiss 700 confocal microscope at a 512x512 pixel resolution, with the pinhole open to the maximum. Only cells expressing both proteins were used for the analysis. Dye uptake was measured by normalizing the EtBr channel to the EGFP channel.

2.1.13. Ethidium Bromide Recovery After Photobleaching Assay

The assay has been previously reported previously (Siu et al., 2016). Transfected Neuro 2a cells were cultured on 35mm glass-bottom dishes and incubated with 10 μM of ethidium bromide in supplemented growth medium for 10 min at 37 °C and 5% CO_2 prior to imaging. Cell pairs expressing Cx27.5-EGFP were selected, and a time-lapse baseline image was recorded. One cell of each cell pair was bleached using the 555 nm laser line with 100% laser power intensity (~40 iterations at 100% intensity). Images were taken every 1 s for 55 s post bleaching. The recovery of ethidium bromide fluorescence after bleaching was measured in two regions of interest (R1 and R2). R1 was placed inside the bleached cell close to the GJP. R2 was placed at the most distant location from the GJP inside the cell to assess background recovery. The fluorescence recovery was calculated using the formula below:

$$\text{Fluorescence recovery (\%)} = \frac{(\text{Faverage}(3\text{min post bleach}) - \text{Fbleach})(\text{Faverage (pre bleach)} - \text{Fbleach})}{(\text{Faverage (pre bleach)} - \text{Fbleach})} \quad (3)$$

2.1.14. Zebrafish Maintenance, Breeding, and Embryo Collection

Adult zebrafish (*Danio rerio*) of strain Tupfel long fin (TL) were obtained from the laboratory of Dr. Wen's lab (Zebrafish Centre for Advanced Drug Discovery, St. Michael's Hospital, Toronto, ON). TL ($Cx27.5^{+/+}$) and Cx27.5 knock-out ($Cx27.5^{-/-}$) strains of zebrafish were used in all experiments. Zebrafish were kept at 28°C in aerated tanks filled with tap water circulating through a bacterial filter system. The fish were maintained at a constant light-dark cycle (14 light:10 dark hours). Breeding was performed in groups of six females and three males according to standard procedures (Brand, M. & Nüsslein-Vollhard, 2002)(**Figure 2.4**). The collected embryos were reared and maintained in E3 medium at 28°C in an incubator. The medium was exchanged the next day, and unhealthy embryos were discarded.

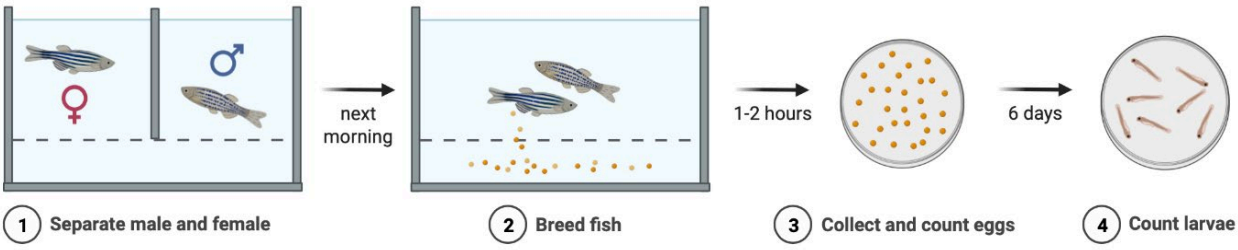

Figure 2.4. Schematic representation of the key steps during breeding procedure. Males and females are combined in the same tank with a divider separating them the day before the breeding. The next morning divider is removed to allow females and males to come together for breeding. After a few hours, eggs are collected and cleaned. In 6 days, larvae are collected and used for the behavioral experiments. The image was created with BioRender.com.

2.1.15. Establishment of TALEN-mediated Cx27.5 Mutant Zebrafish Line

TALEN cRNA pair targeting the *Cx27.5* gene (NM_131811) was microinjected into one-cell staged embryos at a concentration of 12.5 picograms (pg). The TALEN sequences for the *Cx27.5* were 5'-GAACTGGGCGTCATTTT-3' and 5'-GCGTGAACCGACATTCC-3'. To identify mutations generated by TALENs, genomic DNA was extracted from single larva or caudal fins of adult zebrafish. Adult zebrafish were anesthetized with 0.2 mg/ml ethyl 3-aminobenzoate methanesulfonate solution (MS-222, Sigma-Aldrich). Part of the caudal fin (2 mm of the end) was removed using dissecting scissors. The fin segment or larva was then incubated in 100mM NaOH at 95℃ for 15 min. One-tenth volume of 1M Tris (pH 8.0) was added to the extracts to neutralize the NaOH. Finally, 1 volume of TE buffer (pH 8.0) was added. A 250 base pairs (bp) fragment was amplified with PCR using the following primers (**Table 1**). The PCR product was digested with BclI restriction enzyme and run on a 2% agarose gel. Gel-purified PCR products were cloned into the pJet1.2 cloning vector (Life Technologies) and sequenced (Eurofins Genomics LLC, KY, USA) to characterize the indel. Heterozygous (*Cx27.5*$^{+/-}$) F1 mutants were in-crossed to establish homozygous F2 mutants (*Cx27.5*$^{-/-}$). Fish with confirmed knock-out of Cx27.5 were selected for breeding and experiments.

2.1.16. RNA Extraction and Quantitative Real-Time PCR (qRT-PCR)

RNA was extracted from 30 larvae or distinct adult zebrafish tissues using RNeasy Plus Mini Kit (Qiagen) according to the manufacturer's instructions. A total of 1µg of RNA was used to synthesize cDNA with the ReadyScript cDNA Synthesis Kit (Sigma-Aldrich). qPCR was performed using the SsoFast EvaGreen Supermix (Bio-Rad) using the

following oligonucleotide pairs (Table 1). Where possible, primers were designed to span an intron to avoid false detection of genomic DNA. Quantification of 18s rRNA served as a reference gene. Experiments were performed in triplicates using the CFX Connect™ Real-Time PCR Detection System (Bio-Rad). Melt curve analysis was performed to verify that a single amplification product was produced in each reaction. Gene expression values were calculated using the Relative Expression Software Tool software (REST;(Pfaffl et al., 2002).

2.1.17. Immunohistochemistry (IHC) Analysis

Zebrafish larvae were first euthanized in MS-222 solution (0.02% w/v, Sigma-Aldrich). Larvae were then fixed in 4% paraformaldehyde (PFA) overnight at 4oC. Following cryoprotection in 30% sucrose in 1xPBS larvae were embedded in Tissue-Tek O.C.T mounting media. Sections of 10-15 µm thickness were cut on a cryotome (Thermofisher) and mounted on Superfrost™ microscope slides (Thermofisher). Samples were washed three times for 10 min with 1xPBS at RT. Unspecific binding was blocked 5% normal goat serum (NGS, Sigma-Aldrich) in PBST for 1hr at RT. Following blocking, samples were incubated with primary antibody (1:600, rabbit anti-Cx27.5 antibody, Gene Script; 1:100, mouse anti-Cx36/35, Millipore; 1:200, mouse anti-PSD-95, Invitrogen; 1:200, mouse anti-parvalbumin, Sigma-Aldrich Chemie) overnight at 4℃. The anti-Cx27.5 peptide was used at a final concentration of 0.1 µg/ml. The next day, after 3 washes with PBST, Alexa Fluor 488 and Alexa Fluor 568 goat anti-rabbit/mouse secondary antibodies (1:1500, Life Technologies) were applied for 1 hr at RT. The sample was then washed 3 times with PBST followed by one wash with water and was mounted on microscope slides

using ProLong Antifade with DAPI (Thermofisher). Confocal images were collected using Zeiss LSM700 system (Carl Zeiss MicroImaging, Oberkochen, Germany) with Plan-Apochromat 20×/0.8 or Plan-Apochromat 63×/1.3 oil DIC M27 objectives. LSM-ZEN2 software was used to control imaging specifications. During the comparison of wild-type and knock-out tissues, settings for the image collection were kept unchanged. Composite figures were created using Adobe Photoshop 2021.

2.1.18. Behavioral Assays

Zebrafish were raised on a light-dark cycle (14 light:10 dark hours) for 6 days. All behavioral assays were performed on 7 days post-fertilization (dpf) larvae, between 12 pm and 3 pm. Larvae were not fed during the experimental period. A Zebrabox® behavior recording system (ViewPoint Life Technology, Lyon, France) was used for the behavioral recording and analysis unless otherwise specified. OMR assay was performed using a separate custom-built system following the instructions provided here (Štih et al., 2019). The detailed procedures for each assay are described below.

2.1.18.1. Freely Swimming Behavior Assay

At 7 dpf, zebrafish larvae were transferred into a 24-well plate and were allowed to acclimatize inside a recording incubator for 2.5 hours (lights off condition) or 1 hour (lights on condition) before beginning the experiment. The light intensity for the lights on condition was set to 30%. Swimming was tracked for 60 min. The mean traveled distance (mm) and speed (mm/sec) were used for the statistical analysis. Data were recorded every minute.

2.1.18.2. The Visual-Motor Response (VMR) Assay

The VMR assay was executed based on the configurations established elsewhere (Emran et al., 2008). Zebrafish larvae were transferred into a 48-well plate and allowed to acclimatize inside a recording incubator in the dark for 2.5 hours. To obtain the baseline activity data, fish were recorded in the dark for 30 min. The actual test consisted of two trials of alternating light onset (Light-ON) and light offset (Light-OFF) periods. Each period lasted for 30 minutes (a total of 120 min). The light intensity stimulus was set to 100% for the Light-ON and 0% for the Light-OFF condition. Total activity duration was used for the statistical analysis. Data were recorded every second.

2.1.18.3. Optomotor Response (OMR) Assay

The optomotor response is an innate visual behavior of all animals and humans to follow the motion of their surroundings (Bahl & Engert, 2020; Kist & Portugues, 2019; Naumann et al., 2016). OMR experiments were performed using a custom-built apparatus. The stimuli were presented using an ASUS P3B 800-Lumen LED portable projector. An 830 nm long-pass filter (Edmund Optics Inc., USA) was used to block the infrared illumination to aid in the video analysis after. The fish movements were recorded using a USB 3.1 high-speed camera (XIMEA GmbH, Germany) equipped with a 35 mm C Series Fixed Focal Length Lens (Edmund Optics Inc., USA) using XIMEA Windows Software Package. The visual stimuli were generated with an online stimulus generator program called “Moving Grating” (available at http://michaelbach.de/stim/). Larvae (7 dpf) were transferred to a 3 cm plate (Thermo Scientific) and were allowed to acclimatize for

3 min before starting the video recording. The visual stimulus consisted of sequences of black and white bars generated with 64 pixels/cycle spatial frequency. The speed rate was set to 144 pixels/sec and contrast to 100%. Stimuli were presented to larvae (n = 10) for 3 min in the left or right direction. Once the larvae reached the “target zone” (opposite end of the plate), it was counted as a positive response. The proportion of the larvae that reached the “target zone” out of the total number of fish was expressed as a percentage.

2.1.19. Statistical Analysis

Statistical analysis and data presentation were performed using GraphPad Prism 8. Values reported consist of mean ± SEM. The results shown derive from experimental replicates with n ≥ 3. Data were analyzed using the Wilcoxon–Mann–Whitney test.

2.2. General Materials

2.2.1. Biosafety

The research project in this thesis was performed in accordance with federal, provincial, and institutional regulations for the containment Level 2 laboratories located at the Life Science Building (LSB), Department of Biology at York University. Handling, manipulations, and housing of zebrafish was performed in licensed S2 laboratories at the Department of Biology at York University. Animal work was conducted at York University's zebrafish vivarium following the regulations set by the Canadian Council for Animal Care and after the approval of the protocol by the Animal Care Committee (GZ: 2020-7-R3).

2.2.2. Organisms

2.2.2.1. Bacterial Strains

Escherichia coli (*E. coli*) DH5α (Invitrogen, Burlington, Canada)

Genotype: F– Φ80*lac*ZΔM15 Δ (*lac*ZYA-*arg*F) U169 *rec*A1 *end*A1 *hsd*R17 (rK–, mK+) *pho*A *sup*E44 λ– *thi*-1 *gyr*A96 *rel*A1

E. coli NEB 5-alpha competent (New England Biolabs, Whitby, Canada)

Genotype: fhuA2 Δ(argF-lacZ) U169 phoA glnV44 Φ80 Δ(lacZ)M15 gyrA96 recA1 relA1 endA1 thi-1 hsdR17

2.2.2.2. Eukaryotic Strains

Neuroblastoma 2a cells (Neuro 2a cells) were derived from Mus musculus, which were developed by Klebe and Ruddle in 1967 from a strain A albino mouse spontaneous tumour. Neuro2a cells used in this thesis were generously provided by Dr. David C. Spray (Albert Einstein College, NY, USA).

2.2.2.3. Zebrafish

Adult zebrafish (*Danio rerio*) of strain Tupfel long fin (TL) were obtained from the laboratory of Dr. Wen's lab (Zebrafish Centre for Advanced Drug Discovery, St. Michael's Hospital, Toronto, ON). Cx27.5 knock-out line was generated from the wild-type TL line. Handling and housing of zebrafish (*Danio rerio*) were performed according to the CACC guidelines of the Canadian Council for Animal Care (CCAC) after approval of the protocol by the Animal Care Committee (ACC) (GZ#2014-
19 (R3).

2.2.3. Antibodies

Table 2.1. Antibodies used for western blot, immunofluorescence, and IHC experiments.

Name	Species of Origin	Source and Dilution
Anti-GFP	Mouse	Santa Cruz (1:250)
Anti-β-actin	Mouse	Sigma-Aldrich (1:1500)
Anti-HIS	Rabbit	Bethyl Laboratories (1:1000)
Anti-HA	Mouse	Roche (1:500)
Anti-Cx27.5	Rabbit	Gene Script (1:600)
Anti-Cx27.5 peptide (20 µg/ml)	Rabbit	Gene Script (1:200)
Anti-Cx36/35	Mouse	Millipore (1:100)
Anti-PSD-95	Mouse	Invitrogen (1:200)
Anti-Parvalbumin	Mouse	Sigma-Aldrich (1:200)
Anti-mouse iRDye 800	Goat	Li-Cor (1:15000)
Anti-rabbit iRDye 680	Donkey	Li-Cor (1:15000)
Alexa Fluor 488	Goat	Invitrogen (1:15000)
Alexa Fluor 568	Goat	Invitrogen (1:15000)

2.2.4. Commercial Kits

Table 2.2. List of commercial kits utilized for various experimental procedures.

Purpose	Kit and Company Name
Polymerase Chain Reaction	Q5® High Fidelity DNA Polymerase PCR Kit (New England BioLabs)
QIAquick Gel Extraction Kit	Gel Elution of DNA fragments (Qiagen)
Ligation of DNA fragments	CloneJET™ PCR Cloning Kit (Thermo Scientific) Rapid DNA Ligation Kit (Thermo Scientific)

Plasmid DNA Purification	QIAPrep Spin Miniprep Kit (Qiagen)
Restriction DNA analysis	Fast digestion Top Fermentas Kit (Thermo Scientific)
DNA transfection	Effectene Transfection Reagent (Qiagen)
Protease inhibition	Halt™ Protease and Phosphatase inhibition Cocktail (Thermo Scientific)

2.2.5. Oligonucleotides

Table 2.3. Primers used for quantitative Real Time-PCR (qRT-PCR) and genotyping.

Gene	Forward	Reverse	Purpose
Cx27.5	ATGGCCACTGTTTTGACCG	GCTGTTGGGTGTTGCAGATG	Genotyping
18s	TGACTCTTTCGAGGCCCTGTA	TGGAATTACCGCGGCTGCTG	qPCR
Cx27.5	TGCCACTAACACCACCTG	AGGATCCGGAAAATGAAGAGG	qPCR

2.2.6. Solutions and Media

2.2.6.1. Solutions for cell culture

Table 2.4. Solutions used for cell culture and their composition.

Name	Company
10% Formalin	Sigma-Aldrich
Trypsin	Sigma-Aldrich
PBS with/without calcium/magnesium	Sigma-Aldrich
Penicillin and Streptomycin	BioShop
FBS (Fetal Bovine Serum)	Gibco
NEA (Non-essential Amino Acids)	Sigma-Aldrich
Dulbecco's Modified Eagle Medium (DMEM)	Sigma-Aldrich

Mounting Solution: Fluoroshield with DAPI	Sigma-Aldrich
ProLongTM Gold antidade reagent (no DAPI	Invitrogen

2.2.6.2. Solutions for Bacterial Culture

Table 2.5. Solutions used for bacterial culture and their composition.

Name	**Composition**
LB Media	1% bacto tryptone, 0.5% yeast extract, 0.5% NaCl, 50µL/mL of kanamycin or 100µL/mL of ampicillin
LB agar plates	LB medium (1% agar), 50µL/mL of kanamycin or 100µL/mL of ampicillin
SOC medium	2% bacto tryptone, 0.5% yeast extract, 10mM NaCl, 2.5 mM KCl, 10mM $MgCl_2$, 10mM $MgSO_4$, 20 mM glucose

2.2.6.3. Solutions for Biological Methods

Table 2.6. Solutions used for biological methods and their composition.

Name	**Composition**
DNA Loading Buffer	10x FastDigest Green buffer (Fermentas)
1x TAE Gel Loading Buffer	40mM Tris, 20mM acetic acid, 1mM EDTA
Laemmli Sample Buffer	2% SDS, 10% glycerol, 5% β-mercaptoethanol, 0.1% Orange G, 50mM Tris-HCl, pH 6.8

Laemmli Running Buffer	192mM glycine, 0.1% SDS, 25mM Tris-HCl pH 8.3
Staining Solution	Coomassie PAGE BLUE (BioRad)
Blocking Solution	Odyssey Blocking Buffer (Li-Cor Bioscience)
Phosphate Buffered Saline (PBS)	130mM NaCl, 28mM KCl, 10mM Na_2HPO_4, 1.8mM KH_2PO_4, pH 7.4
Stock salts for E3	40g Instant Ocean Salt, 1L Distilled water
E3 medium for raising zebrafish embryos	1.5ml of stock salts in 1L of distilled water (60 µg/ml)

2.2.7. Software

Table 2.7. Software and tools used for publication and thesis completion

Purpose	**Name**
Image Processing	ImageJ, Adobe Photoshop 2020
Primer Design and PCR Analysis	NCBI/Primer-BLAST
Analyses of DNA Sequences and Sequence Data	SnapGene Viewer
Sequence alignments	Clustal Omega
Microscope Image Software	ZEN 2010, ZEN Black, (Carl Zeiss Microscopy)
Protein/DNA concentration	Nanodrop2000
Statistical Analysis	Prism 9 (GraphPad)
Text processing	Microsoft Word

Chapter 3. Endocytosis of Connexin 36 is Mediated by Interaction with Caveolin-1

This chapter is modified from the following original published article:

Kotova, A., Timonina, K., & Zoidl, G. R. (2020). Endocytosis of connexin 36 is mediated by interaction with caveolin-1. *International Journal of Molecular Sciences*, *21*(15), 5401. doi.org/10.3390/ijms21155401

Authors:

Anna Kotova [1],

Ksenia Timonina [1]

Georg R. Zoidl [1,2,*]

Affiliations:

[1] Department of Biology, York University, Toronto, ON M3J 1P3, Canada
[2] Department of Psychology, York University, Toronto, ON M3J 1P3, Canada
***** Author to whom correspondence should be addressed.

Author Contributions

Designed the study and wrote the manuscript (A.K., G.R.Z.); executed experiments (A.K., K.T.); analyzed data (A.K., K.T.). All authors have read and agreed to the published version of the manuscript.

Funding: Canada Research Chair program and NSERC-DG (GRZ)

Conflicts of Interest: The authors declare no conflict of interest.

In Brief:

The gap junctional protein connexin 36 has been shown to interact with a lipid raft protein called caveolin-1, however, the functional relevance of this interaction remains unknown. In this study, we explore the effect of caveolin-1 on the intracellular and membrane transport of connexin 36. Our data indicate that the interaction between connexin 36 and caveolin-1 is involved in the connexin 36 internalization through a caveolin-dependent pathway.

Highlights:

- Connexin 36 and caveolin-1 co-localize and interact in Neuro 2a cells
- Interaction between connexin 36 and caveolin-1 is dependent on intracellular calcium levels
- Caveolin-1 enhances vesicular transport of connexin 36 but inhibits its membrane dynamics
- Caveolin-1 depletes levels of connexin 36 from the membrane via endocytosis

3.1. Abstract

The gap junctional protein connexin 36 (Cx36) has been co-purified with the lipid raft protein caveolin-1 (Cav-1). The relevance of an interaction between the two proteins is unknown. In this study, we explored the significance of Cav-1 interaction in the context of intracellular and membrane transport of Cx36. Co-immunoprecipitation assays and Förster resonance energy transfer analysis (FRET) were used to confirm the interaction between the two proteins in the Neuro 2a cell line. We found that the Cx36 and Cav-1

interaction was dependent on the intracellular calcium levels. By employing different microscopy techniques, we demonstrated that Cav-1 enhances the vesicular transport of Cx36. Pharmacological interventions coupled with cell surface biotinylation assays and FRET analysis revealed that Cav-1 regulates membrane localization of Cx36. Our data indicate that the interaction between Cx36 and Cav-1 plays a role in the internalization of Cx36 by a caveolin-dependent pathway.

3.2. Introduction

The intracellular transport of connexins, their assembly and channel formation, and removal are governed by complex interactions with regulatory, transport, and structural proteins (Laird, 2010; Thévenin et al., 2013). The turnover of connexins from the cell membrane is, in particular, challenging for connexin 36 (Cx36), the major component of electrical synapses. In these gap junctions of the brain, Cx36 has been found in axo-axonal, axo-dendritic, and dendro-dendritic contact sites (Nagy et al., 2018, 2019; Nagy & Rash, 2017). It is reasonable to expect that each type of contact site presents a distinct local environment with both unique and shared complements of Cx36-interacting proteins enabling on-demand protein transport and removal.

One of the most notable interacting partners of Cx36 is the Ca2+/calmodulin dependent protein kinase II (CaMKII) (Alev et al., 2008). Cx36 also exhibits a unique property called the “run-up” phenomenon, in which its conduction increases 10-fold (Del Corsso et al., 2012). The deletion of CaMKII binding and phosphorylation regions in Cx36 led to the loss of this “run-up” property, signifying that this interaction is essential for the functional plasticity of electrical synapses formed by Cx36. Calmodulin (CaM), another

multifunctional calcium signaling protein, has also been shown to bind Cx36 (Burr et al., 2005). Both CaMKII and CaM share a binding motif and interact with Cx36 competitively. Cx36 also interacts with scaffolding proteins (Li et al., 2012), proteins of the zonula occludens family (Li et al., 2000, 2009), or protein kinases (Bazzigaluppi et al., 2017; H. Y. Wang et al., 2015). A recent study demonstrated that Cx36 interaction with tubulin potentiates the synaptic strength of Cx36 by tubulin-mediated delivery of channels to the gap junction plaques (Brown et al., 2019).

Several connexins, including Cx36, have been shown to interact with a membrane/lipid raft protein called Caveolin-1 (Langlois et al., 2008; A. L. Schubert et al., 2002). However, the functional role of the Cx36/Cav-1 interaction has yet to be established. Caveolins are the primary components of caveolae and are involved in cellular processes such as transcytosis, potocytosis, endocytosis, and signal transduction (Cohen et al., 2004). While caveolae, the flask-like invaginations of the plasma membrane, are known to exist in numerous cell types except for neurons, caveolins can be expressed in neurons independently of caveolae (Head & Insel, 2007). This family of proteins is composed of three members: caveolin-1, caveolin-2, and caveolin-3, which have been reported to be expressed in many cell types, including neurons (Boulware et al., 2007; Galbiati et al., 1998). Analogous to Cx36 (Condorelli et al., 1998), Cav-1 is expressed in hippocampal neurons (Bu et al., 2003). Recent studies have linked the expression of caveolins in the brain to the regulation of various neuronal processes, including hippocampal plasticity (Braun & Madison, 2000; Gaudreault et al., 2005). Lipid rafts are vital for synapse development, maintenance, and stabilization (Mauch et al., 2001; Willmann et al., 2006). Cav-1 targets various neurotrophic receptors such as

NMDA, AMPA, Trk, and GPC, (Bilderback et al., 1999; Björk et al., 2010; Head et al., 2008, 2011) to the rafts, and also regulates components of the actin cytoskeleton (Head et al., 2011). Cav-1 has also been shown to regulate the activity of several channels (Toselli et al., 2005; Trouet et al., 1999, 2001), and it has been suggested that the rafts might be involved in connexin trafficking (Locke et al., 2005).

Here, the role of Cav-1 in regulating the Cx36 function was investigated in the Neuro 2a cell line. We demonstrated that the Cx36/Cav-1 interaction is calcium-dependent using Förster Resonance Energy Transfer Analysis (FRET) and co-immunoprecipitation (CoIP). Total Internal Reflection Fluorescence (TIRF) and Fluorescence Recovery After Photobleaching (FRAP) determined the role of Cav-1 on intracellular transport and membrane dynamics of Cx36. Pharmacological interventions, together with FRET and cell surface biotinylation assays, confirmed the involvement of Cav-1 in the endocytosis of Cx36. Our results suggest that an increased Cx36/Cav-1 interaction may be a key mechanism implicated in the caveolin-dependent endocytosis of Cx36. We expect that these findings have implications for the spatial regulation of Cx36 and its turnover in the plasma membrane.

3.3. Results

3.3.1. Cx36 co-localizes with and is in close proximity to Cav-1 in Neuro 2a cells

To investigate the co-localization patterns of Cx36 and Cav-1, Neuro 2a cells were double transfected with Cx36-HIS and Cav-1-HA. Proteins were labeled with the corresponding primary antibodies and imaged 48 hr post-transfection. Cx36 and Cav-1 co-localize in the intracellular compartments and partly at the cell membrane (**Figure**

3.1A, arrows). Co-localization quantification revealed that Cx36 and Cav-1 co-localize significantly more intracellularly than at the membrane (Intracellular: 0.51 ± 0.028, n = 27; Membrane: 0.35 ± 0.032, n = 27; p = 0.0010) (**Figure 3.1B**).

Neuro 2a cells were double transfected with Cx36-ECFP and Cav-1-DsRed to investigate proximity between these two proteins using FRET. FRET efficiency above the threshold of 1.7% signified that proximity between two proteins is less than 10nm, meaning that they are close enough to interact with each other (**Figure 3.1C**). Because Cx36 monomers oligomerize into hexamers, Cx36-Cx36 pairs served as a positive control with a FRET efficiency value of 10.27 ± 0.60 (n = 40). Cells transfected with fluorescent tags alone served as a negative control. ECFP-DsRed pair displayed the FRET efficiency value of 2.82 ± 0.28 (n = 30). The value above the threshold can be explained by the partial dimerization of the fluorescent tags. FRET efficiency between Cx36-ECFP and Cav-1-DsRed pair was 5.73 ± 0.47 (n = 86) and was significantly different from the negative control group (p = 0.0001). This result proved that the two proteins were close enough to interact with each other. To assess whether the protein tags have an equal impact on the interaction, the tags were switched (Cx36-DsRed and Cav-1-ECFP). FRET efficiency was not significantly different (5.94 ± 0.40, n = 100, p = 0.4538), suggesting that protein tags are interchangeable and have minimal impact on FRET efficiency.

To confirm the interaction between Cx36 and Cav-1, a CoIP assay was performed. Neuro 2a cells were double transfected with Cx36-HIS and Cav-1-HA, and the HIS antibody was used to pull down the protein complexes. The expression of the proteins of interest in the lysate (input) and elution (CoIP) fractions was confirmed with western blot

analysis (**Figure 3.1D**). Low levels of Cx36 co-immunoprecipitated with Cav-1, suggesting a weak or transient interaction.

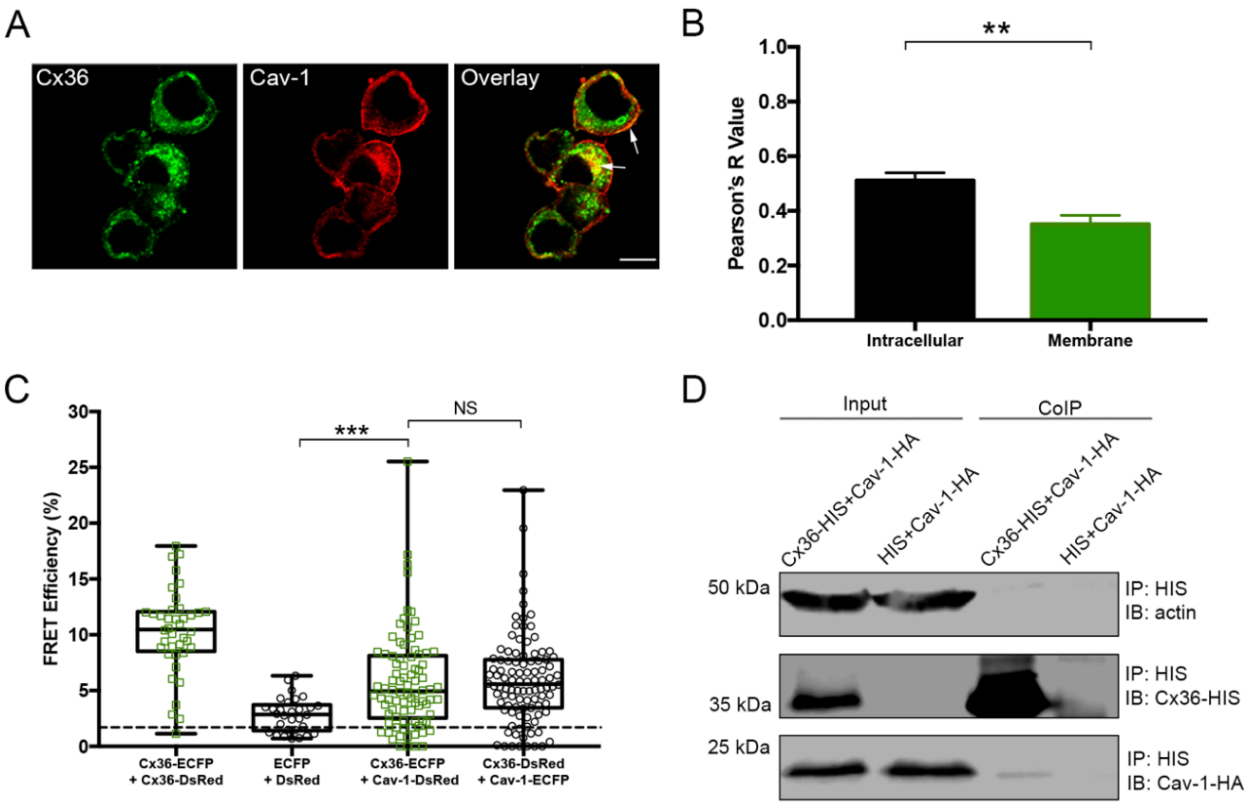

Figure 3.1. Co-localization, Förster Resonance Energy Transfer Analysis (FRET), and co-immunoprecipitation (CoIP) analysis of Cx36 and Cav-1. (A) Neuro 2a cells transfected with Cx36-HIS and Cav-1-HA were labeled with anti-HIS and anti-HA antibodies. Cx36 and Cav-1 displayed co-localization in the intracellular compartments and partly at the membrane (white arrows). Scale bar: 10 μm. (B) Co-localization quantification of the Cx36-HIS and Cav-1-HA intracellularly and at the membrane. Error bars show standard error of the mean. Sample sizes were the following: Intracellular: n = 27; Membrane: n = 27. (C) FRET efficiencies. Cx36-ECFP and Cx36-DsRed pair served as a positive control while ECFP and DsRed pair served as a negative control. Cx36-ECFP and Cav-1-DsRed pair showed high FRET efficiency, signifying that two proteins are close to one another. The exchange of tags on both proteins (Cx36-DsRed and Cav-1-ECFP) had no significant effect on FRET efficiency. The dotted line represents the threshold of 1.7% (equals to 10nm distance between FRET pairs). Error bars show the minimum and maximum values. Sample sizes were the following: Cx36-ECFP + Cx36-DsRed: n = 40; ECFP + DsRed: n = 30; Cx36-ECFP + Cav-1-DsRed: n = 86; Cx36-DsRed + Cav-1-ECFP: n = 100. (D) CoIP of Cx36 and Cav-1. HIS antibody was used to pull down the Cx36-HIS and Cav-1-HA complex. Neuro 2a cells double transfected with HIS and Cav-1-HA served as a negative control. Input lanes (cell lysates) show protein levels prior to the assay. CoIP lanes represent eluted protein complexes. A low amount of Cav-1 eluted together with Cx36 signified weak or transient interaction. Anti-HA and anti-HIS

antibodies detected Cav-1 and Cx36 proteins, respectively. An anti-ß-actin antibody served as a loading control. IP: immunoprecipitation; IB: immunoblotting. Mann-Whitney U (two tailed) significance test, ** $p < 0.01$, *** $p < 0.001$, NS—not significant.

3.3.2. Calcium enhances the interaction between Cx36 and Cav-1

Due to the existing relationship between calcium and Cx36, we tested whether an influx of intracellular calcium would strengthen the interaction between Cx36 and Cav-1. We first tested the effect of Ionomycin (Iono) and 1,2-bis (2-aminophenoxy) ethane-N, N, N', N'-tetraacetate (BAPTA) pharmacological agents on FRET efficiency between Cx36 and Cav-1 (**Figure 3.2A**). Treatment with 2 µM Iono, a calcium ionophore, significantly increased FRET efficiency between Cx36-ECFP and Cav-1-DsRed pairs (7.33 ± 0.37, $n = 85$, $p = 0.0004$). Treatment with 24 µM BAPTA, a calcium chelator, served as a negative control to Iono and significantly decreased FRET efficiency (3.015 ± 0.25, $n = 42$, $p = 0.0001$).

Because Iono enhanced the FRET efficiency between Cx36 and Cav-1 and BAPTA showed the opposite effect, the involvement of calcium in Cx36 and Cav-1 interaction was further explored. The possibility that calcium would strengthen the interaction between these two proteins was tested using CoIP assay. Prior to lysing, cells were treated with 2 µM Iono for 10 min. HIS antibody was used to pull down the protein complexes. Both Cx36 and Cav-1 were found in the elution fraction (**Figure 3.2B**). This assay further confirmed that an increase in the intracellular calcium strengthens the interaction between Cx36 and Cav-1.

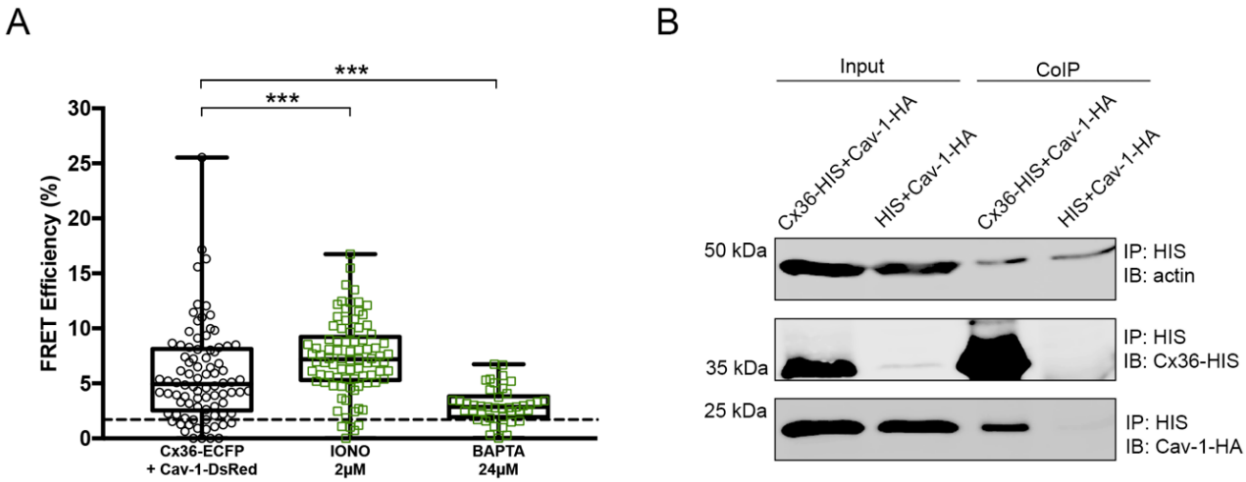

Figure 3.2. Interaction between Cx36 and Cav-1 is strengthened upon Ionomycin incubation. (A) FRET efficiencies of the Cx36-ECFP and Cav-1-DsRed pair under the action of Iono and BAPTA pharmacological agents. The dotted line represents the threshold of 1.7% (equals to 10nm). Error bars show the minimum and maximum values. Sample sizes were the following: Cx36-ECFP + Cav-1-DsRed: n = 86; Iono: n = 85; BAPTA: n = 42. (B) CoIP of Cx36-HIS and Cav-1-HA after stimulation with Iono. HIS antibody was used to pull down the Cx36-HIS and Cav-1-HA complex. Neuro 2a cells double transfected with HIS and Cav-1-HA served as a negative control. Input lanes (cell lysates) show protein levels prior to the assay. CoIP lanes represent eluted protein complexes. Cav-1 eluted together with Cx36, signifying that calcium is required to strengthen the interaction between the two proteins. Anti-HA and anti-HIS antibodies detected Cav-1 and Cx36 proteins, respectively. An anti-ß-actin antibody served as a loading control. IP: immunoprecipitation; IB: immunoblotting. Mann-Whitney U (two tailed) significance test, ***$p < 0.001$.

3.3.3. Cx36 and Cav-1 co-localize more with Golgi than the ER and Their interaction is reduced with BFA treatment

The next step was to determine in which intracellular location the Cx36/Cav-1 interaction occurs. Co-localization studies with the Golgi marker, galactosyltransferases, and the endoplasmic reticulum (ER) organelle marker, calreticulin, were performed. Neuro 2a cells were double transfected with the following pairs: Cx36-HIS and ER-DsRed, Cx36-HIS and Golgi-DsRed (**Figure 3.3A**), Cav-1-HIS and ER-DsRed and Cav-1-HIS and Golgi-DsRed (**Figure 3.3B**). Cx36 showed more co-localization with the Golgi

marker than with ER (Cx36 and ER: 0.61 ± 0.024, *n* = 30; Cx36 and Golgi: 0.76 ± 0.034, *n* = 21; *p* = 0.0008) (**Figure 3.3C**). Cav-1 showed the same co-localization pattern (Cav-1 and ER: 0.58 ± 0.028, *n* = 21; Cav-1 and Golgi: 0.71 ± 0.024, *n* =19; *p* = 0.0018).

This result led us to believe that Cx36 and Cav-1 are likely to interact in the Golgi apparatus. To explore this idea, Brefeldin A (BFA), a pharmacological agent that blocks transport between ER and Golgi (Misumi et al., 1986), was employed. Neuro 2a cells were transfected with Cx36-ECFP and Cav-1-DsRed and incubated with BFA for 6 hr prior to FRET analysis. FRET efficiency between the Cx36 and Cav-1 post BFA treatment (3.76 ± 0.40, *n* = 91) was significantly decreased when compared to untreated cells (5.73 ± 0.47, *n* = 86, *p* = 0.0003) (**Figure 3.3D**). This result further confirmed that a population of Cx36 and Cav-1 proteins were interacting in the Golgi apparatus.

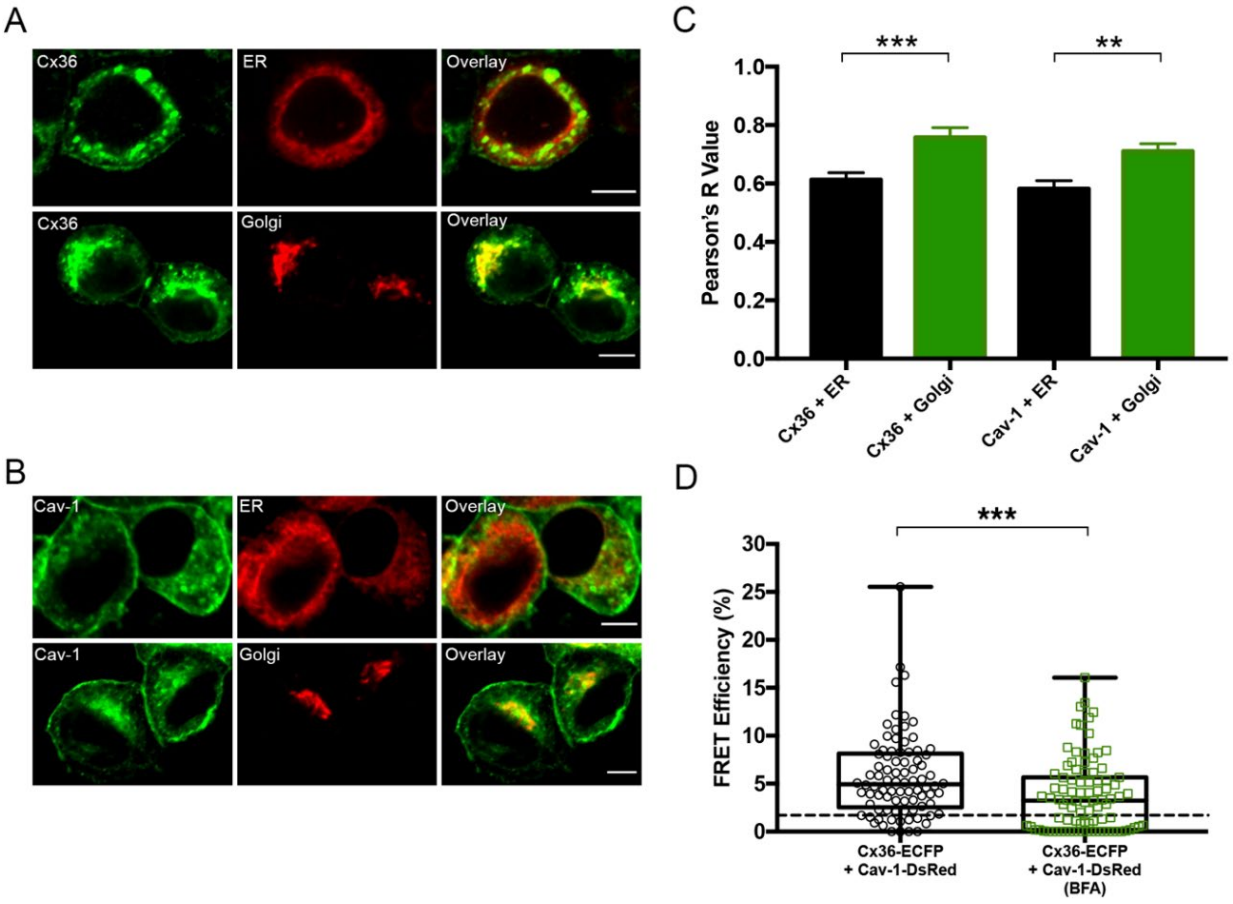

Figure 3.3. Co-localization with cellular markers and FRET analysis of Cx36 and Cav-1 post Brefeldin A (BFA) treatment. (A, B) Co-localization of Cx36-HIS and Cav-1-HA with DsRed-tagged calreticulin (ER marker), and DsRed-tagged galactosyltransferases (Golgi apparatus marker). HIS-tagged Cx36 was detected using an anti-HIS antibody and HA-tagged Cav-1 was detected using an anti-HA antibody. Alexa Fluor 568 was used as a secondary antibody. Scale bar: 5 μm (C). Co-localization quantification of the Cx36 and Cav-1 with the organelle markers. Error bars show standard error of the mean. Sample sizes were the following: Cx36 and ER: n = 30; Cx36 and Golgi: n = 20; Cav-1 and ER: n = 21; Cav-1 and Golgi: n = 19. (D) FRET efficiencies of Neuro 2a cells transfected with Cx36 and Cav-1 with and without BFA treatment. The threshold of 1.7% (equals to 10nm) is represented by the dotted line. Error bars show the minimum and maximum values. Sample sizes were the following: Cx36-ECFP + Cav-1-DsRed: n = 86; BFA: n = 91. Mann-Whitney U (two tailed) significance test, **p < 0.01, ***p < 0.001.

3.3.4. Cav-1 affects both vesicular and membrane transport of Cx36

To further explore the importance of the interaction between Cx36 and Cav-1 we examined the effect of Cav-1 overexpression on the intracellular transport of Cx36. Neuro 2a cells transfected with Cx36-EGFP and Cav-1-HA or with Cx36-EGFP and HA were subjected to TIRF microscopy. Trafficking dynamics of the individual vesicles, illuminated in the submembrane space, were recorded over the 1-min duration (**Figure 3.4A–D**). Vesicles double transfected with both Cx36 and Cav-1 demonstrated increased displacement (Cx36: 1.28 ± 0.062, n = 1107; Cx36 and Cav-1: 1.50 ± 0.061, n = 1349; p < 0.0001) (**Figure 3.4A**), mean speed (Cx36: 0.14 ± 0.014, n = 1107; Cx36 and Cav-1: 0.20 ± 0.016, n = 1349; p < 0.0001) (**Figure 3.4B**), maximum speed (Cx36: 0.64 ± 0.037, n = 1107; Cx36 and Cav-1: 0.75 ± 0.037, n = 1349; p < 0.0001) (**Figure 3.4C**) and minimum speed (Cx36: 0.043 ± 0.013, n = 1107; Cx36 and Cav-1: 0.056 ± 0.014, n = 1349; p < 0.0001 (**Figure 3.4D**).

To assess whether Cav-1 has an effect on the membrane dynamics and gap-junction regeneration of Cx36, FRAP microscopy was employed. Gap junctions were

used as regions of interest (**Figure 3.4E**). FRAP analysis revealed that fluorescent recovery of the Cx36-EGFP and Cav-1-HA transfected cells was significantly lower than of Cx36-EGFP and HA transfected cells (Cx36: 14.77 ± 2.136, n = 27; Cx36 and Cav-1: 11.04 ± 1.444, n = 29; p = 0.0467) (**Figure 3.4F**). However, both types of cells exhibited the same trend in recovery (**Figure 3.4G**). These results demonstrated that while Cav-1 increases the dynamics of the intracellular transport of Cx36, it reduces the gap junction plaque recovery, signifying that a lower amount of Cx36 is reaching the membrane in the presence of Cav-1. Taken together, these results suggest that Cav-1 enhances the retrograde transport of Cx36.

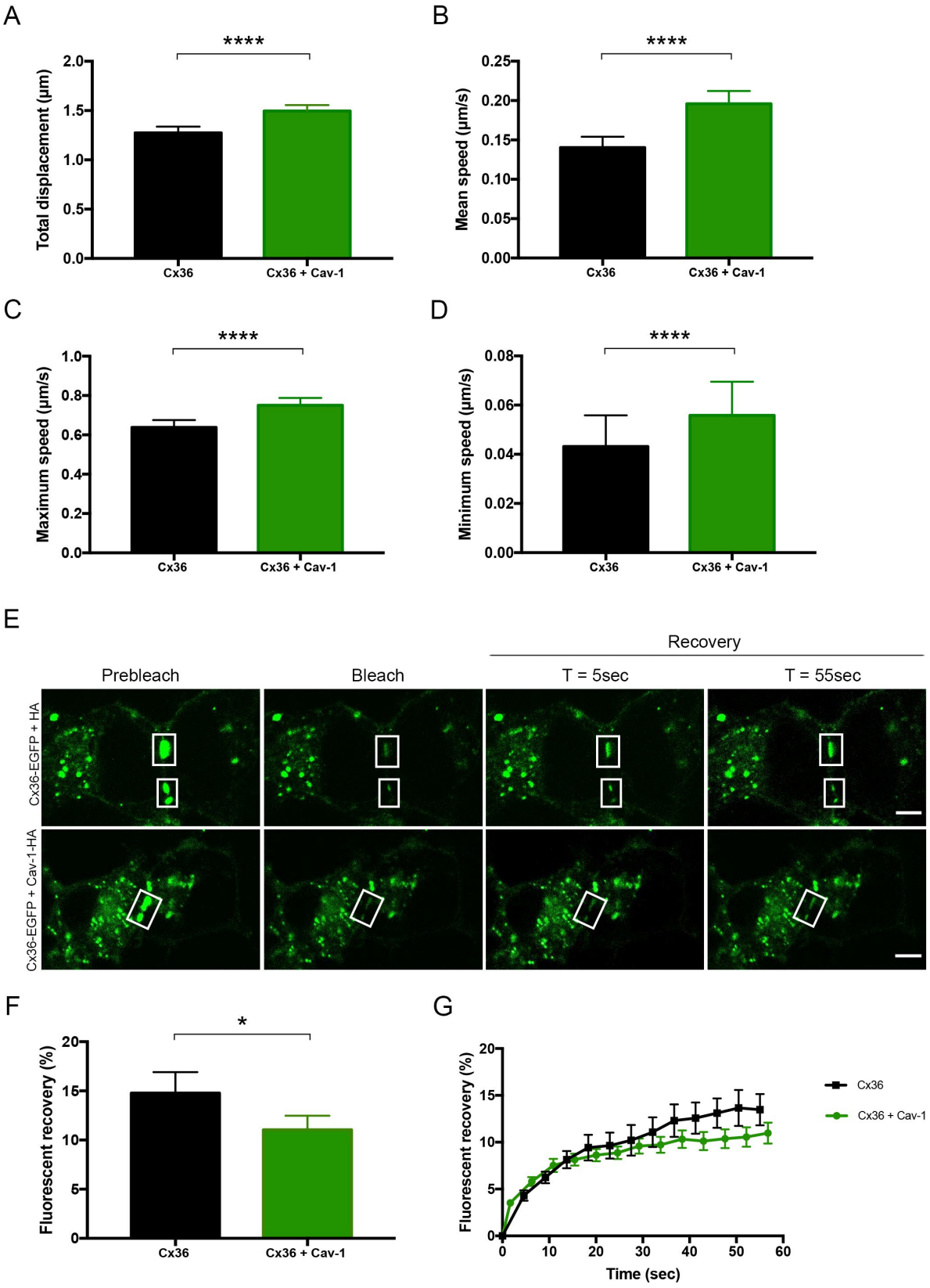

Figure 3.4. The effect of Cav-1 on vesicular transport and membrane dynamics of Cx36. Total Internal Reflection Fluorescence (TIRF) microscopy was used to resolve the

vesicular transport of Cx36-EGFP. Cav-1 significantly amplified displacement (A) and the mean (B), maximum (C), and minimum speed of Cx36 (D). Error bars show standard error of the mean. Sample sizes were the following: Cx36-EGFP and HA: n = 1107; Cx36-EGFP and Cav-1-HA: n = 1349. (E) FRAP analysis of cells transfected with Cx36-EGFP and HA or Cx36-EGFP and Cav-1-HA showing selected regions (white rectangles) pre bleaching, immediately after bleaching, and recovery 5 and 55 s post bleaching. Scale bar: 5 μm. (F) The bar graph displays the total % fluorescent recovery of the selected gap junction regions, 55 s post bleaching. Error bars show standard error of the mean. Sample sizes were the following: Cx36-EGFP: n = 23; Cx36-EGFP and Cav-1-HA: n = 24. (G) Overall trends in % recovery measured every 5 s, over the 55-s duration. Error bars show standard error of the mean. Mann-Whitney U (two tailed) significance test, *p < 0.05, ****p < 0.0001.

3.3.5. Cav-1 depletes levels of Cx36 from the membrane via endocytosis

After establishing that Cav-1 has an effect on the intracellular transport of Cx36, we tested whether the same held for the membrane expression of Cx36. To assess the effect of Cav-1 on gap junction assembly or disassembly, the gap junction plaque area was measured in Cx36-EGFP and HA or Cx36-EGFP and Cav-1-HA transfected cells (**Figure 3.5A).** The gap junction plaque area of Cx36 and Cav-1 transfected cells was significantly lower when compared to Cx36 transfected cells (Cx36: 1.87 ± 0.19, n = 45; Cx36 and Cav-1: 1.28 ± 0.098, n = 48; p = 0.0230) (**Figure 3.5B**).

To further compare levels of Cx36 at the membrane, cell surface biotinylation assay was performed. While Cx36 is a transmembrane protein containing two extracellular loops, Cav-1 does not contain any extracellular domains; therefore, Cav-1 is unable to undergo cell surface biotinylation (**Figure 3.5C**). Cx36-HIS and HA or Cx36-HIS and Cav-1-HA transfected cells were biotinylated at the cell surface and pulled down with streptavidin (**Figure 3.5D**). Levels of Cx36 were notably lower when cells were also transfected with Cav-1, suggesting that Cav-1 depletes Cx36 from the membrane. To test whether this effect is due to the Cav-1 mediated endocytosis of Cx36, we employed the

pharmacological agent Dynasore. Prior to cell surface biotinylation, cells transfected with Cx36 and Cav-1 were incubated with 50 μM Dynasore for 1 hr. As expected, once endocytosis was blocked with Dynasore (Kirchhausen et al., 2008), levels of Cx36 were restored to baseline. **Figure 3.5E** displays the expected increase in the membrane expression of Cx36 once Dynasore is applied. Unlike Cx36, Cav-1 is predominately expressed in the membrane, therefore, a minor increase in the membrane localization is observed.

To confirm the specificity of this drug on the interaction, we examined the effect of Dynasore on FRET efficiency between Cx36 and Cav-1 (**Figure 3.5F**). Prior to the FRET analysis, cells transfected with Cx36-ECFP and Cav-1-DsRed were incubated with 50 μM Dynasore for 1 hr. FRET efficiency between Cx36 and Cav-1 was significantly reduced upon Dynasore application, further suggesting that Cx36 and Cav-1 are interacting during the internalization pathway (no treatment: 4.00 ± 0.46, n = 55; Dynasore: 2.67 ± 0.33, n = 64, p = 0.0350).

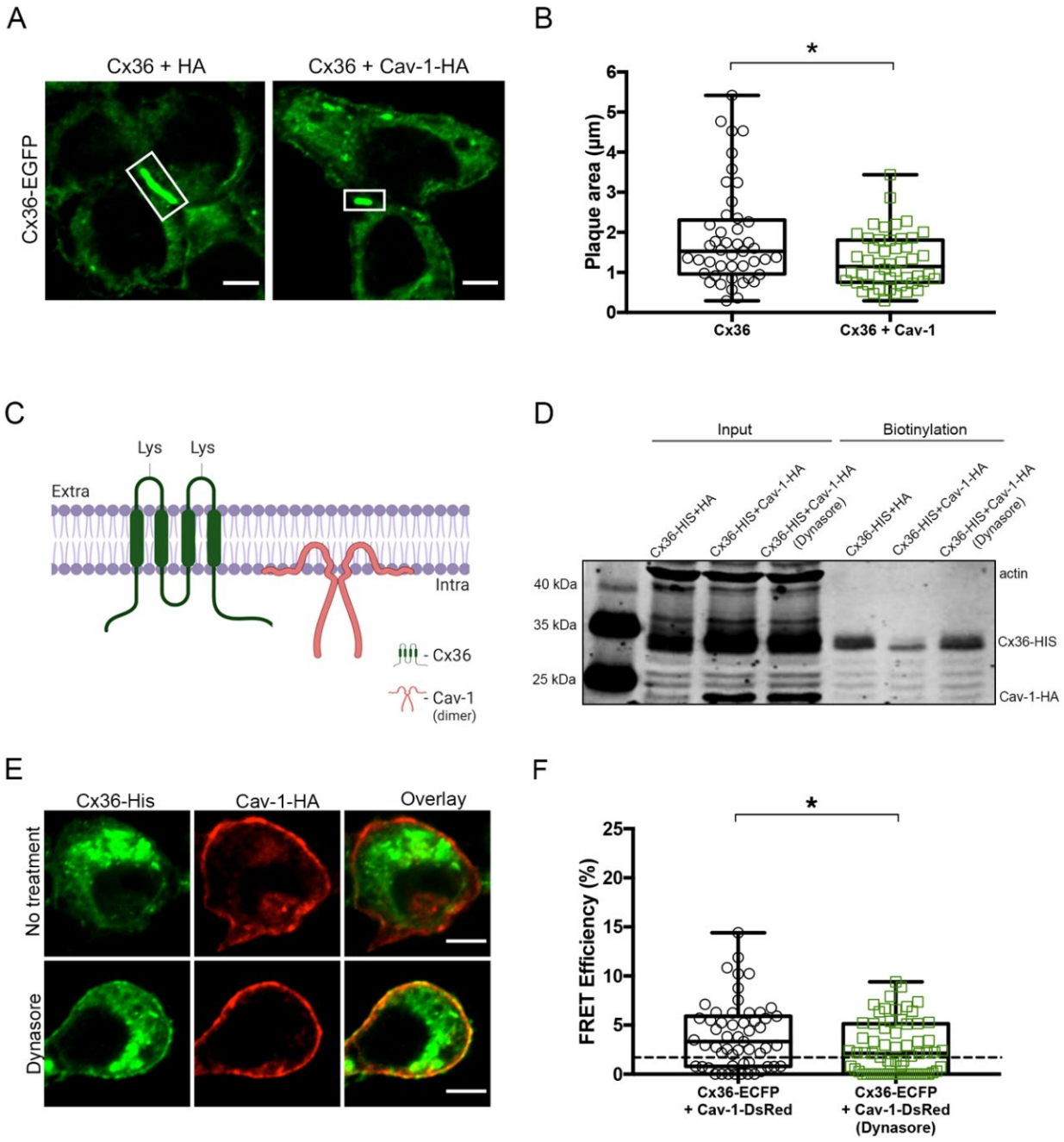

Figure 3.5. Cav-1 regulates levels of Cx36 at the membrane. (A) Representative images of Cx36 gap junction plaques (in white boxes) in live cells transfected with Cx36-EGFP and HA or Cx36-EGFP and Cav-1-HA. Scale bar: 5µm. (B) Gap junction plaque areas of cells double transfected with Cx36-EGFP and Cav-1-HA were significantly reduced when compared to cells transfected with Cx36-EGFP and HA. Error bars show the minimum and maximum values. Sample sizes were the following: Cx36-EGFP: n = 45; Cx36-EGFP and Cav-1-HA: n = 48. (C) Topological representation of Cx36 and Cav-1 structures. Unlike Cav-1, Cx36 possesses two extracellular loops which can undergo cell surface biotinylation. The image was created with BioRender.com. (D) Cell surface

biotinylation assay displaying the effect of Cav-1 on levels of Cx36 at the membrane. Total cell lysates (Input) show expression of both Cx36 and Cav-1. The streptavidin pull-down fractions (Biotinylation) show that membrane levels of Cx36 were depleted in cells double transfected with Cav-1. Treatment with Dynasore restored membrane levels of Cx36 to baseline. Anti-HIS and anti-HA antibodies were used to detect Cx36 and Cav-1 proteins, and an anti-ß-actin antibody was used as an internal control. (E) Cx36 and Cav-1 transfected cells pre and post Dynasore treatment. Increased membrane expression of Cx36 can be observed post treatment. Scale bar: 5 µm. (F) FRET efficiencies of Neuro 2a cells transfected with Cx36 and Cav-1 with and without Dynasore treatment. The threshold of 1.7% (equals to 10 nm) is represented by the dotted line. Error bars show the minimum and maximum values. Sample sizes were the following: Cx36-ECFP + Cav-1-DsRed: n = 55; Dynasore: n = 64. Mann-Whitney U (two tailed) significance test, *p < 0.05.

3.4. Discussion

Connexins have a short half-life of only a few hours (Fallon & Goodenough, 1981; Laird et al., 1991; H. Y. Wang et al., 2015), suggesting that efficient mechanisms must exist to control and facilitate on-demand genesis and removal from gap junctions. A previous study identified the lipid raft protein Cav-1 (A. L. Schubert et al., 2002) as a candidate involved in the dynamic turnover of several connexins, including Cx36. Here, we employed Neuro 2a cells to characterize the interaction between Cx36 and Cav-1 further. CoIP and FRET analysis showed the interaction between both proteins. Various microscopy techniques, coupled with pharmacological interference, determined the role of Cav-1 in mediating endocytosis of Cx36.

Connexins undergo internalization through clathrin-mediated endocytosis (Fiorini et al., 2008; Gumpert et al., 2008; Piehl et al., 2007). Entire or partial gap junction plaques are internalized as double-membrane vesicles, termed annular gap junctions or connexosomes (Falk et al., 2009; Jordan et al., 2001). Connexins have also been shown to localize within lipid rafts (A. L. Schubert et al., 2002), suggesting the possibility of internalization through caveolae-dependent endocytosis. Gap junctions are usually much

larger than lipid rafts (Thévenin et al., 2013), and the internalization of entire plaques by this alternative pathway is unlikely. Instead, under normal physiological conditions, connexins destined for degradation are removed from the center of the plaque (Gaietta et al., 2002; Lauf et al., 2002). Endocytosis of Cx36 by a caveolin-mediated pathway might be one of the different pathways used by cells for dynamic control of gap junction mediated communication.

Caveolins have been implicated in the internalization of several different proteins (Hernández-Deviez et al., 2008; J. Liu et al., 2005; Marchiando et al., 2010; Shi & Sottile, 2008; Shigematsu et al., 2003; Sun et al., 2010). Re-expression of Cav-1 in Cav-1 negative cells resulted in increased endocytosis of β1 integrins and fibronectin (Shi & Sottile, 2008). We observed the same effect on Cx36, as Cav-1 overexpression resulted in an increased membrane depletion. Dynasore has been used effectively to inhibit caveolar endocytosis and prevented occludin internalization (Marchiando et al., 2010). Here, Dynasore, an endocytosis inhibitor, counteracted the action of Cav-1.

Some proteins, including glutamate transporters, rely on Cav-1 for both endocytosis and exocytosis (González et al., 2007). The disruption of the Cav-1 function has been shown to cause intracellular retention and accumulation of glycosylphosphatidylinositol-linked proteins, angiotensin II type 1 receptor, and dysferlin (Hernández-Deviez et al., 2006; Sotgia et al., 2002; Wyse et al., 2003). Dysferlin is endocytosed rapidly in cells lacking Cav-1, signifying that Cav-1 is required for dysferlin's retention at the cell surface (Hernández-Deviez et al., 2008). In the case of Cx36, Cav-1 is not required for the trafficking to the cell surface, suggesting that alternative

mechanisms facilitate exocytic transport. The interaction of Cx36 with tubulin is an example of this process (Brown et al., 2019).

Caveolin-1 has also been suggested to function as negative regulators of caveolae-dependent endocytosis (Hernández-Deviez et al., 2008; Le et al., 2002; Nabi & Le, 2003). However, this seems to be the mechanism for cell lines expressing stable levels of Cav-1. Cell lines with limited Cav-1 expression tend to show the opposite effect. In 293T cells, Cav-1 expression is below the detectable levels, and Cav-1 overexpression leads to an increased turnover of the TGF-β receptor (Di Guglielmo et al., 2003). Like 293T, Neuro 2a cells do not express detectable levels of Cav-1 (Gorodinsky & Harris, 1995; Scherer et al., 1997). Our results also indicate increased endocytosis with Cav-1 overexpression. This evidence suggests that Cav-1 is a positive regulator of Cx36 endocytosis in Neuro 2a cells.

Both Cx36 and Cav-1 co-localized more efficiently with the Golgi apparatus than with ER. Further, the interaction between the two proteins was inhibited with BFA. BFA is widely used as an inhibitor of transport between ER and Golgi as it leads to Golgi disassembly (Misumi et al., 1986). However, BFA has also been shown to block the transport function of COPI vesicles (Peyroche et al., 1999), which are known to be involved in the retrograde recycling transport from Golgi to ER (Springer et al., 1999). Analogous to the Golgi-ER fusion, the trans-Golgi network (TGN) fuses with the endosomal recycling system upon BFA addition (Lippincott-Schwartz et al., 1991). TGN-endosome fusion impairs trafficking from endosomes, and the vesicles are retained in this compartment. FRET efficiency reduction between Cx36 and Cav-1 upon BFA incubation indicated that the proteins are retained in endosomes and are unable to interact in the

Golgi apparatus during the retrograde pathway. The interaction was not fully abolished, as Cx36 and Cav-1 are likely interacting in the retained compartment or are interacting at the sites unaffected by BFA, such as vesicles leaving the membrane.

We also determined that the interaction between Cx36 and Cav-1 is calcium-dependent. Ionomycin raises intracellular calcium levels (Morgan & Jacob, 1994), and such conditions are typically found during synaptic activity in neurons (Gamble & Koch, 1987). Specifically for Cx36, Ionomycin significantly increases the extent of the “run-up” and thus increases its conductance (Del Corsso et al., 2012). Interestingly, CaM is able to interact with Cx36 only when intracellular calcium levels are elevated (Siu et al., 2016). A similar mechanism is indicative of Cx36 interaction with Cav-1, as the interaction levels increase with a rise in intracellular calcium. An influx of calcium has been shown to regulate intracellular transport. Also, the speed of both endocytosis and exocytosis is tightly controlled by intracellular calcium levels (Sankaranarayanan & Ryan, 2001). Specifically, in retinal bipolar cells, where Cx36 is highly expressed (Han & Massey, 2005), calcium influx selects the fast mode of endocytosis at the synaptic terminals (Neves et al., 2001). On the contrary, the application of BAPTA leads to membrane retrieval by a slower mechanism. Dynamin and synaptophysin, critical regulators of endocytosis, have been shown to interact in the presence of high concentrations of calcium (Daly et al., 2000). Their interaction is indicative of a rapid and specialized mechanism of endocytosis. This is consistent with our results and supports that Cav-1 is a mediator of rapid endocytosis of Cx36 (**Supplementary Figure 3.1A**).

The principal findings of this research provide insights into the life cycle of Cx36, specifically the regulation of its trafficking mechanisms. They highlight the role of Cav-1

in rapid, clathrin-independent endocytosis of Cx36 by maintaining the pool of releasable vesicles contributing to the dynamic functions of this connexin.

3.5. Supplementary Figures

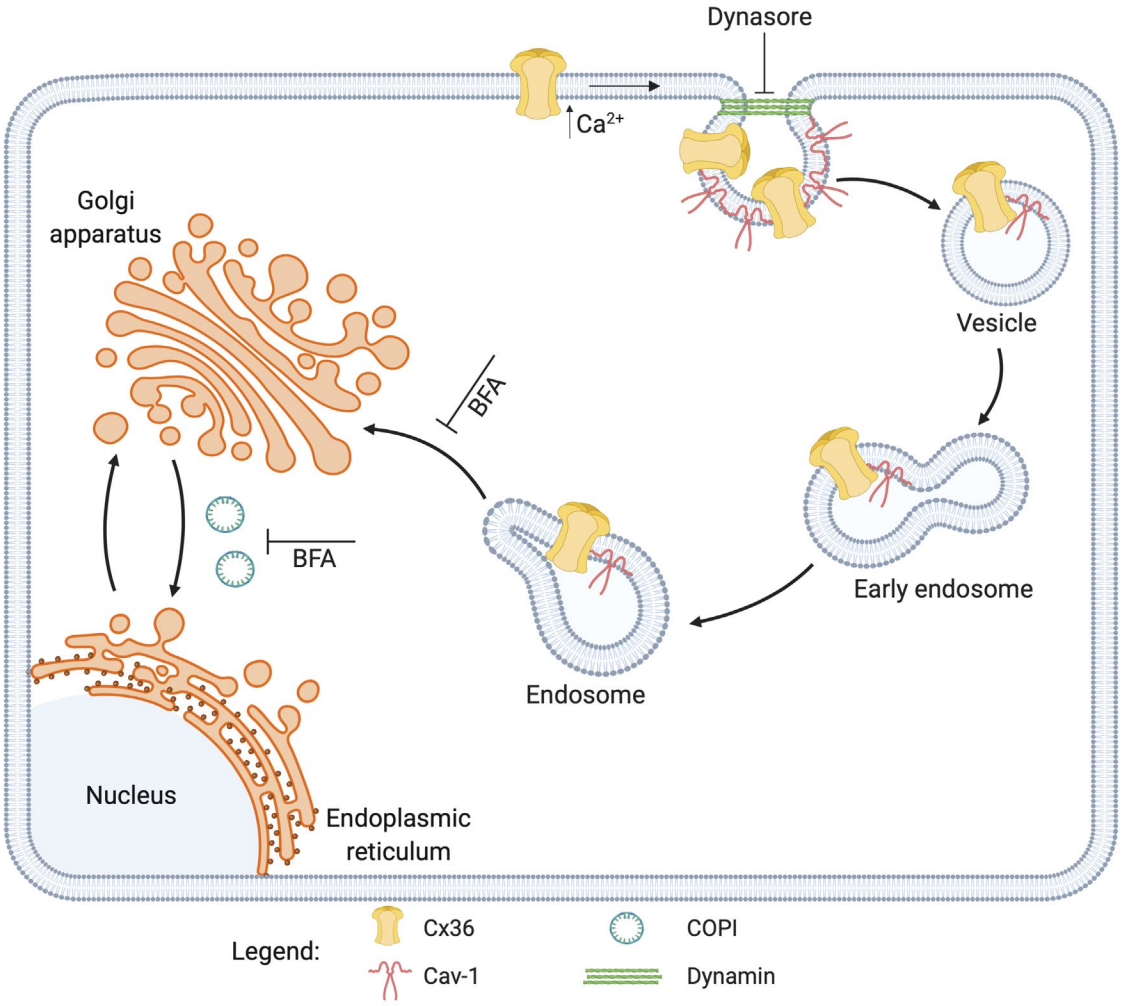

Supplementary Figure 3.1. Schematic representation showing caveolin-dependent endocytosis pathway of Cx36. An influx of calcium (Ca^{2+}) enhances the interaction between Cx36 and Cav-1 and triggers endocytosis of Cx36. Pharmabiotic agent dynasore blocks dynamin and thus endocytosis at the early membrane invagination. Brefeldin A (BFA) blocks transport between endosomes and Golgi apparatus and the retrograde transport from Golgi to endoplasmic reticulum. Both agents show a decrease in the interacting population of Cx36 and Cav-1 suggesting that both proteins interact at various stages of the endocytic pathway. The image was created with BioRender.com.

Chapter 4. Heterotypic and Heteromeric Oligomerization Capabilities of Cx36/Cx35b and Cx27.5

4.1. Introduction

Gap junction channels provide a direct connection between adjacent cells by enabling the exchange of small molecules. Gap junctions are composed of connexin proteins, and different connexins have been shown to form channels with different permeability and gating characteristics (Stauffer & Unwin, 1992). Moreover, gap junction channels are known to contain more than one connexin isoform (Cottrell & Burt, 2005; Koval, 2006). These connexin channels are referred to as heterotypic when two hemichannels consisting of two different isoforms dock to each other. When each hemichannel is composed of two or more different types of connexin subunits, the connexin channels are referred to as heteromeric. These variabilities in the oligomerization allow for the formation of unique channels with distinctive gating abilities that could not be achievable with single connexin isoform channels. Moreover, not all connexins are compatible to form heteromeric or heterotypic channels, further enabling a network of specific interconnected cells.

The retina is a highly synchronized and interconnected tissue where gap junctions play a crucial role (J. O'Brien & Bloomfield, 2018). Different heteromeric and heterotypic gap junctions allow for specialized connections between different cell types. Cx36 is a major neuronal connexin and has been shown to express in a multitude of cells in the retina, such as cones (Feigenspan et al., 2004; E. J. Lee et al., 2003; J. O'Brien et al., 2004; J. J. O'Brien et al., 2012; J. Zhang & Wu, 2004), bipolar (Arai et al., 2010; Feigenspan et al., 2004; Han & Massey, 2005; J. O'Brien et al., 2004), amacrine

(Feigenspan et al., 2001; Mills et al., 2001), and ganglion cells (Degen et al., 2004; Hidaka et al., 2002; Hoshi & Mills, 2009; T. Schubert et al., 2005).

However, thus far, Cx36 hasn't shown an ability to hetero-oligomerize or dock with other connexins. Cx27.5 is a novel connexin that has been discovered in the zebrafish retina (Dermietzel et al., 2000). Cx27.5 can form heterotypic channels with Cx44.1 and Cx55.5, and curiously these channels show distinct features from the homotypic Cx27.5 channels. Cx27.5 is expressed in ganglion cells as well as cells of the inner nuclear layer, such as amacrine cells. Because of the shared localization between Cx36 and Cx27.5, the ability to form heteromeric and heterotypic channels between these proteins is of significant interest.

The heteromeric and heterotypic compatibility of mouse Cx36 and Cx35b (a zebrafish orthologue of Cx36) (A. C. Miller et al., 2017) with zebrafish Cx27.5 was explored in the Neuro 2a cell line. Förster Resonance Energy Transfer Analysis (FRET) and co-immunoprecipitation (CoIP) were used to prove the interaction of Cx36/Cx35b with Cx27.5. Membrane interaction was confirmed via a combination of cell surface biotinylation and co-immunoprecipitation assays. Membrane and intracellular trafficking dynamics were assessed via Total Internal Reflection Fluorescence (TIRF) and Fluorescence Recovery After Photobleaching (FRAP). Functional properties of the heteromeric channels were assessed with dye uptake and dye transfer assays. Immunohistochemistry analysis was used to explore the co-localization of Cx35b and Cx27.5 in the zebrafish tissue. Our results suggested that Cx35b and Cx27.5 form mobile heteromeric channels that assemble into more open conformation, allowing for increased dye uptake and transfer. These results further supported the notion that the potential for

compatible heteromeric channel formation likely shapes the functional connectivity and plasticity of the retinal circuits.

4.2. Results

4.2.1. Cx27.5 and Cx36 co-localize and interact in Neuro 2a cells

To investigate whether Cx36 and Cx27.5 co-localize in Neuro 2a cells, cells were double transfected with Cx36-DsRed and Cx27.5-EGFP and imaged 48 hr post-transfection. Cx36 and Cx27.5 co-localized in the intracellular compartments (**Figure 4.1A**, arrows).

Neuro 2a cells were then double transfected with Cx36-DsRed and Cx27.5-EGFP to investigate whether these two proteins are in close proximity via FRET. FRET efficiency above the threshold of 1.07% signified that proximity between two proteins is less than 10nm, and thus these proteins are close enough to interact with each other (**Figure 4.1B**). Like other Cx proteins, Cx36 monomers oligomerize into hexamers, and thus Cx36-Cx36 pair served as a positive control with a FRET efficiency value of 9.43 ± 1.18 (n = 28). Cells transfected with fluorescent tags alone served as a negative control. EGFP-DsRed pair displayed the FRET efficiency value of 0.18 ± 0.05 (n = 30). FRET efficiency between Cx36-DsRed and Cx27.5-EGFP pair was 3.01 ± 0.34 (n = 53) and was significantly different from the negative control group ($p < 0.0001$). This result proved that the two proteins were close enough to interact with each other.

To confirm the interaction between Cx36 and Cx27.5, a CoIP assay was performed. Neuro 2a cells were double transfected with Cx36-HIS and Cx27.5-EGFP, and the HIS antibody was used to pull down the protein complexes. The expression of

the proteins of interest in the lysate (input) and elution fractions was confirmed with western blot analysis (**Figure 4.1C**). The presence of Cx27.5 in the elution fraction, but its absence in the negative control, confirmed the Cx36/Cx27.5 interaction.

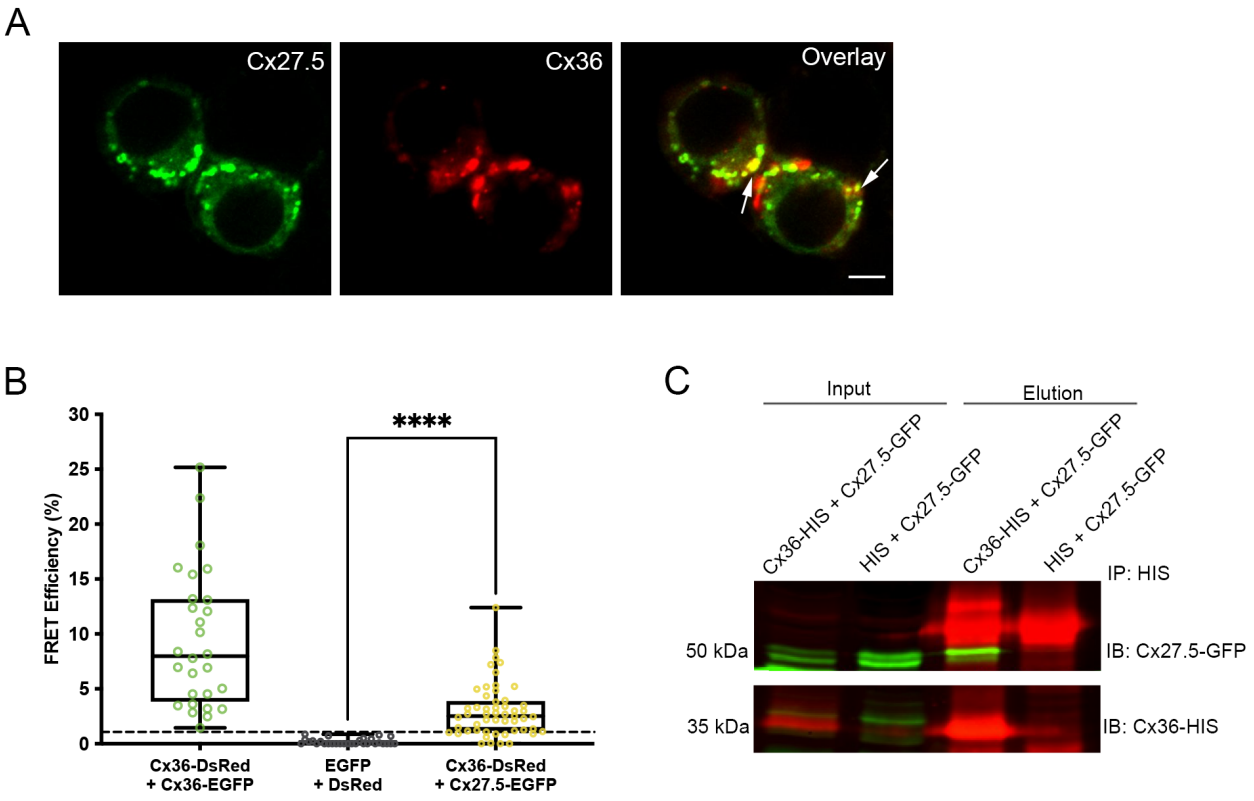

Figure 4.1. Co-localization, Förster Resonance Energy Transfer Analysis (FRET), and co-immunoprecipitation (CoIP) analysis of Cx36 and Cx27.5. (A) Neuro 2a cells transfected with Cx36-DsRed and Cx27.5-EGFP. Cx36 and Cx27.5 displayed co-localization in the intracellular compartments (white arrows). Scale bar: 5 µm. (B) FRET efficiencies. Cx36-EGFP and Cx36-DsRed pair served as a positive control while EGFP and DsRed pair served as a negative control. Cx36-DsRed and Cx27.5-EGFP pair showed high FRET efficiency, signifying that the two proteins are close to one another. The dotted line represents the threshold of 1.07% (equals to 10nm distance between FRET pairs). Error bars show the minimum and maximum values. Sample sizes were the following: Cx36-EGFP + Cx36-DsRed: n = 28; ECFP + DsRed: n = 30; Cx36-DsRed + Cx27.5-EGFP: n = 53. (C) CoIP of Cx36 and Cx27.5. HIS antibody was used to pull down the Cx36-HIS and Cx27.5-EGFP complex. Neuro 2a cells double transfected with HIS and Cx27.5-EGFP served as a negative control. Input lanes (cell lysates) show protein levels prior to the assay. Elution lanes represent eluted protein complexes. Anti-GFP and anti-HIS antibodies detected Cx27.5 and Cx36 proteins, respectively. IP:

immunoprecipitation; IB: immunoblotting. Mann-Whitney U (two-tailed) significance test, **** $p < 0.0001$.

4.2.2. Cx27.5 and Cx35b co-localize and interact in Neuro 2a cells

Because Cx27.5 is a zebrafish connexin, a zebrafish orthologue of mammalian Cx36 was chosen to confirm the interaction and to perform further experiments. Cx35b is one of the four zebrafish orthologues of Cx36 (A. C. Miller et al., 2017). We began the investigation with a co-localization analysis between Cx35b and Cx27.5. Neuro 2a cells were double transfected with Cx35b-DsRed and Cx27.5-EGFP and imaged 48 hr post-transfection. Cx35b and Cx27.5 co-localize in the intracellular compartments as well as at the membrane regions, specifically gap junctions (**Figure 4.2A**, arrows).

Neuro 2a cells were then double transfected with Cx35b-DsRed and Cx27.5-EGFP to investigate whether these two proteins are in close proximity, via FRET. Cx35b-Cx35b pair served as a positive control with a FRET efficiency value of 8.96 ± 0.96 (n = 29) while pair with corresponding fluorescent tags served as a negative control (0.18 ± 0.05, n = 30) (**Figure 4.2B**). As co-localization was observed both intracellularly and at the gap junction, FRET was used to quantify and compare the interaction strength at both compartments. FRET efficiency between Cx35b-DsRed and Cx27.5-EGFP pair in the intracellular compartments was 3.76 ± 0.43 (n = 60), however significantly higher efficiency was detected at the gap junction plaques (7.50 ± 1.69, n = 18, p = 0.0488). FRET efficiency between Cx35b and Cx27.5 pair was significantly higher than the negative control at both compartments (Intracellular: $p < 0.0001$; GJP: $p < 0.0001$).

To confirm the interaction between Cx35b and Cx27.5, a CoIP assay was performed. Neuro 2a cells were double transfected with Cx35b-HIS and Cx27.5-EGFP,

and the HIS antibody was used to pull down the protein complexes. The expression of the proteins of interest in the lysate (input) and elution fractions was confirmed with western blot analysis (**Figure 4.2C**). The presence of Cx27.5 in the elution fraction, but its absence in the negative control, confirmed the Cx35b/Cx27.5 interaction.

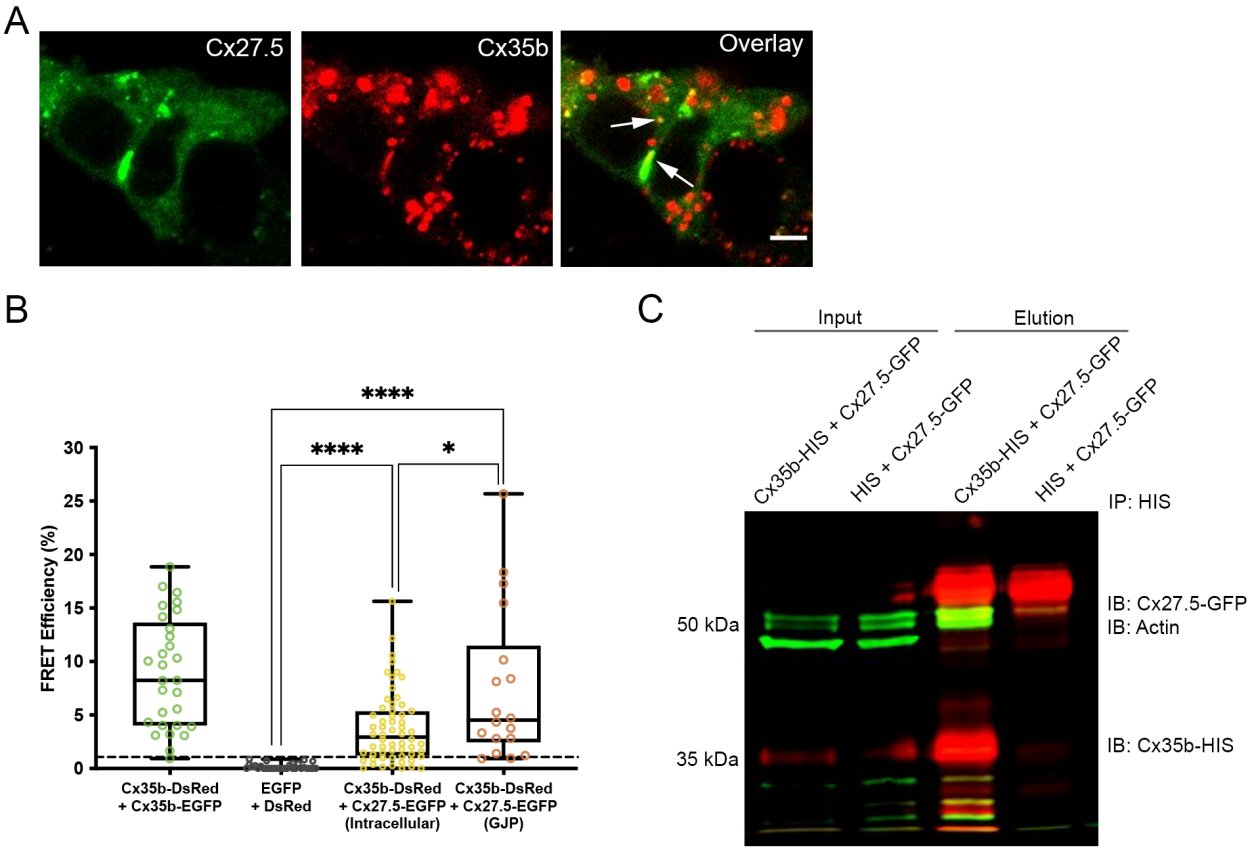

Figure 4.2. Co-localization, Förster Resonance Energy Transfer Analysis (FRET), and co-immunoprecipitation (CoIP) analysis of Cx35b and Cx27.5. (A) Neuro 2a cells transfected with Cx35b-DsRed and Cx27.5-EGFP. Cx35b and Cx27.5 displayed co-localization in the intracellular compartments as well as at the membrane (white arrows). Scale bar: 5 µm. (B) FRET efficiencies. Cx35b-EGFP and Cx35b-DsRed pair served as a positive control while EGFP and DsRed pair served as a negative control. Cx35b-DsRed and Cx27.5-EGFP pair showed high FRET efficiency intracellularly and even higher efficiency at the gap junction plaques (GJP). The dotted line represents the threshold of 1.07% (equals to 10nm distance between FRET pairs). Error bars show the minimum and maximum values. Sample sizes were the following: Cx35b-EGFP + Cx35b-DsRed: n = 29; ECFP + DsRed: n = 30; Cx35b-DsRed + Cx27.5-EGFP (intracellular): n = 60; Cx35b-DsRed + Cx27.5-EGFP (GJP): n = 18. (C) CoIP of Cx35b-HIS and Cx27.5-EGFP. HIS antibody was used to pull down the Cx35b-HIS and Cx27.5-EGFP complex. Neuro 2a cells double transfected with HIS and Cx27.5-EGFP served as a negative control. Input

lanes (cell lysates) show protein levels prior to the assay. Elution lanes represent eluted protein complexes. Anti-GFP and anti-HIS antibodies detected Cx27.5 and Cx35b proteins, respectively. An anti-ß-actin antibody served as a loading control. IP: immunoprecipitation; IB: immunoblotting. Mann-Whitney U (two-tailed) significance test, **** $p < 0.0001$, * $p < 0.05$.

4.2.3. Cx27.5 and Cx35b form mobile heteromeric channels at the membrane

As Cx27.5 and Cx35b co-localize at the membrane (**Figure 4.2A**) and FRET efficiency is significantly higher at the gap junction plaque area (**Figure 4.2B**), we confirmed the membrane interaction of these two proteins by combining cell surface biotinylation and co-immunoprecipitation assays (**Figure 4.3A**). Cells transfected with Cx35b-HIS and Cx27.5-EGFP or HIS and Cx27.5-EGFP were labelled with biotin and subjected to co-immunoprecipitation. Eluted proteins, which contain Cx35b-HIS interacting partners, were further purified with streptavidin to isolate biotinylated proteins localized at the membrane. Both Cx35b and Cx27.5 were detected in the elution fraction and signify a population of Cx35b and Cx27.5 that interact specifically at the membrane. These results suggested that Cx35b and Cx27.5 form heteromeric channels at the membrane.

To assess whether the membrane dynamics of Cx35b and Cx27.5 heteromeric channels differ from homomeric Cx27.5 channels, FRAP microscopy was employed. Gap junctions were used as regions of interest (**Figure 4.3B**). FRAP analysis revealed that fluorescent recovery of the Cx35b-DsRed and Cx27.5-EGFP transfected cells was significantly higher than of DsRed and Cx27.5-EGFP transfected cells (Cx27.5: 9.31 ± 1.39, $n = 17$; Cx27.5 and Cx35b: 13.79 ± 1.67, $n = 22$; $p = 0.0101$) (**Figure 4.3C**). The overall trends in recovery were similar between the two populations (**Figure 4.3D**).

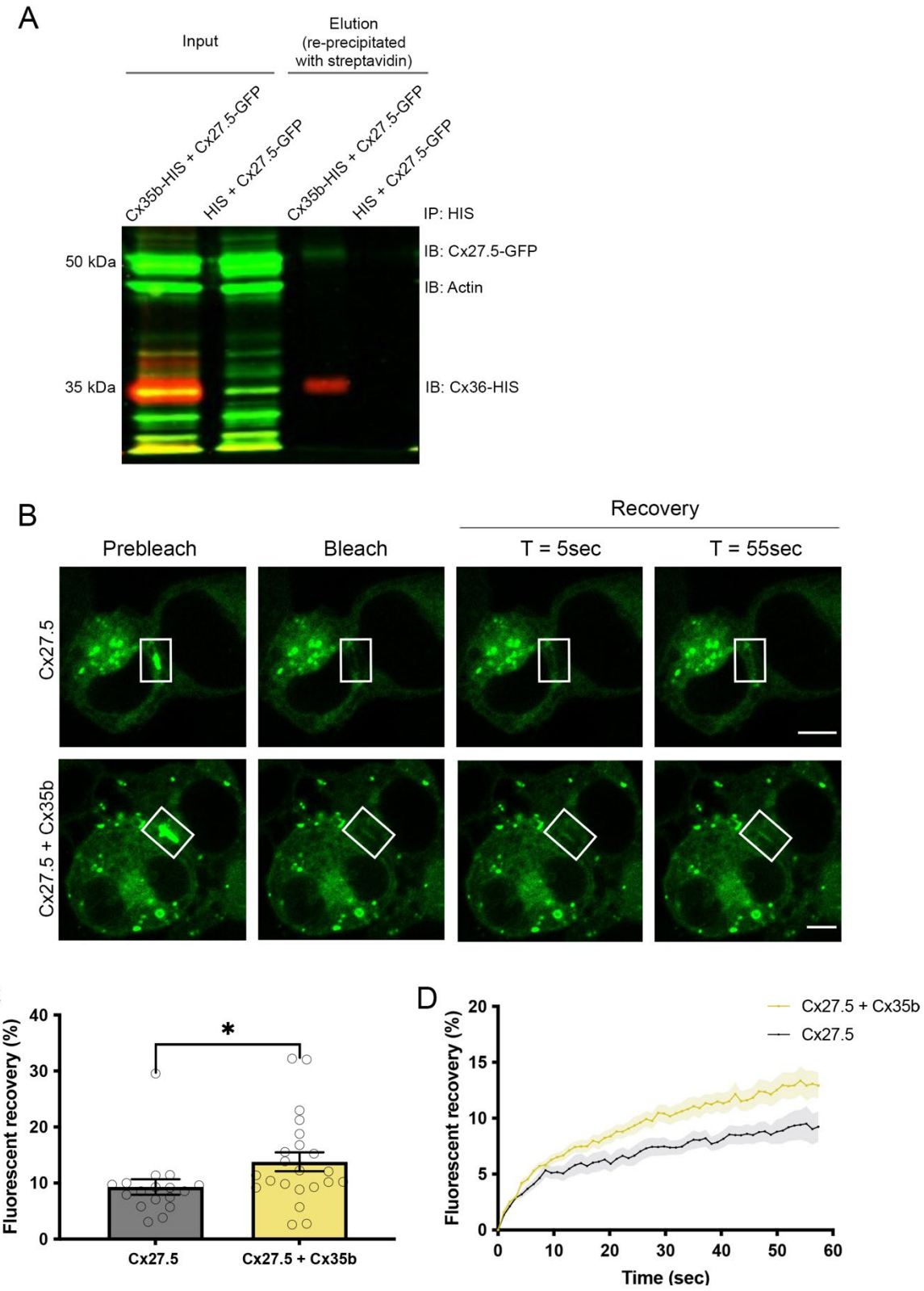

Figure 4.3. Assessment of membrane interaction and dynamics of Cx35b and Cx27.5. (A) Co-immunoprecipitation of biotinylated proteins to isolate interacting partners

of Cx35b at the membrane. Total cell lysates (Input) show expression of both Cx35b and Cx27.5. The streptavidin pull-down fractions (Elution) show both proteins, signifying membrane interaction. Anti-HIS and anti-GFP antibodies were used to detect Cx35b and Cx27.5 proteins, and an anti-ß-actin antibody was used as an internal control. IP: immunoprecipitation; IB: immunoblotting. (B) FRAP analysis of cells transfected with Cx27.5-EGFP and DsRed or Cx27.5-EGFP and Cx35b-DsRed showing selected regions (white rectangles) pre bleaching, immediately after bleaching, and recovery 5 and 55 s post bleaching. Only gap junctions expressing both proteins were selected for the analysis. Scale bar: 5 µm. (C) The bar graph displays the total % fluorescent recovery of the selected gap junction regions, 55 s post bleaching. Error bars show the standard error of the mean. Sample sizes were the following: Cx27.5-EGFP and DsRed: n = 17; Cx27.5-EGFP and Cx35b-DsRed: n = 22. (D) Overall trends in % recovery measured every 5 s, over the 55-s duration. Error bars show the standard error of the mean. Mann-Whitney U (two tailed) significance test, *p < 0.05.

4.2.4. Vesicles containing both Cx27.5 and Cx35b display enhanced dynamics

To explore the intracellular dynamics at a vesicular stage, we examined the quantitative kinetics of Cx35b and Cx27.5 containing vesicles. Neuro 2a cells transfected with Cx27.5-EGFP and Cx35b-DsRed or with Cx27.5-EGFP and DsRed were subjected to TIRF microscopy. Trafficking dynamics of the individual vesicles were recorded over the 1-min duration. Vesicles expressing both proteins were selected for the analysis. Vesicles double transfected with both Cx27.5 and Cx35b demonstrated increased vesicular diameter (Cx27.5: 1.14 ± 0.044, n = 235; Cx27.5 and Cx35b: 1.48 ± 0.049, n = 308; p < 0.0001) (**Figure 4.4A**), track length (Cx27.5: 4.85 ± 0.30, n = 235; Cx27.5 and Cx35b: 7.23 ± 0.48, n = 308; p = 0.0007) (**Figure 4.4B**), and track duration Cx27.5: 26.76 ± 1.37, n = 235; Cx27.5 and Cx35b: 33.58 ± 1.20, n = 308; p < 0.0001) (**Figure 4.4C**). Vesicular speed showed no changes between the two groups (Cx27.5: 0.29 ± 0.024, n = 235; Cx27.5 and Cx35b: 0.32± 0.023, n = 308; p = 0.6277 (**Figure 4.4D**).

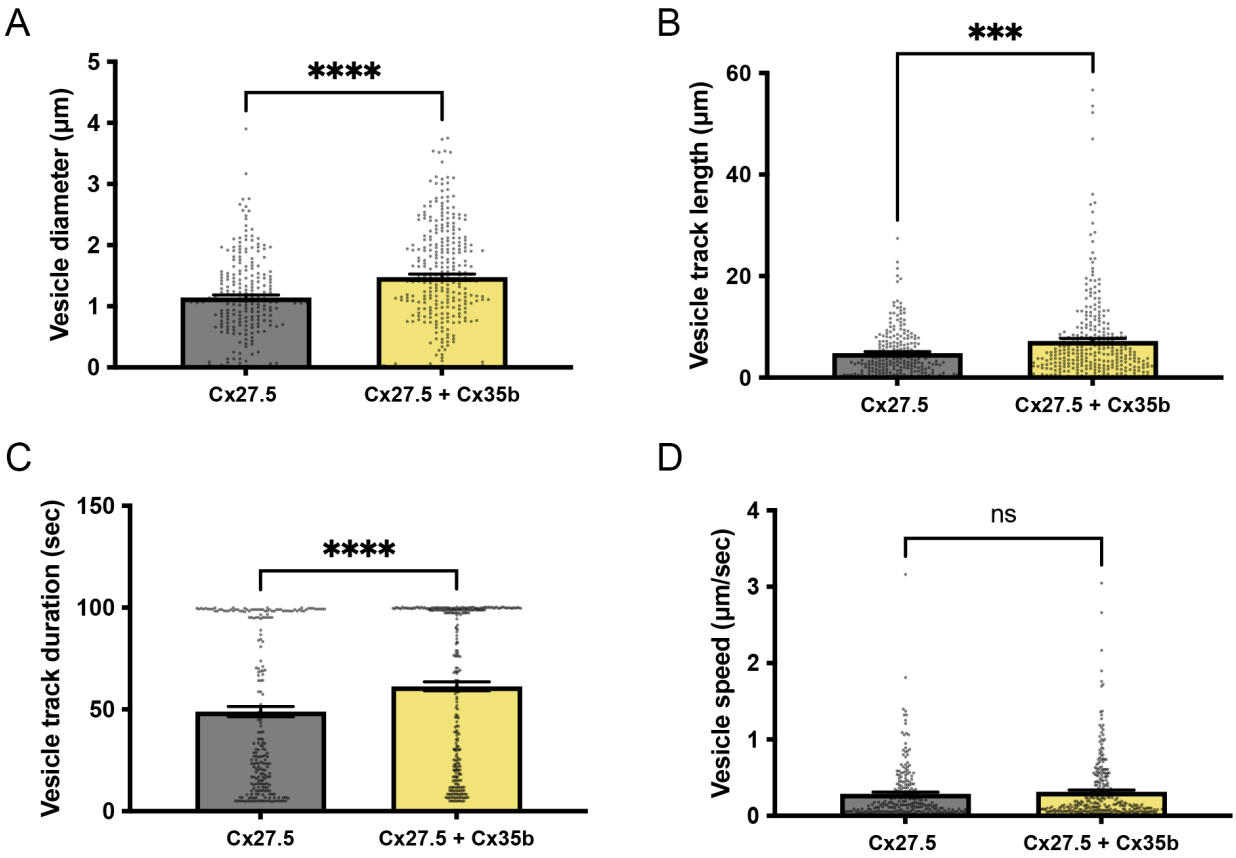

Figure 4.4. Transport dynamics of Cx35b and Cx27.5 vesicles. Total Internal Reflection Fluorescence (TIRF) microscopy was used to resolve the vesicular transport of Cx27.5-EGFP. Vesicles containing both Cx27.5-EGFP and Cx35b-DsRed showed significantly increased (A) diameter, (B) track length, and (C) track duration. (D) The speed of Cx27.5-EGFP and Cx35b-DsRed containing vesicles was not different from vesicles containing Cx27.5-EGFP and DsRed. Vesicle dynamics were measured per second over the course of 1 minute. Error bars show the standard error of the mean. Sample sizes were the following: Cx27.5-EGFP and DsRed: n = 235; Cx27.5-EGFP and Cx35b-DsRed: n = 308. Mann-Whitney U (two-tailed) significance test, ****p < 0.0001, ***p < 0.001, ns—not significant.

4.2.5. Cx27.5 and Cx35b heteromeric channels allow for increased dye transfer

To determine whether the functional profile of heteromeric channels composed of Cx35b and Cx27.5 differs from homomeric Cx27.5 channels, EtBr uptake assays were employed. We first assessed the functional dynamics of heteromeric channels with a dye uptake assay (**Figure 4.5A**). Cells were transfected with Cx27.5-EGFP and ECFP empty

vector or Cx27.5-EGFP and Cx35b-ECFP, and total dye uptake was recorded after 5 minutes of EtBr (10uM) application. Cells transfected with Cx27.5-EGFP and Cx35b-ECFP showed significantly higher increase in the dye uptake when compared to the control group (Cx27.5: 1.87 ± 0.17, *n* = 83; Cx27.5 and Cx35b: 3.32 ± 0.39, *n* = 86; *p* = 0.0001).

We further investigated these differences in channel properties by examining the functionality of gap junction plaques composed of Cx35b and Cx27.5 with EtBr uptake and recovery after photobleaching assay (**Figure 4.5B**). Cells were transfected with Cx27.5-EGFP and ECFP empty vector or Cx27.5-EGFP and Cx35b-ECFP, and fluorescent recovery in the area under the gap junction plaque was measured. This assay allowed us to determine how much dye passes thought the gap junction plaque from the neighboring into the photobleached cell of interest. Cells transfected with Cx27.5-EGFP and Cx35b-ECFP showed significantly higher fluorescent recovery when compared to the control group (Cx27.5: 21.91 ± 3.97, *n* = 45; Cx27.5 and Cx35b: 33.13 ± 4.23, *n* = 40; *p* = 0.0095). Both assays suggest that heteromeric hemichannels, as well as gap junction plaques composed of Cx35b and Cx27.5 assemble into more open conformation, allowing for increased dye uptake and transfer.

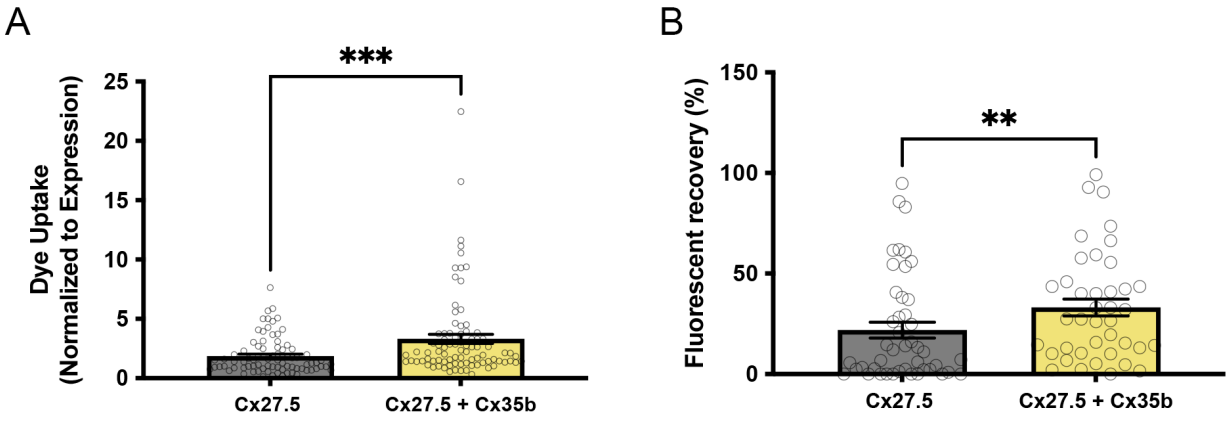

Figure 4.5. Functional profile of heteromeric Cx27.5 and Cx35b hemichannels and gap junctions. (A) Dye uptake quantification of cells transfected with Cx27.5-EGFP and ECFP or Cx27.5-EGFP and Cx35b-ECFP. Values correspond to total dye uptake after 5 minutes of EtBr (10uM) application. Expression of Cx27.5-EGFP was used for normalization. Cells expressing both proteins were selected for the analysis. Sample sizes were the following: Cx27.5-EGFP and ECFP: n = 83; Cx27.5-EGFP and Cx35b-ECFP: n = 86. (B) EtBr uptake and recovery after photobleaching assay analysis of Cx27.5-EGFP and ECP or Cx27.5-EGFP and Cx35b-ECFP expressing cells. Recovery in the region next to gap junction plaque was recorded after photobleaching of the entire cell after 10 minutes of EtBr (10uM) application. The bar graph displays the total % fluorescent recovery of the selected regions, 55 s post bleaching. Only gap junctions expressing both proteins were selected for the analysis. Sample sizes were the following: Cx27.5-EGFP and ECFP: n = 45; Cx27.5-EGFP and Cx35b-ECFP: n = 40. Error bars show the standard error of the mean. Mann-Whitney U (two-tailed) significance test, ***p < 0.001, **p < 0.01, ns—not significant.

4.2.6. Cx27.5 and Cx35b co-localize in the inner plexiform layer of the zebrafish retina

To further examine oligomerization between Cx35b and Cx27.5, we performed immunohistochemistry analysis on 7 dpf zebrafish retina sections (Figure 4.6). Sections were labeled with antibodies against Cx36/35 and Cx27.5. Cx27.5 antibody showed discrete labeling in the inner plexiform layer (IPL). Cx36/35 antibody showed labeling in the outer nuclear layer, outer plexiform layer, inner plexiform layer, and ganglion cell layer. Limited overlap between two proteins was observed in the IPL of the retina.

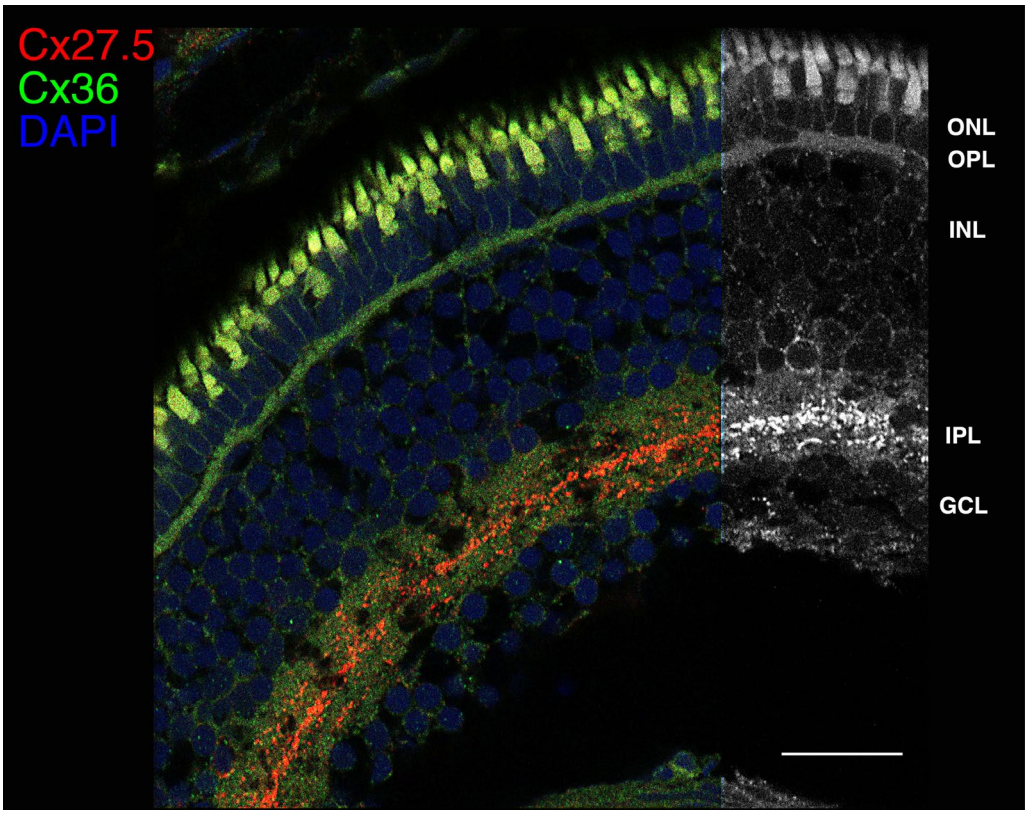

Figure 4.6. Co-localization analysis of Cx27.5 and Cx35b in the larval zebrafish retina. Confocal images of horizontal sections of 7 dpf retina stained by immunohistochemistry with antibodies against Cx27.5 (red) and Cx36/35b (green). The nucleus is stained with DAPI (blue). ONL, outer nuclear layer; OPL, outer plexiform layer; INL, inner nuclear layer; IPL, inner plexiform layer; GCL, ganglion cell layer. Scale bar: 20μm.

4.3. Discussion

Multiple types of connexins are often expressed in the same tissues, which often results in the formation of heteromeric and heterotypic channels. Here, we explored the compatibility of zebrafish Cx35b and Cx27.5. Cx35b is an orthologue of mammalian Cx36, which belongs to the delta class of connexins (A. C. Miller et al., 2017), while Cx27.5 is an orthologue of mammalian Cx32 and belongs to the beta class (Dermietzel et al., 2000; Eastman et al., 2006; McLachlan et al., 2003; Valiunas et al., 2004). It is a general understanding that connexins from different classes do not form heteromeric channels as

they often possess a different heteromeric specificity motif in the transition between the cytoplasmic loop (CL) and third transmembrane (TM3) domains (Largrée et al., 2003; Smith et al., 2012). Cx35b contains a conserved arginine residue (R) at position 180 (referred to as R type connexins) (**Supplementary Figure 4.1A, C**). In contrast Cx27.5 contains a di-tryptophan ("WW") motif at positions 132 and 133 (W type connexins) (**Supplementary Figure 4.1B, C**).

The control of hetero-oligomerization by R and W motifs is most likely indirect and due to the differences in the cellular pathways that connexins follow during oligomerization. R type connexins, specifically Cx43 and Cx46, are stabilized as monomers in the endoplasmic reticulum (ER) and only oligomerize after transport to the trans-Golgi network (TGN) (Koval et al., 1997; Maza et al., 2005; Musil & Goodenough, 1993). It is believed that other R connexins follow the same pathway, but this has yet to be determined. Cx36 has been shown to undergo Golgi mediated trafficking (H. Y. Wang et al., 2015); however, its oligomerization occurs in the ER (Tetenborg et al., 2022), which most likely holds for Cx35b due to the shared homology of the two proteins. Trafficking dynamics of Cx27.5 are not well studied yet but due to its homology to Cx32, it is reasonable to speculate that the two proteins share similar oligomerization pathways. W type connexins like Cx32 are believed to oligomerize in the ER (George et al., 1999; Kumar et al., 1995). The above information suggests that both Cx35b and Cx27.5 share similar oligomerization routes and thus could oligomerize with each other.

The other motif believed to be involved in the heteromeric oligomerization of connexins is located in the N terminus (Largrée et al., 2003). The two positions are referred to as P1 and P2. In position1, connexins of alpha class usually contain a

negatively charged residue such as aspartic acid or glutamic acid, while connexins of class beta contain small non-charged residues like serine or glycine. In position 2, connexins of the alpha class usually contain a polar residue such as lysine, asparagine, glutamine, or glutamic acid, while connexins of class beta contain a small non-charged glycine. Residues 1-10 of β-connexins are predicted to lie within the channel pore, and the N-terminal domain might form the channel vestibule (Largrée et al., 2003). Therefore, the differences in the amino acid residues could lead to the different structural conformation of the N-terminal domain, making the heteromeric assembly unlikely.

Cx27.5, like other class beta connexins, contains a serine residue at position 11 (P1) and glycine residue at position 12 (P2) (**Supplementary Figure 4.1B, C**). Cx35b, belonging to the delta class of connexins, contains different residues to class alpha and beta. Cx35b contains alanine both at position 13 (P1) and at position 14 (P2) (**Supplementary Figure 4.1A, C**). Perhaps small alanine residues of Cx35b provide better compatibility with serine and glycine residues of Cx27.5, unlike amino acids of alpha class, and thus the formation of heteromeric channels between the two proteins is possible. Another study showed that once the N terminal of connexin is truncated, connexins from different classes are able to form heteromeric channels, as shown by their ability to co-immunoprecipitate together (Ahmad et al., 1998). The same didn't hold true when the C terminus was removed. The apparent lack of discrimination between different subunit isotypes observed with the N-terminal-truncated connexin peptides suggests the crucial role of the N terminus in the connexin oligomerization.

While our co-localization and co-immunoprecipitation data pointed to the formation of heteromeric channels composed of Cx27.5 and Cx35, the possibility of heterotypic

channels cannot be ruled out. The heterotypic motif is located in extracellular loop domain two. Cx27.5, like Cx32, belongs to group 1 and possesses a so-called K-N motif with a lysine (K) residue in position 167 and asparagine (N) in position 175 (**Supplementary Figure 4.1B, C**). Group 2 connexins have a histidine (H) residue instead of asparagine. Cx35b, however, has a glutamic acid residue in position 213 and a lysine residue in position 221 and therefore doesn't belong to either group 1 or group 2 (**Supplementary Figure 4.1A, C**). Like 35b, Cx31 also does not belong to a group and has been shown to be compatible with connexins from both group 1 and group 2, including Cx32 (Abrams et al., 2006; Elfgang et al., 1995). Moreover, heterotypic compatibility seems to be more flexible and permits unusual docking interactions. For example, group 1 Cx46 has been demonstrated to be heterotopically compatible with both group 1 (K-N) type connexins (Cx26, Cx32, Cx50) and group 2 (H) connexin (Cx43) (T. W. White et al., 1995). This suggests that the possibility of heterotypic channel formation between Cx35b and Cx27.5 is highly plausible.

Our results showed that channels composed of Cx35b and Cx27.5 are significantly more mobile both intercellularly and at the membrane. Increased dynamics possibly allow for fast delivery to the points of contact when there is demand for these specialized channels. Another interesting aspect was an increased dye uptake and transfer for the heteromeric/heterotypic Cx27.5/Cx35b channels when compared to the homomeric Cx27.5 channels. This is not unexpected as channels that are formed by different connexins often have different conductance and permeability properties (Cottrell & Burt, 2001). The ability to allow more dye through suggests a more open conformation, and thus these channels are likely to possess distinct permeability and conductance features.

Immunohistochemistry analysis showed co-localization of Cx35b and Cx27.5 in the IPL of the retina. IPL is known to be the point of contact for the synapses between amacrine, bipolar interneurons, and the retinal ganglion cells (Euler et al., 2014). Cx27.5 has been previously reported to be expressed in the amacrine cells (Dermietzel et al., 2000), while Cx36 is known to be expressed in bipolar, amacrine, and ganglion cells (J. O'Brien & Bloomfield, 2018). This suggests that the heteromeric or heterotypic Cx35b/Cx27.5 channels are most likely formed between either of these three cell types (**Supplementary Figure 4.2**).

Overall, our data suggested that Cx35b and Cx27.5 oligomerization leads to the formation of specialized gap junction channels that are needed to couple distinct cell types in the inner plexiform layer of the retina. By allowing for the connection between different cell types, heteromeric and heterotypic gap junction channels can shape the plasticity of the electrical circuits in the retina.

4.4. Supplementary Figures

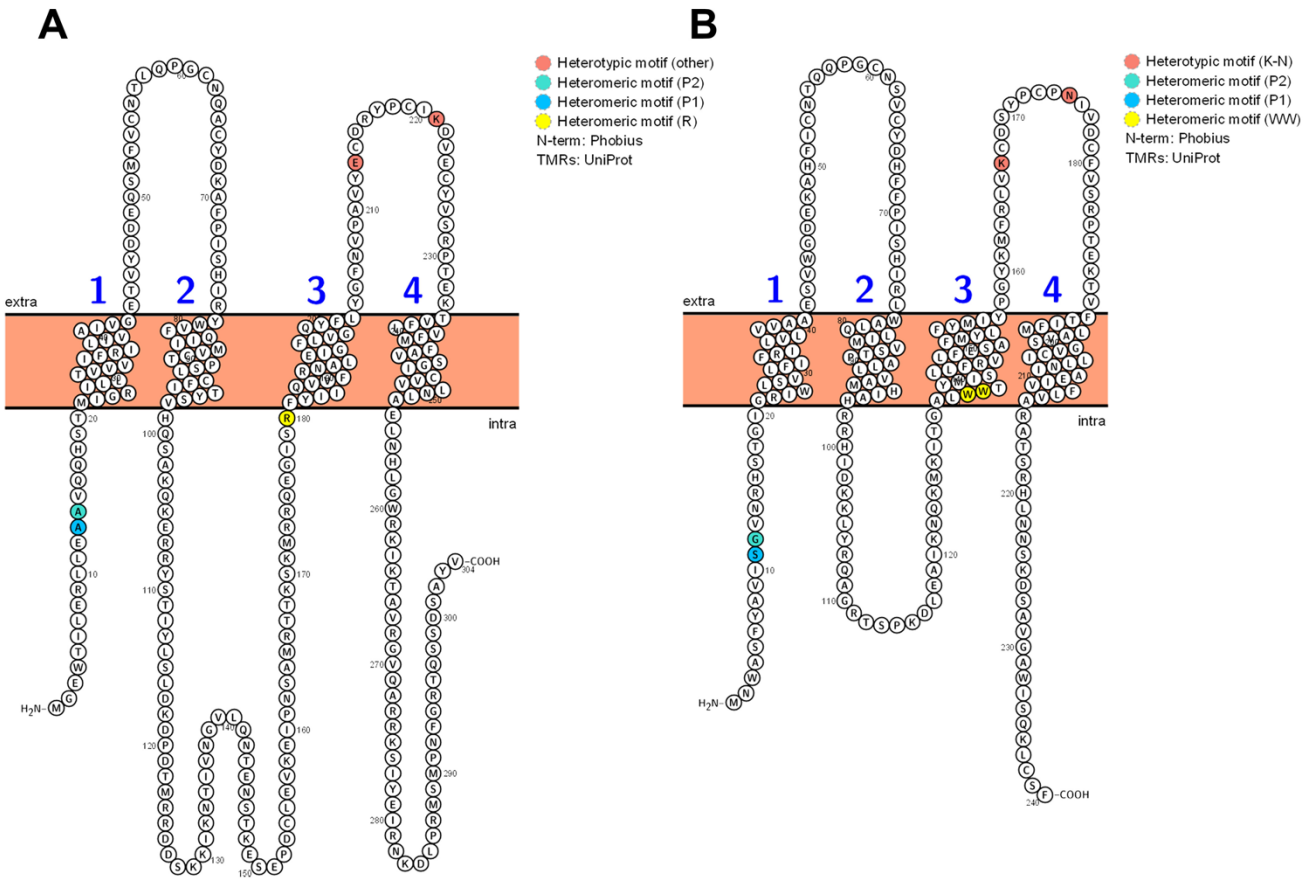

Supplementary Figure 4.1. Heteromeric and heterotypic sequence motifs of Cx35b and Cx27.5. Transmembrane topology of Cx35b (A) and Cx27.5 (B) highlighting critical heteromeric and heterotypic sequence motifs. Images were created with Protter software. (C) Sequence alignment between Cx35b and Cx27.5 highlighting key residues. Heteromeric P1 and P2 motifs are highlighted in blue, heteromeric R and W motifs are highlighted in yellow and heterotypic motifs are highlighted in red. Alignments were performed using Pairwise Sequence Alignment with EMBOSS Needle.

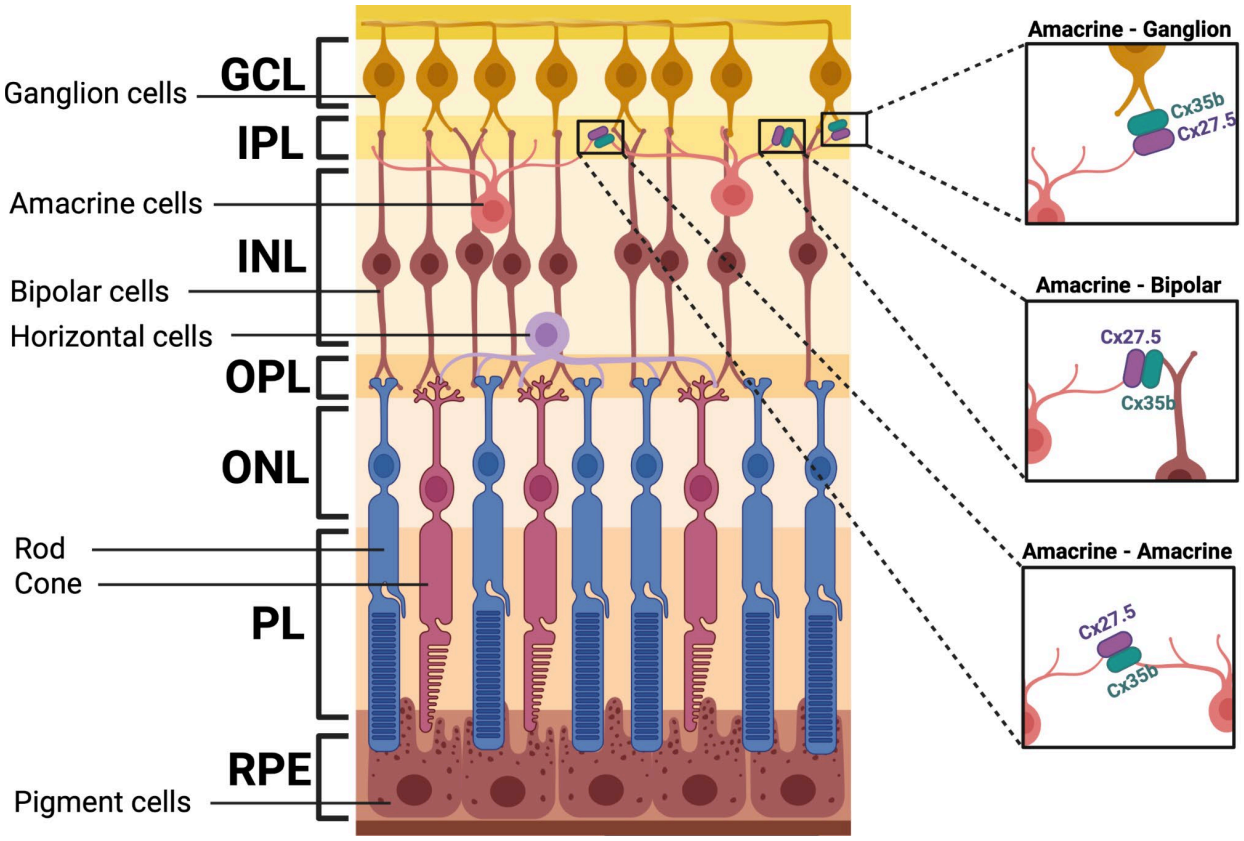

Supplementary Figure 4.2. Schematic of the retinal anatomy, showing potential electrical synapses formed by Cx35b and Cx27.5. The illustration shows key layers of the retina and different cell types contained within each layer on the left. Zoomed-in insets on the right show potential cell to cell connections mediated by Cx35b and Cx27.5 heterotypic channels. The image was created with BioRender.com. GCL: ganglion cell layer; IPL: inner plexiform layer; INL: inner nuclear layer; OPL: outer plexiform layer; ONL: outer nuclear layer; PL: photoreceptor layer; RPE: retinal photoreceptor layer.

Chapter 5. Connexin 27.5 is Critical for Visual Perception and Processing in Zebrafish

5.1. Introduction

Intercellular communication is essential for the behavior coordination of the individual cells. The most widely distributed cell structures involved in cell-to-cell communication are gap junctions. Gap junctions are formed by protein channels that couple neighboring cells and allow for the passage of small molecules and ions. These channels are formed by a family of integral membrane proteins called connexins (Stauffer & Unwin, 1992). Connexin 27.5 (Cx27.5) is a novel isoform that was first identified in the zebrafish retina (Dermietzel et al., 2000). Specifically in the retina, Cx27.5 showed labeling of subpopulations of neurons in the inner nuclear layer and the ganglion cell layer. The overall Cx27.5 expression has been shown to be restricted to the brain, retina, and ear (Chang-Chien et al., 2014; Dermietzel et al., 2000; Zoidl et al., 2008).

Cx27.5 shares homology with both mammalian connexin 26 (Cx26) and connexin (Cx32). Phylogenetic tree analysis places zebrafish Cx27.5 closer to mammalian Cx32 than Cx26 (**Supplementary Figure 5.1A**) even though the sequence similarity is higher between Cx27.5 and Cx26 (72.2%) (**Supplementary Figure 5.1B**) than Cx32 (65.2%) (**Supplementary Figure 5.1C**). Cx27.5 channels display moderate voltage-dependent channels and low conductance (Dermietzel et al., 2000). These properties of Cx27.5 are more similar to those of Cx32 than Cx26, as Cx26 displays weak voltage sensitivity (Barrio et al., 1991) and large conductance (Bukauskas et al., 1995). Mutations in Cx32 are known to lead to the Charcot-Marie-Tooth neuropathy X type 1 (CMTX1) syndrome (Janssen et al., 1997). Cx32 gene *(GJB1)* is X-linked, leading to moderate-to-severe

motor and sensory neuropathy in males with typically mild-to-no symptoms in carrier females. Sensorineural deafness, cases of optic atrophies (Stojkovic et al., 1999), and central nervous system deficits (Hu et al., 2019; Wen et al., 2018) have been reported suggesting that both central and peripheral nervous systems are affected by this disease. The homology between Cx27.5 and Cx32 suggests that these proteins might share a similar functional profile.

To determine the functional significance of the Cx27.5 protein, we employed transcription activator-like effector nucleases (TALEN) to generate a knock-out zebrafish model ($Cx27.5^{-/-}$). A loss of function mutation allowed us to investigate the role of Cx27.5 in zebrafish larvae. Because of the previously identified expression in the brain and sensory organs, like the eye and ear, and homology to the mammalian Cx32, we hypothesized that zebrafish lacking Cx27.5 would exhibit sensory and cognitive deficits.

5.2. Results

5.2.1. TALEN mediated knock-out of Cx27.5

Cx27.5 gene consists of two exons and one intron (**Figure 5.1A**). The beginning of exon 2, which contains a BclI restriction endonuclease recognition sequence, was chosen as a target site for TALEN-mediated mutagenesis. TALEN cRNA pair targeting the Cx27.5 gene was microinjected into one-cell staged embryos at a concentration of 12.5 picograms (pg). DNA sequence analysis confirmed that TALENs generated small deletions ranging between 9 and 25 bp (**Figure 5.1B**). A wild-type (WT) Cx27.5 protein is composed of 254 amino acids with N and C termini (**Figure 5.1C**). A 25 bp deletion resulted in a frameshift which led to a premature stop codon at amino acid 18, and the

majority of the protein is not translated. Fish with this specific mutation were chosen to generate a homozygous knock-out line through rounds of breeding. The restriction fragment length polymorphism test (RFLP) of the genomic DNA of 4 randomly selected Cx27.5-/- fish was used to confirm the loss of the BclI restriction site in the F1 generation (**Figure 5.1D**).

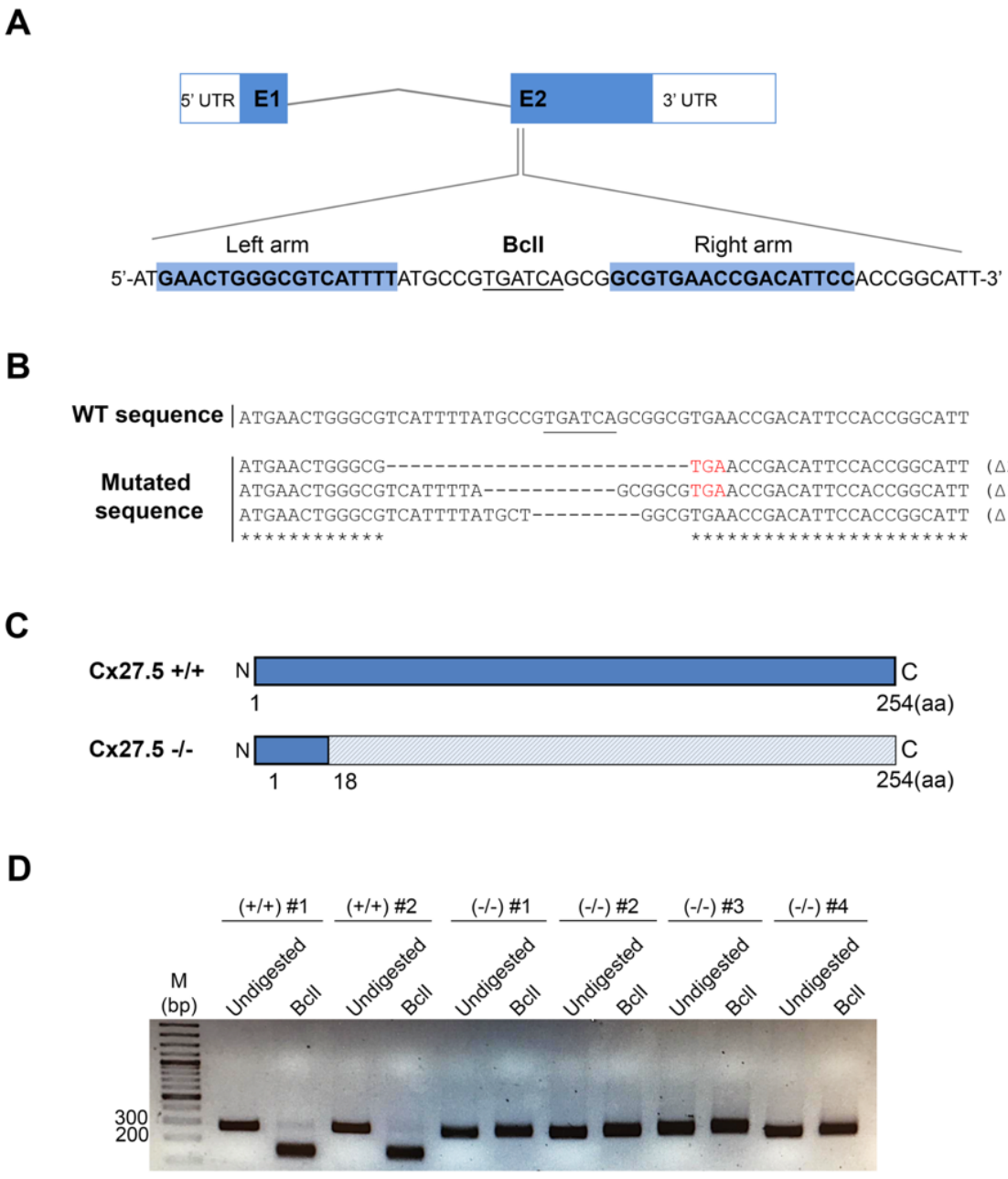

Figure 5.1. Generation of Cx27.5-/- zebrafish with TALENs. (A) The zebrafish Cx27.5 gene contains two exons (E1 and E2). The left and right TALENs sequences are highlighted in blue. The BclI restriction site, which is used as a diagnostic site, is underlined. (B) A sequence alignment of WT and mutated sequences demonstrate 9 to 25 bp deletions. Stop codons are labeled in red. (C) A 25 bp deletion caused a frameshift, which resulted in a premature stop codon at amino acid (aa) 18. (D) The RFLP assay demonstrates the loss of the BclI restriction site in the F1 generation of Cx27.5-/- fish.

5.2.2. Characterization of Cx27.5$^{-/-}$ larvae

To investigate the differences between Cx27.5$^{+/+}$ and Cx27.5$^{-/-}$ larvae, we started by comparing the survival rate between the two groups. The number of live embryos was counted 24 hours post-fertilization and expressed as a percentage to display the survival rate. Cx27.5$^{-/-}$ embryos showed a decreased survival rate when compared to the WT control (Cx27.5$^{+/+}$: 88.22 ± 2.42, n = 13; Cx27.5$^{-/-}$: 20.81 ± 4.81, n = 13, p < 0.0001) (**Figure 5.2A**). To further examine the low survival rate, embryos were observed 4 hours post-fertilization. Cx27.5$^{-/-}$ embryos seemed to arrest their development during the 4-cell stage of the cleavage period, typically observed 1 hour post-fertilization (Kimmel et al., 1995) (**Figure 5.2B**). The control Cx27.5$^{+/+}$ embryos reached the sphere stage of the blastula period, which is expected 4 hours post-fertilization. At 7dpf, the survived Cx27.5$^{-/-}$ larvae looked very similar to their control counterparts, and no substantial anatomic defects were observed (**Figure 5.2C**). However, the body length measurements revelated that Cx27.5$^{-/-}$ larvae are shorter than control larvae (Cx27.5$^{+/+}$: 4.31 ± 0.049, n = 12; Cx27.5$^{-/-}$: 3.96 ± 0.074, n = 13 p = 0.0006.) (**Figure 5.2D**). Next, the expression levels of Cx27.5 mRNA were compared between the knock-out and control groups. No significant reduction in Cx27.5 mRNA levels was observed in the Cx27.5$^{-/-}$ larva, signifying that a 25 bp deletion did not lead to the nonsense-mediated mRNA decay (p = 0.361) (**Figure 5.2E**).

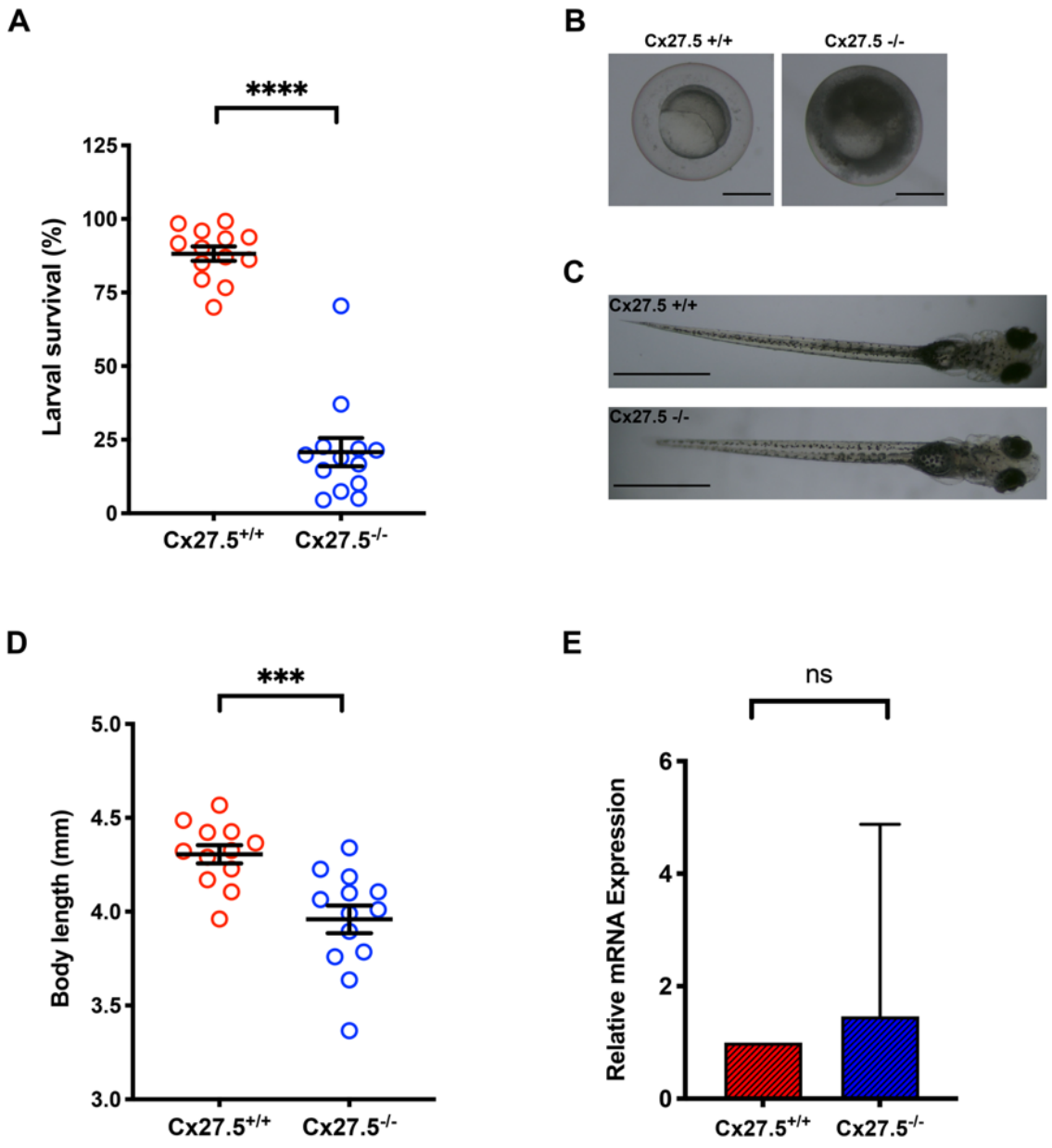

Figure 5.2. Characterization of Cx27.5-/- larvae. (A) Survival rate comparison between Cx27.5+/+ and Cx27.5-/- larvae 24 hours post-fertilization. Sample sizes were the following: Cx27.5+/+: n = 13, Cx27.5-/-: n = 13. (B) Cx27.5+/+ and Cx27.5-/- zebrafish embryos 4 hours post-fertilization. Scale bar = 0.5 mm. (C) Cx27.5+/+ and Cx27.5-/- larvae at 7 dpf showing regular morphology. Scale bar = 1 mm. (D) The head-to-tail body length measurement of Cx27.5+/+ and Cx27.5-/- larvae at 7 dpf. Sample sizes were the following: Cx27.5+/+: n = 12, Cx27.5-/-: n = 13. (E) qRT-PCR analysis of Cx27.5 expression in Cx27.5-/- and control larvae at 7 dpf. 18s rRNA was used as the reference gene. Cx27.5+/+ was used as the control group. Data were collected in three independent experiments in triplicate for each gene. Error bars show the standard error of the mean. ***p < 0.001, ****p < 0.0001, ns – not significant.

5.2.3. Cx27.5 mRNA expression in adult and larvae zebrafish tissues

To determine the physiological importance of the Cx27.5 protein, we first assessed its mRNA expression pattern. For this purpose, various tissues of adult zebrafish were collected and subjected to mRNA extraction followed by qPCR. In line with previous reports (Chang-Chien et al., 2014; Zoidl et al., 2008), Cx27.5 expression was detected in the retina, and this tissue was used as a reference condition (normalized to 1) (**Figure 5.3A**). Cx27.5 expression levels were most prominent in the optic tectum and mid/hindbrain region (Optic tectum: $p < 0.000$; Mid/hindbrain: $p < 0.000$). Minimal Cx27.5 expression was detected in the heart and liver (Heart: $p = 0.006$; Liver: $p < 0.000$).

Next, the temporal expression pattern of Cx27.5 was assessed (**Figure 5.3B**). Cx27.5 mRNA levels were measured in 30 whole larva aged between 1 and 7dpf. Expression at 1 dpf was used as a reference condition. Cx27.5 expression was minimal at 2 pdf ($p = 0.936$) and significantly increased from 3 dpf (3 dpf: $p = 0.003$; 4 dpf: $p = 0.007$; 5 dpf: $p = 0.017$; 6 dpf: $p = 0.013$). The highest expression was observed at 7pdf ($p < 0.000$).

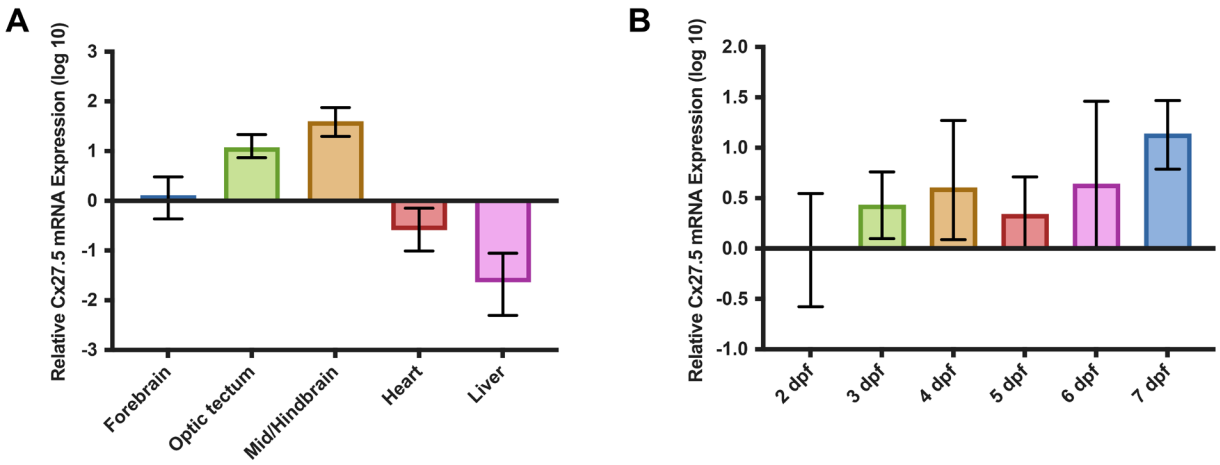

Figure 5.3. Spatiotemporal expression of Cx27.5 mRNA in zebrafish. (**A**) Real- time qPCR analysis of Cx27.5 mRNA expression in WT adult zebrafish tissues. Total RNA was isolated from different tissues and used for cDNA synthesis. Retinal Cx27.5 expression was used as a reference condition and was normalized to 1. 18s rRNA was used as the reference gene (**B**) Real-time qPCR analysis of Cx27.5 mRNA expression in zebrafish larva collected from 1 to 7 dpf. Total RNA was isolated from 30 whole larvae at different ages and used for cDNA synthesis. Larval expression at 1 dpf was used as a reference condition and was normalized to 1. 18s rRNA was used as the reference gene. Data was collected in three independent experiments in triplicate for each gene. Error bars show the standard error of the mean.

5.2.4. Cx27.5 protein expression in the retina and brain of larvae zebrafish

Protein expression of Cx27.5 in larvae showed to be most prominent in the forebrain region and the inner plexiform layer of the retina (IPL) (**Figure 5.4A**). While the antibody staining wasn't completely abolished, Cx27.5$^{-/-}$ larvae showed a marked reduction in expression. With peptide control, the specific Cx27.5 expression was lost, and only dispersed background staining can be observed, which proves the specificity of antibody binding (**Figure 5.4B**). To narrow down the specific cell types that express Cx27.5 in the IPL of the retina, we performed double labeling immunohistochemistry experiments with PSD-95 and parvalbumin markers. PSD-95 is found at postsynaptic sites of bipolar cells in the IPL (Massey, 1990; Massey & Redburn, 1987). No co-localization of Cx27.5 and PSD-95 suggests that bipolar cells do not express Cx27.5 (**Figure 5.4C**). Another marker we employed was parvalbumin. A parvalbumin antibody was used as a marker for the subtype of glycinergic amacrine cells called AII amacrine cells (Haverkamp & Wässle, 2000; Rice & Curran, 2000; Yeo et al., 2009). The double labeling with Cx27.5 and parvalbumin antibody showed no co-localization, suggesting that Cx27.5 is not expressed by parvalbumin-positive AII amacrine cells (**Figure 5.4D**).

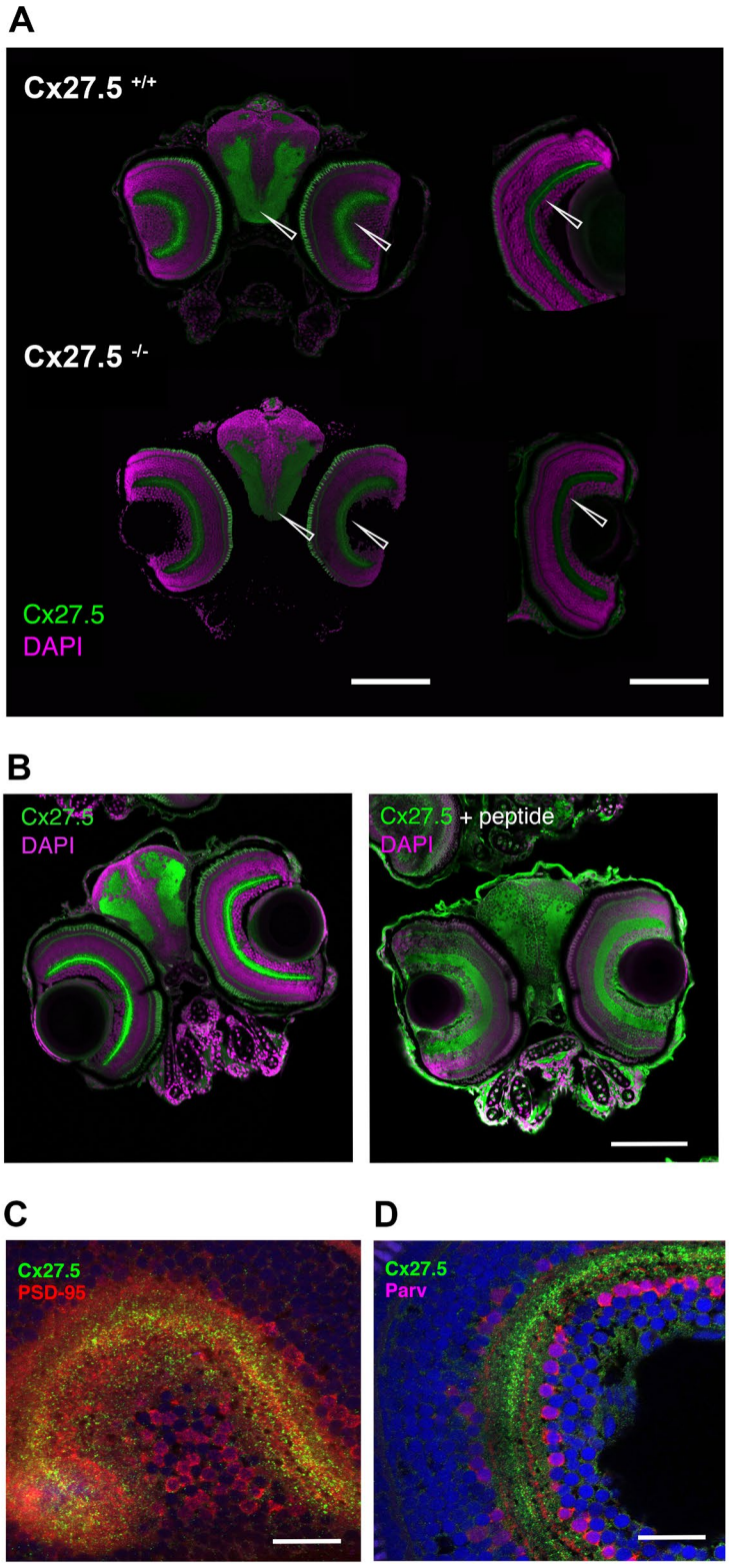

Figure 5.4. Expression of Cx27.5 protein in zebrafish larvae. Immunohistochemistry analysis of Cx27.5 expression in 7dpf larvae. (**A**) The section shows Cx27.5 expression in the forebrain and retina (green). Arrows point to notable expression in the forebrain

region and inner plexiform layer of retina. Cx27.5-/- larvae show a reduction in Cx27.5 expression. The nucleus is stained with DAPI (purple). Scale bar: 100μm. (**B**) Specific Cx27.5 expression pattern is lost upon addition of an antibody peptide control. The nucleus is stained with DAPI (purple). Scale bar: 100μm. Co-expression analysis of Cx27.5 (green) with PSD-95 (red) (**C**) and parvalbumin (purple) (**D**). The nucleus is stained with DAPI (blue). Scale bar: 20μm.

5.2.5. Loss of Cx27.5 alters freely swimming behavior in the dark

To determine whether any major sensory and motor deficits are present in the $Cx27.5^{-/-}$ fish, locomotion tracking experiments were performed. Larvae were transferred into a 24 well plate at 7 dpf and their movements were tracked for a total of 1 hour under light (30% light intensity) or dark (0% light intensity) conditions. Under the light condition, the total distance traveled of $Cx27.5^{-/-}$ was no different from the control $Cx27.5^{+/+}$ ($Cx27.5^{+/+}$: 1114 ± 65.93, n = 44; $Cx27.5^{-/-}$: 1111 ± 64.90, n = 43, p = 0.7902) (**Figure 5.4A, B**). No differences were observed in the swimming speed between the two groups ($Cx27.5^{+/+}$: 22.87 ± 1.29, n = 44; $Cx27.5^{-/-}$: 22.12 ± 1.37, n = 43, p = 0.5179) (**Figure 5.4C, D**). However, under complete darkness $Cx27.5^{-/-}$ fish traveled a shorter distance ($Cx27.5^{+/+}$: 689.8 ± 61.05, n = 44; $Cx27.5^{-/-}$: 503.5 ± 35.61, n = 43, p = 0.0194) (**Figure 5.4E, F**) and showed a decrease in their speed ($Cx27.5^{+/+}$: 17.20 ± 1.372, n = 44; $Cx27.5^{-/-}$: 12.32 ± 0.5779, n = 43, p = 0.0030) (**Figure 5.4G, H**) when compared to the $Cx27.5^{+/+}$ control.

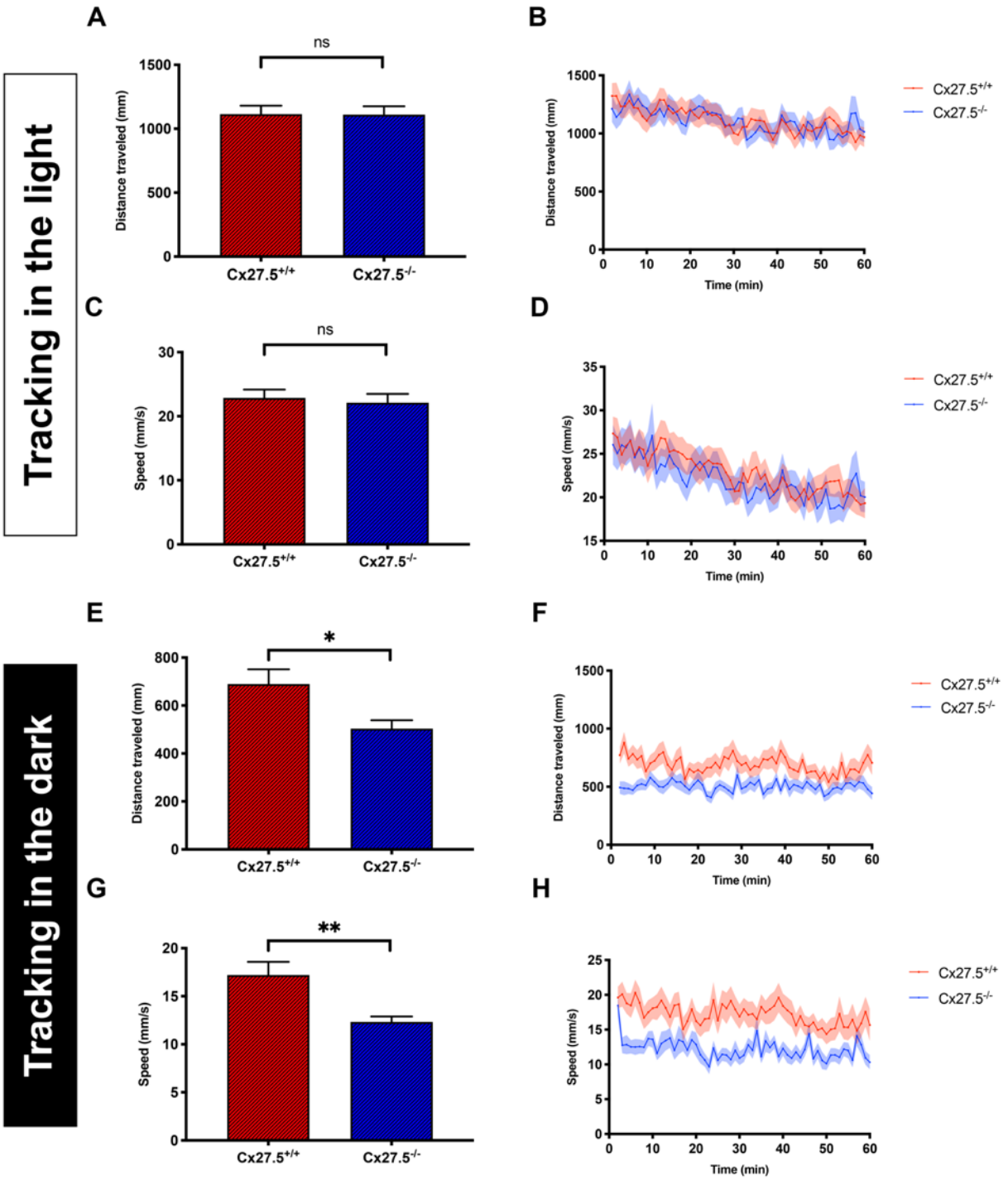

Figure 5.5. Locomotion activity of Cx27.5$^{-/-}$ larvae under light and dark conditions. Total distance traveled and mean speed of 7dpf Cx27.5-/- and Cx27.5+/+ larvae (**A, C**) with their corresponding experimental traces (**B, D**) tracked under light condition (30% light intensity). Total distance traveled and mean speed of 7dpf Cx27.5-/- and Cx27.5+/+ larvae (**E, G**) with their corresponding experimental traces (**F, H**) tracked under dark condition (0% light intensity). Fish were tracked for one hour, and data were collected

every minute. Sample sizes were the following: Cx27.5+/+: n = 44, Cx27.5-/-: n = 43. Error bars show the standard error of the mean. *p < 0.05, **p < 0.01, ns - not significant.

5.2.6. Cx27.5-/- larvae exhibit hypersensitive visual-motor response (VMR)

Because the aforementioned results showed differences in locomotion activity between the two groups only during the dark cycle, we decided to further explore the effect the light stimulus has on Cx27.5$^{-/-}$ larvae. For this purpose, we employed a modified VMR assay (Emran et al., 2008). 7 dpf larvae were transferred into a 48 well plate, and their response to the abrupt light ON (100% light intensity) or light OFF (0% light intensity) condition was tested. The Cx27.5$^{-/-}$ larvae had the same baseline levels of activity as Cx27.5$^{+/+}$ control; however, they seem to exhibit a hyperreactivity response to the light transitions (**Figure 5.5A**). When the lights were changed from light OFF to light ON Cx27.5$^{-/-}$ larvae showed an increase in their activity when compared to the control (Cx27.5$^{+/+}$: 0.433 ± 0.023, n = 80; Cx27.5$^{-/-}$: 0.599 ± 0.019, n = 120, p <0.0001) (**Figure 5.5B, C**). On the contrary, the activity of Cx27.5$^{-/-}$ larvae was no different from the control when lights were changed from light ON to light OFF (Cx27.5$^{+/+}$: 0.434 ± 0.031 n = 80; Cx27.5$^{-/-}$: 0.475 ± 0.027, n = 120, p = 0.3150) (**Figure 5.5D, E**). The values are the average of the second trial as it represents a more robust and reliable behavior. Overall, Cx27.5$^{-/-}$ larvae appear to be hypersensitive to the abrupt light transition but only when it is changed from OFF to ON.

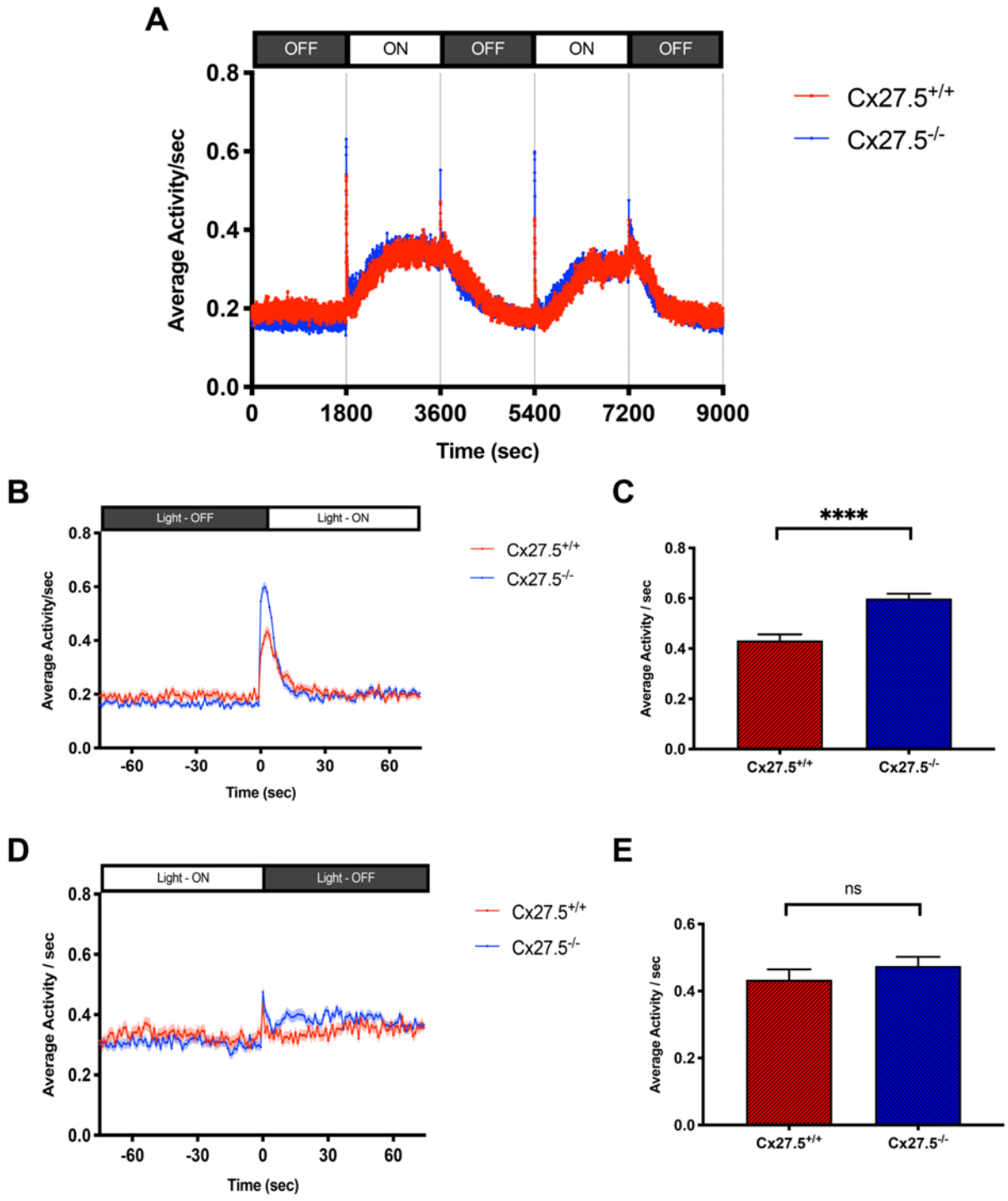

Figure 5.6. Visual-motor response (VMR) of Cx27.5$^{-/-}$ larvae. (**A**) The line graph shows the average activity of Cx27.5$^{+/+}$ and Cx27.5$^{-/-}$ larvae during the alternating periods of light OFF (0% light intensity) and ON (100% light intensity). The activity was defined as the fraction of frames per second that a larva spent being active (swimming). (**B, D**) The line graph shows the change in activity as the light changes from Light-OFF to Light-ON or Light-ON to Light-OFF. Activity is shown from 1 minute (min) preceding and 1 min

succeeding the light switch. (**C, E**) The average activity comparison between two groups right at the light switch. The values are the average of the second trial from five independent tests. Data was collected every second. Sample sizes were the following: $Cx27.5^{+/+}$: n = 80, $Cx27.5^{-/-}$: n = 120. Error bars show the standard error of the mean. ****p < 0.0001, ns - not significant.

5.2.7. Optomotor response (OMR) declines in the absence of Cx27.5

To further explore the involvement of Cx27.5 in visual processing, we subjected the 7 dpf larva to the OMR assay. The OMR is a visual behavior in which motion observed in the surroundings is followed. (Bahl & Engert, 2020; Kist & Portugues, 2019; Naumann et al., 2016). Once larvae see the moving stimulus (black and white stripes), they follow it. The sample larvae distribution prior to and after the right-ward visual stimulus is displayed in **Figure 5.6A**. $Cx27.5^{-/-}$ larvae displayed a decrease in their ability to follow the right-ward moving stimulus, after 1.5 min ($Cx27.5^{+/+}$: 73.75 ± 3.24, n = 80; $Cx27.5^{-/-}$: 51.52 ± 1.34, n = 80, p = 0.0002) and 3 min of stimulus presentation ($Cx27.5^{+/+}$: 73.75 ± 4.60, n = 80; $Cx27.5^{-/-}$: 52.59 ± 2.25, n = 80, p = 0.0022) (**Figure 5.6B**). Same as with right-ward stimulus, $Cx27.5^{-/-}$ larvae exhibited decreased ability to follow the left-ward moving stimulus, both after 1.5 min ($Cx27.5^{+/+}$: 67.50 ± 4.53, n = 80; $Cx27.5^{-/-}$: 40.23 ± 3.05, n = 80, p = 0.0011) and 3 min ($Cx27.5^{+/+}$: 75.00 ± 4.23, n = 80; $Cx27.5^{-/-}$: 47.79 ± 3.72, n = 80, p = 0.0011) (**Figure 5.6C**). Thus, Cx27.5 appears to play a role in encoding and perception of the motion direction signals.

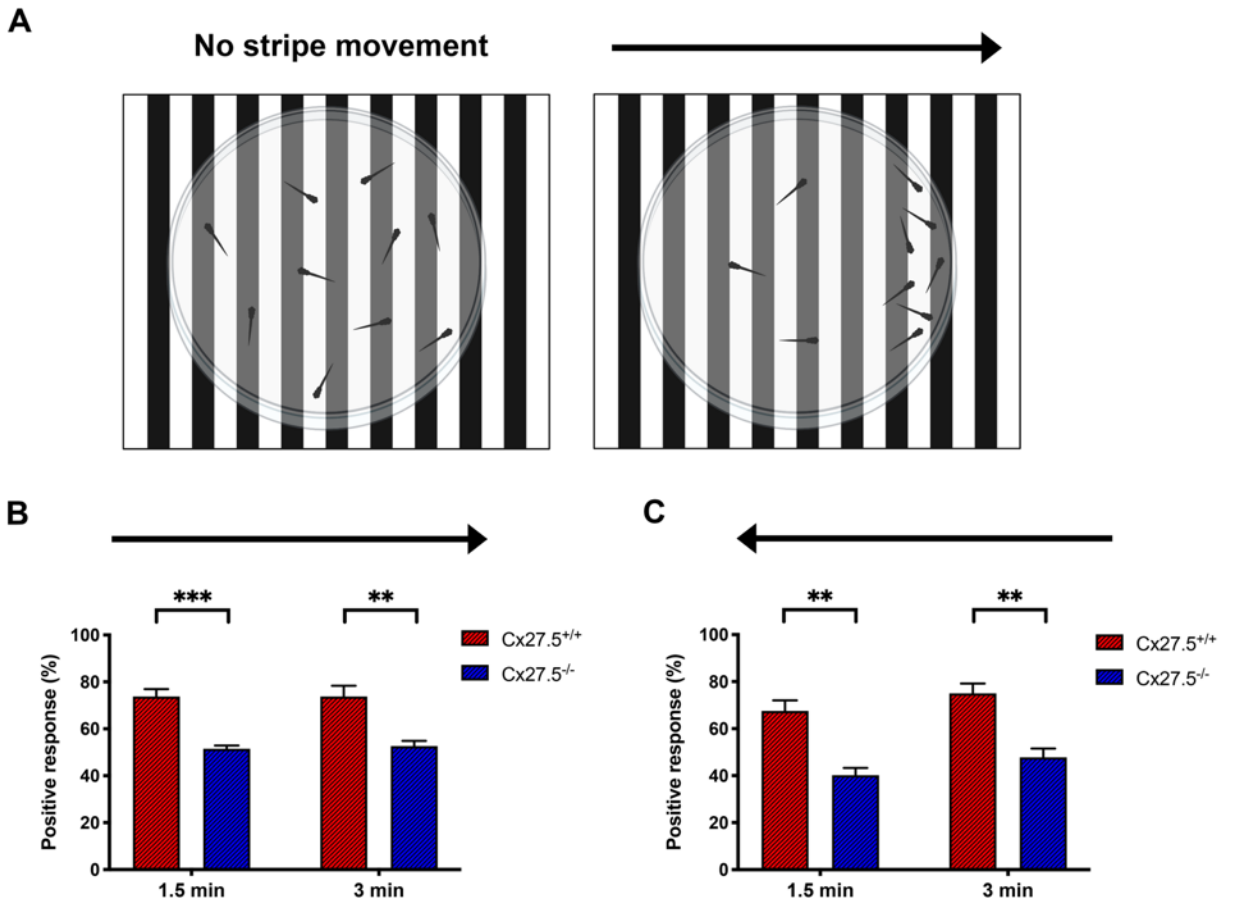

Figure 5.7. Optomotor response (OMR) of Cx27.5$^{-/-}$ larvae. (**A**) A model of the OMR test chamber set up showing larvae distribution prior to and after the right-ward visual stimulus. The image was created with BioRender.com. (**B**) Percentage of Cx27.5$^{+/+}$ and Cx27.5$^{-/-}$ larvae exhibiting a positive OMR response to the moving right-ward stimulus and (**C**) left-ward stimulus. The positive response was calculated after 1.5 min and 3 min of stimulus presentation. Spatial frequency = 64 pixels/cycle, speed = 144 pixels/sec, contrast setting = 100%. Ten larvae were used in each experiment. Sample sizes were the following: Cx27.5$^{+/+}$: n = 80, Cx27.5$^{-/-}$: n = 80. Error bars show the standard error of the mean. **p < 0.01, ***p < 0.001.

5.3. Discussion

The establishment of the Cx27.5$^{-/-}$ zebrafish line enabled us to study the role of Cx27.5 in visual and cognitive processing in a live animal. The knock-out of the Cx27.5 gene did not lead to gross anatomical defects, and visually the Cx27.5$^{-/-}$ larvae looked indistinguishable from the Cx27.5$^{+/+}$ control. However, Cx27.5$^{-/-}$ larvae were of reduced length, and most notably, Cx27.5$^{-/-}$ embryos had a significant reduction in the survival rate. The majority of Cx27.5$^{-/-}$ embryos seemed to arrest their development during the 4-cell stage of the cleavage period, typically observed 1 hour post-fertilization (Kimmel et al., 1995). As mentioned earlier, Cx27.5 shares 72.2% sequence homology with Cx26 (**Supplementary Figure 5.1B**). Interestingly, at 10.5 days post-coitum, Cx26$^{-/-}$ mouse embryos were significantly smaller than the wild-type or heterozygous littermates (Gabriel et al., 1998). No obvious malformation could be detected, but around day 11 days post-coitum, the homozygous knock-out embryos died. Their results suggest that Cx26 gap junction channels are essential for the transfer of maternal nutrients, such as glucose, and embryonic waste products in the mouse placenta. It is possible that Cx27.5 possesses a similar function, and the transfer of nutrients from the yolk to the embryo, which is critical for embryogenic development, is compromised.

Accurate VMR responsiveness requires an intact retina (Fernandes et al., 2012) and photoreceptor populations with distinct spectral properties (Burton et al., 2017). The altered response of Cx27.5$^{-/-}$ larvae to dark-to-light transitions suggests a specific deficiency in the visual system. This deficiency is most likely due to a misregulation in the network of cells involved in the “ON” pathways that are responsible for processing the incoming light. We have shown that Cx27.5 expression is restricted to the brain and

retina, which is in line with previous reports (Chang-Chien et al., 2014; Zoidl et al., 2008). Specifically in the retina, Cx27.5 expression is most prominent in the IPL layer. IPL layer is known to contain the synapses between the amacrine and bipolar interneurons and the retinal ganglion cells (Euler et al., 2014). The majority of the synapses in the IPL are formed by amacrine cells suggesting that these cells are most likely the ones expressing Cx27.5 (**Supplementary Figure 5.2**). The co-localization experiments with the PSD-95 marker further pointed out that Cx27.5 is most likely expressed in a subset of amacrine cells.

The inner half of the IPL, where Cx27.5 is localized, contains cell connections that are involved in the “ON” network pathways and get depolarized upon an increase in illumination. The initial processing of the VMR Light-ON and VMR Light-OFF responses is influenced by different classes of photoreceptors. Zhang and colleagues showed an increased VMR Light-ON response upon stimulation with Schisandrin B component in a cone deficient zebrafish mutant (L. Zhang et al., 2016). The authors concluded that the above compound most likely acted on the rods and led to an enhanced light sensation in the zebrafish mutants. Scotopic vision is dependent on the synapses between ON-cone bipolar cells and amacrine cells in the IPL, which maintain the signaling through the primary rod pathway (Deans et al., 2002; Güldenagel et al., 2001). The expression of Cx27.5 in the IPL and the aberrant VMR Light-ON response suggested that Cx27.5 might be a key player in the rod-mediated light “ON” pathway. While we were unable to narrow down the specific cell type that expresses Cx27.5, IPL is critical for visual processing, and Cx27.5 could be involved in the pathway contributing to the negative regulation of the ON pathway, and its absence would lead to the enhanced VMR response.

In the positive OMR, the larva swims to follow moving visual stimuli (Bahl & Engert, 2020; Kist & Portugues, 2019; Naumann et al., 2016). The OMR test can be used to evaluate the spatial acuity in zebrafish, as fish will swim in the direction of perceived motion. As expected, 7 dpf larvae were able to elicit OMR and follow the visual stimulus. This is in line with the previous reports depicting this response in fish as early as 5 dpf (Portugues & Engert, 2011; Rainy et al., 2016; Stiebel-Kalish et al., 2012). In zebrafish, processing and encoding of both presence and direction of motion are largely governed by direction-selective ganglion cells (DSGCs) (Briggman et al., 2011; Ding et al., 2016; Naumann et al., 2016; Taylor & Vaney, 2002). Cx27.5$^{-/-}$ larvae showed a significantly reduced OMR when compared to the control group.

We were able to exclude parvalbumin expressing AII amacrine cells as the cells expressing Cx27.5. However, up to thirty distinct subpopulations of amacrine cells have been discovered and moving forward antibodies which detect other subtypes in the zebrafish will need to be identified. It is worth mentioning that a subtype of amacrine cells, called starburst amacrine cells, plays an important role in the signal transmission to the direction-sensitive retinal ganglion cells and thus is a key contributor to the detection of directional motion and direction selectivity (Taylor & Smith, 2012). Our OMR data suggested that starburst amacrine cells might be the subtype that expresses Cx27.5, as Cx27.5 knock-out led to the disruption in the directional motion detection.

Overall, our data pointed to an involvement of Cx27.5 in the network responsible for processing motion direction signals. Further, the results suggested that Cx27.5 could be a critical modulator of the pathways converging in the IPL layer and thus is critical for visual perception.

5.4. Supplementary Figures

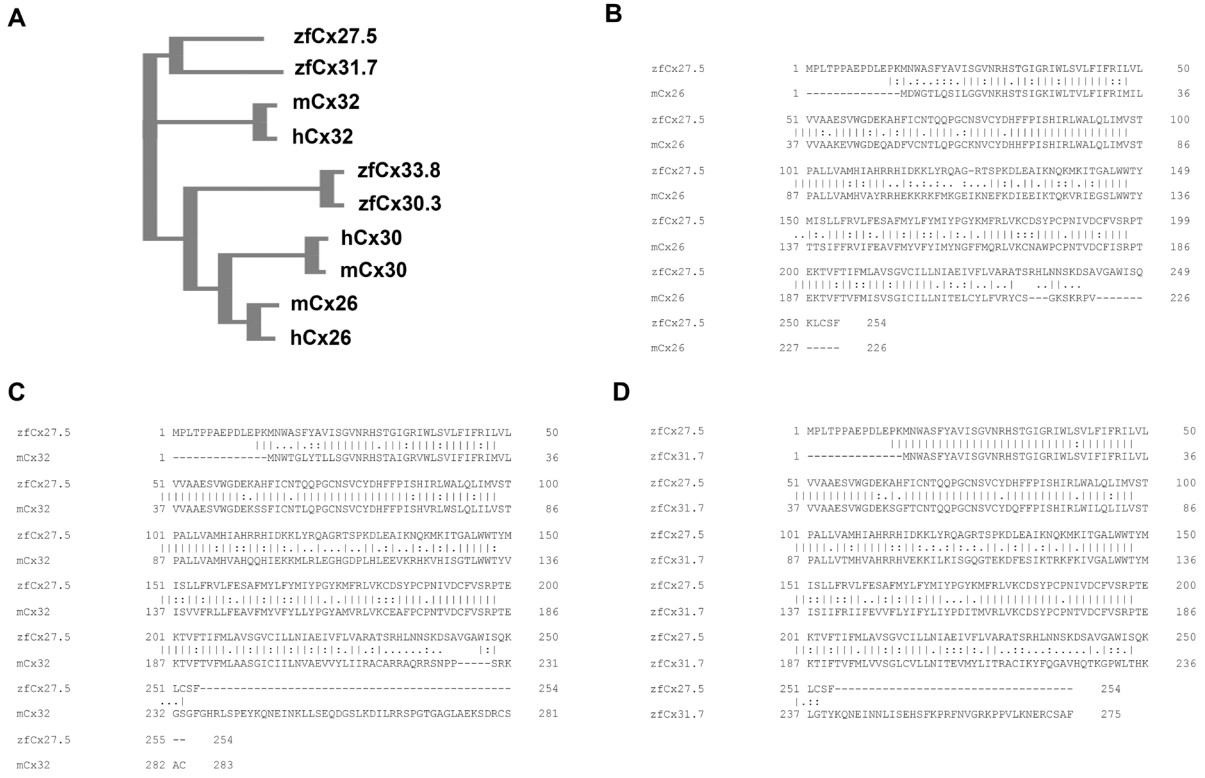

Supplementary Figure 5.1. Phylogenetic tree and sequence comparisons of zebrafish Cx27.5 paralogue and orthologues. Phylogenic tree consisting of proteins closely related to Cx27.5. zfCx27.5 is more closely related to mCx32 and hCx32. Phylogenic tree was created with Simple Phylogeny EMBL-EBI. (B) Sequence alignment between zebrafish Cx27.5 and mouse Cx26 shows a similarity score of 72.2%, identity score of 56.1%, and gap score of 11.8%. (C) Sequence alignment between zebrafish Cx27.5 and mouse Cx32 shows a similarity score of 65.2%, identity score of 52.6% and gap score of 22.2%. (D) Sequence alignment between zebrafish Cx27.5 and zebrafish Cx31.7 shows a similarity score of 70.6%, identity score of 58.5%, and gap score of 17.0%. Alignments were performed using Pairwise Sequence Alignment with EMBOSS Needle EMBL-EBI. zf: zebrafish; m: mouse; h: human.

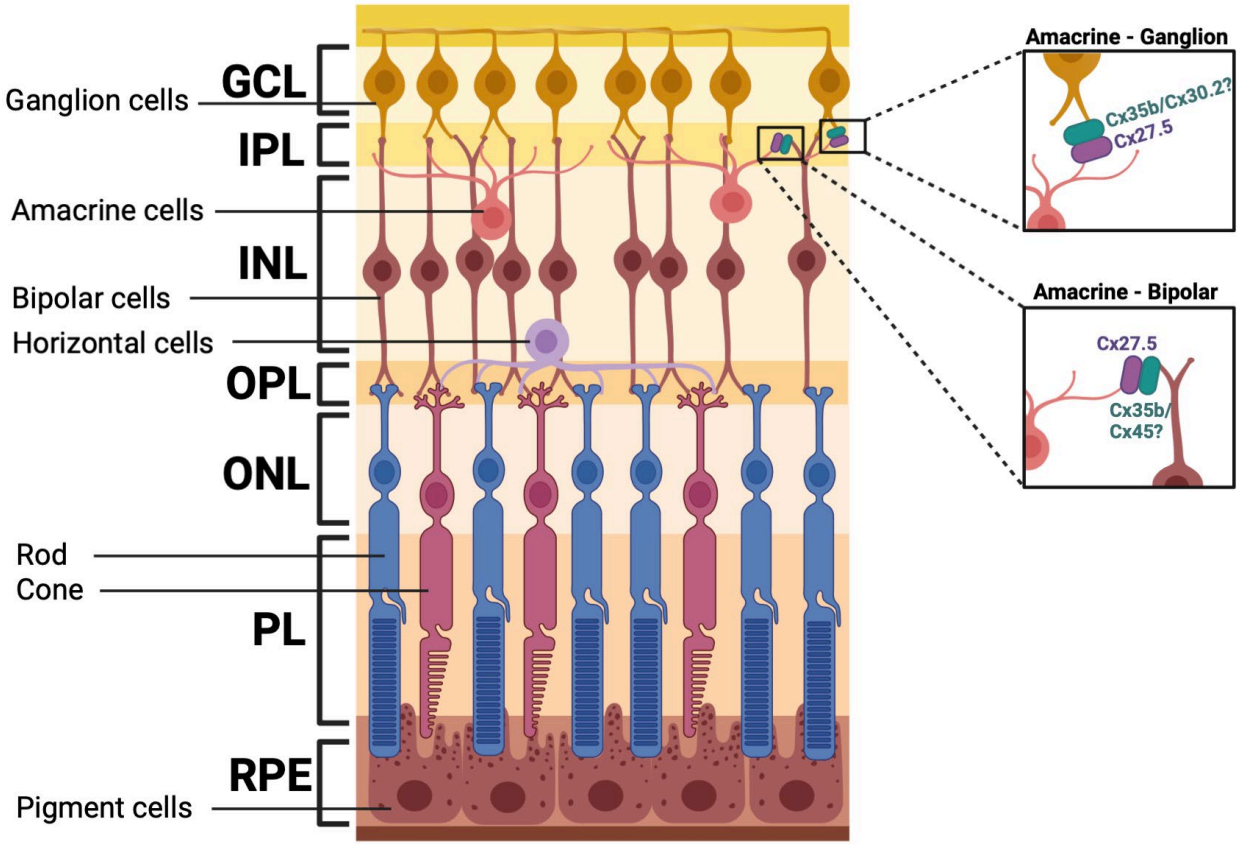

Supplementary Figure 5.2. Schematic of the retinal anatomy, showing electrical synapses containing Cx27.5. The illustration shows key layers of the retina and different cell types contained within each layer on the left. Zoomed-in insets on the right show Cx27.5 in the amacrine cells connecting with other retinal connexins in bipolar and ganglion cells. The image was created with BioRender.com. GCL: ganglion cell layer; IPL: inner plexiform layer; INL: inner nuclear layer; OPL: outer plexiform layer; ONL: outer nuclear layer; PL: photoreceptor layer; RPE: retinal photoreceptor layer.

Chapter 6. Concluding Remarks and Future Directions

6.1. Summary

The overall findings in this thesis uncovered the importance of molecular mechanisms governing the regulation and function of neuronal connexins. Connexins possess high turnover rates, which is believed to be instrumental in synaptic plasticity. The high turnover rates are likely mediated by various interacting partners that connexins interact with at different stages of their life cycle. Various proteins have been shown to affect the delivery to and from the membrane as well as intracellular trafficking between different cellular compartments. In chapter 3, the interaction between Cx36 and Cav-1 was explored in the Neuro 2a cell line and showed to be calcium-dependent. As Cav-1 is a mediator of caveolin-dependent endocytosis, the effect of Cav-1 overexpression on the trafficking dynamics of Cx36 was explored. Cav-1 overexpression led to enhanced vesicular and membrane transport of Cx36. With pharmacological intervention, we concluded the involvement of Cav-1 in endocytosis, specifically through the rapid and calcium-dependent pathway.

Chapter 4 focused on connexin oligomerization as a means of regulation. When different connexin isoforms oligomerize together to form a single hemichannel, this hemichannel is referred to as a heteromeric. The docking of two distinct channels is referred to as heterotypic channels. Both conformations allow for the formation of highly specialized gap junction channels, which are required to connect a multitude of different cell types. Because the retina is known to be an ideal tissue to study gap junctional regulation and connectivity, the potential oligomerization capability of two connexins highly expressed in the retina, Cx35b and Cx27.5, was explored. Cx35b and Cx27.5

channels showed distinct trafficking features, intracellularly and at the membrane, compared to homomeric channels. Moreover, Cx35b/Cx27.5 channels displayed a difference in their function by showing an increased dye uptake and transfer. These results suggested that Cx35b/Cx27.5 channels can shape the signal transmission in a specific manner. As we showed co-localization between Cx35b and Cx27.5 in the inner plexiform layer of the retina, the most likely cell types expressing the above proteins were narrowed down to bipolar, amacrine, and ganglion cells. The connection between the above cell types may rely on the heteromeric/heterotypic gap junctions as opposed to a homomeric/homotypic channel.

As we began to uncover a potential role of Cx27.5 in the retinal connectivity, a knock-out zebrafish line was employed to continue this exploration further. The knock-out larvae demonstrated significant visual deficiencies when compared to the wild-type. The increased startle upon light stimulation suggested that the signaling transmission between ON-cone bipolar cells and amacrine cells was altered or lost. Furthermore, Cx27.5 knock-out larvae could not perceive and encode directional motion signals. The above results together, with protein expression analysis, implied that Cx27.5 is expressed by starburst amacrine cell type. These cells are known for their critical function in the detecting directional motion and direction selectivity, and thus the absence of Cx27.5 gap junctions might affect the electrical communication between amacrine and ganglion cells.

6.2. Future Directions

Interaction between Cx36 and Cav-1 proved to be an essential mediator of the caveolin-dependent endocytosis of Cx36. One possible future direction would be to employ immunoprecipitation followed by a mass spectrometry analysis to identify

potential interacting partners of Cx36. By establishing an interacting network of Cx36, not only the specialized endocytosis mechanism of Cx36 could be elucidated, but new regulators of Cx36 function can be established.

Further studies can be used to pinpoint whether the channels formed between Cx35b and Cx27.5 are heteromeric or heterotypic or whether both types of channels can be observed. Two different cell lines, each stably expressing only Cx35b or Cx27.5, can be employed to determine this. Once the stable expression is established, cells from the different cell lines can be mixed to determine if heterotypic channels can be formed between the different cells. However, a stable expression often comes with its challenges. Specifically, for Cx36, rapid loss of expression is often observed in the stable cell lines making further investigations challenging.

Electrophysiology is essential for the functional studies of gap junction properties. The technique can determine whether the mixed Cx35b/Cx27.5 channels display increased signal transmission, as seen with the functional dye assays. This can further explain how distinct properties of heteromeric/heterotypic channels can aid in the fine-tuning of the electrical synapses between different cell types. Lastly, while we began to explore co-localization patterns of Cx35b and Cx27.5, this should be further explored. The specific cell types the mixed channels are attributed to can be identified by employing different cell markers.

Like other connexins, Cx27.5 has a paralog, which is Cx31.7 (Eastman et al., 2006) with the sequence similarity of 70.6% (**Supplementary Figure 5.1D**). The knock-out fish line of the paralogue should be generated and inbred with Cx27.5 knock-out to obtain a double knock-out line. It would be appealing to observe how the behavioral characteristics

of this line would differ from the current Cx27.5 knock-out line. Often, the presence of another paralogue rescues the effect of the single knock-out, leading to an either reduced or entirely absent phenotype. Another important direction for future research is to knock-in Cx27.5 back into the knock-out line to show the rescue of the observed phenotype. Alternatively, a rescue by transgenic expression under the control of an amacrine cell promoter can be performed, once the exact amacrine cell type expressing Cx27.5 is known. This would further reinforce the specificity of the observed deficiencies in the knock-out line.

Cx35b and Cx27.5 are highly expressed in the retina and show oligomerization capabilities as described in Chapter 4; thus, it would be beneficial to observe the behavioral outcomes in a fish line lacking both Cx35b and Cx27.5. As the above proteins show partial co-localization, the deletion of both genes would most likely cause a significant disruption in visual processing. This would help to narrow down the specific pathways within the retina that employ both Cx35b and Cx27.5.

The immunohistochemistry results show that Cx27.5 knock-out tissues display a partial signal from the Cx27.5 antibody. This could be attributed to the cross-reactivity of the antibody with other connexin isoforms. To rectify this, one possible solution is to adjust the immunohistochemistry protocols to determine the most optimal stringent conditions that will eliminate any residual binding but will not strip the antibody completely.

Lastly, both immunohistochemistry and mRNA localization assays showed a significant signal of Cx27.5 in the brain. The role of Cx27.5 in cognitive processing can be explored by employing several behavioral assays such as T-maze assays, social

preference tests, prey-capture assays, shoaling tests, to test for possible deficiencies in the Cx27.5 knock-out line.

6.3. Conclusion

This thesis focused on multifaced regulatory mechanisms and the function of neuronal connexins. Gap junctions are critical building blocks of the electrical synapses, and the outcomes will contribute to the understanding of the mechanisms that govern and shape neuronal connectivity and signal transmission. In the retina, these mechanisms can help further understand the role and function of each cell type and uncover potential network misregulations that often result in visual abnormalities. With the involvement of gap junction proteins in neurodegenerative diseases such as Parkinson's and amyotrophic lateral sclerosis, the above research and its continuation could potentially have implications even in the therapeutic avenues.

BIBLIOGRAPHY

Abrams, C. K., Freidin, M. M., Verselis, V. K., Bargiello, T. A., Kelsell, D. P., Richard, G., Bennett, M. V. L., & Bukauskas, F. F. (2006). Properties of human connexin 31, which is implicated in hereditary dermatological disease and deafness. *Proceedings of the National Academy of Sciences of the United States of America*, *103*(13), 5213–5218. https://doi.org/10.1073/pnas.0511091103

Ahmad, S., Diez, J. A., George, C. H., & Evans, W. H. (1999). Synthesis and assembly of connexins in vitro into homomeric and heteromeric functional gap junction hemichannels. *Reactions*, *253*, 247–253.

Ahmad, S., Iriondo, J. D., & Howard Evans, W. (1998). Cell-free synthesis and assembly of connexins into functional gap junction hemichannels. *Biochemical Society Transactions*, *26*(3), 2703–2716. https://doi.org/10.1042/bst026s304

Ai, Z., Fischer, A., Spray, D. C., Brown, A. M. C., & Fishman, G. I. (2000). Wnt-1 regulation of connexin43 in cardiac myocytes. *Journal of Clinical Investigation*, *105*(2), 161–171. https://doi.org/10.1172/JCI7798

Alev, C., Urscheld, S., Sonntag, S., Zoidl, G., Fort, A. G., Höher, T., Matsubara, M., Willecke, K., Spray, D. C., & Dermietzel, R. (2008). The neuronal connexin36 interacts with and is phosphorylated by CaMKII in a way similar to CaMKII interaction with glutamate receptors. *Proceedings of the National Academy of Sciences of the United States of America*, *105*(52), 20964–20969. https://doi.org/10.1073/pnas.0805408105

Allen, K., Fuchs, E. C., Jaschonek, H., Bannerman, D. M., & Monyer, H. (2011). Gap junctions between interneurons are required for normal spatial coding in the hippocampus and short-term spatial memory. *Journal of Neuroscience*, *31*(17), 6542–6552. https://doi.org/10.1523/JNEUROSCI.6512-10.2011

Arai, I., Tanaka, M., & Tachibana, M. (2010). Active roles of electrically coupled bipolar cell network in the adult retina. *Journal of Neuroscience*, *30*(27), 9260–9270. https://doi.org/10.1523/JNEUROSCI.1590-10.2010

Archard, H. O., & Denys, F. R. (1979). Development of annular gap junctions in guinea pig epithelia. *Journal of Oral Pathology & Medicine*, *8*(4), 187–197. https://doi.org/10.1111/j.1600-0714.1979.tb01885.x

Bahl, A., & Engert, F. (2020). Neural circuits for evidence accumulation and decision making in larval zebrafish. *Nature Neuroscience*, *23*(1), 94–102. https://doi.org/10.1038/s41593-019-0534-9

Barrio, L. C., Suchyna, T., Bargiello, T., Xu, L. X., Roginski, R. S., Bennett, M. V. L., & Nicholson, B. J. (1991). Gap junctions formed by connexins 26 and 32 alone and in combination are differently affected by applied voltage. *Proceedings of the National Academy of Sciences of the United States of America*, *88*(19), 8410–8414. https://doi.org/10.1073/pnas.88.19.8410

Bazzigaluppi, P., Isenia, S. C., Haasdijk, E. D., Elgersma, Y., De Zeeuw, C. I., van der Giessen, R. S., & de Jeu, M. T. G. (2017). Modulation of murine olivary connexin 36 gap junctions by PKA and CaMKII. *Frontiers in Cellular Neuroscience*, *11*(December), 1–11. https://doi.org/10.3389/fncel.2017.00397

Belluardo, N., Mudò, G., Trovato-Salinaro, A., Le Gurun, S., Charollais, A., Serre-Beinier, V., Amato, G., Haefliger, J. A., Meda, P., & Condorelli, D. F. (2000).

Expression of Connexin36 in the adult and developing rat brain. *Brain Research*, *865*(1), 121–138. https://doi.org/10.1016/S0006-8993(00)02300-3
Bennett, B. C., Purdy, M. D., Baker, K. A., Acharya, C., Mcintire, W. E., Stevens, R. C., Zhang, Q., Harris, A. L., Abagyan, R., & Yeager, M. (2016). An electrostatic mechanism for Ca 2+ -mediated regulation of gap junction channels. *Nature Communications*, *7*. https://doi.org/10.1038/ncomms9770
Bennett, M. V. L., & Zukin, R. S. (2004). Electrical Coupling and Neuronal Synchronization in the Mammalian Brain. *Neuron*, *41*(4), 495–511. https://doi.org/10.1016/S0896-6273(04)00043-1
Berthoud, V. M., Minogue, P. J., Laing, J. G., & Beyer, E. C. (2004). Pathways for degradation of connexins and gap junctions. *Cardiovascular Research*, *62*(2), 256–267. https://doi.org/10.1016/j.cardiores.2003.12.021
Bilderback, T. R., Gazula, V. R., Lisanti, M. P., & Dobrowsky, R. T. (1999). Caveolin interacts with Trk A and p75(NTR) and regulates neurotrophin signaling pathways. *Journal of Biological Chemistry*, *274*(1), 257–263. https://doi.org/10.1074/jbc.274.1.257
Biswas, S. K., & Lo, W. K. (2007). Gap junctions contain different amounts of cholesterol which undergo unique sequestering processes during fiber cell differentiation in the embryonic chicken lens. *Molecular Vision*, *13*(February), 345–359.
Björk, K., Sjögren, B., & Svenningsson, P. (2010). Regulation of serotonin receptor function in the nervous system by lipid rafts and adaptor proteins. *Experimental Cell Research*, *316*(8), 1351–1356. https://doi.org/10.1016/j.yexcr.2010.02.034
Blatow, M., Rozov, A., Katona, I., Hormuzdi, S. G., Meyer, A. H., Whittington, M. A., Caputi, A., & Monyer, H. (2003). A novel network of multipolar bursting interneurons generates theta frequency oscillations in neocortex. *Neuron*, *38*(5), 805–817. https://doi.org/10.1016/S0896-6273(03)00300-3
Bloomfield, S. A., & Volgyi, B. (2009). The diverse functional roles and regulation of neuronal gap junctions in the retina. *Nat Rev Neurosci*, *10*(7), 495–506. https://doi.org/nrn2636 [pii]\r10.1038/nrn2636
Boulware, M. I., Kordasiewicz, H., & Mermelstein, P. G. (2007). Caveolin proteins are essential for distinct effects of membrane estrogen receptors in neurons. *Journal of Neuroscience*, *27*(37), 9941–9950. https://doi.org/10.1523/JNEUROSCI.1647-07.2007
Brand, M., M. G., & Nüsslein-Vollhard, C. (2002). Keeping and raising zebrafish, in Zebrafish: A practical approach. *Oxford University Press*. https://doi.org/10.1017/S0016672303216384
Braun, J. E. A., & Madison, D. V. (2000). A novel SNAP25-caveolin complex correlates with the onset of persistent synaptic potentiation. *Journal of Neuroscience*, *20*(16), 5997–6006. https://doi.org/10.1523/jneurosci.20-16-05997.2000
Briggman, K. L., Helmstaedter, M., & Denk, W. (2011). Wiring specificity in the direction-selectivity circuit of the retina. *Nature*. https://doi.org/10.1038/nature09818
Brown, C. A., Del Corsso, C., Zoidl, C., Donaldson, L. W., Spray, D. C., & Zoidl, G. (2019). Tubulin-Dependent Transport of Connexin-36 Potentiates the Size and Strength of Electrical Synapses. *Cells*, *8*(10), 1146. https://doi.org/10.3390/cells8101146

Bu, J., Bruckner, S. R., Sengoku, T., Geddes, J. W., & Estus, S. (2003). Glutamate regulates caveolin expression in rat hippocampal neurons. *Journal of Neuroscience Research*, *72*(2), 185–190. https://doi.org/10.1002/jnr.10556

Bukauskas, F. F., Elfgang, C., Willecke, K., & Weingart, R. (1995). Heterotypic gap junction channels (connexin26 - connexin32) violate the paradigm of unitary conductance. *Pflügers Archiv European Journal of Physiology*, *429*(6), 870–872. https://doi.org/10.1007/BF00374812

Burr, G. S., Mitchell, C. K., Keflemariam, Y. J., Heidelberger, R., & O'Brien, J. (2005). Calcium-dependent binding of calmodulin to neuronal gap junction proteins. *Biochemical and Biophysical Research Communications*, *335*(4), 1191–1198. https://doi.org/10.1016/j.bbrc.2005.08.007

Burrill, J. D., & Easter, S. S. (1995). The first retinal axons and their microenvironment in zebrafish: Cryptic pioneers and the pretract. *Journal of Neuroscience*, *15*(4), 2935–2947. https://doi.org/10.1523/jneurosci.15-04-02935.1995

Burton, C. E., Zhou, Y., Bai, Q., & Burton, E. A. (2017). Spectral properties of the zebrafish visual motor response. *Neuroscience Letters*. https://doi.org/10.1016/j.neulet.2017.03.002

Butkevich, E., Hülsmann, S., Wenzel, D., Shirao, T., Duden, R., & Majoul, I. (2004). Drebrin is a novel connexin-43 binding partner that links gap junctions to the submembrane cytoskeleton. *Current Biology*, *14*(8), 650–658. https://doi.org/10.1016/j.cub.2004.03.063

Cade, L., Reyon, D., Hwang, W. Y., Tsai, S. Q., Patel, S., Khayter, C., Joung, J. K., Sander, J. D., Peterson, R. T., & Yeh, J. R. J. (2012). Highly efficient generation of heritable zebrafish gene mutations using homo-and heterodimeric TALENs. *Nucleic Acids Research*, *40*(16), 8001–8010. https://doi.org/10.1093/nar/gks518

Cameron, D. A., & Carney, L. H. (2000). Cell mosaic patterns in the native and regenerated inner retina of zebrafish: Implications for retinal assembly. *Journal of Comparative Neurology*, *416*(3), 356–367. https://doi.org/10.1002/(SICI)1096-9861(20000117)416:3<356::AID-CNE7>3.0.CO;2-M

Chang-Chien, J., Yen, Y. C., Chien, K. H., Li, S. Y., Hsu, T. C., & Yang, J. J. (2014). The connexin 30.3 of zebrafish homologue of human connexin 26 may play similar role in the inner ear. *Hearing Research*, *313*, 55–66. https://doi.org/10.1016/j.heares.2014.04.010

Chanson, M., Kotsias, B. A., Peracchia, C., & O'Grady, S. M. (2007). Interactions of connexins with other membrane channels and transporters. *Progress in Biophysics and Molecular Biology*, *94*(1–2), 233–244. https://doi.org/10.1016/j.pbiomolbio.2007.03.002

Christian, M., Cermak, T., Doyle, E. L., Schmidt, C., Zhang, F., Hummel, A., Bogdanove, A. J., & Voytas, D. F. (2010). Targeting DNA double-strand breaks with TAL effector nucleases. *Genetics*, *186*(2), 756–761. https://doi.org/10.1534/genetics.110.120717

Christie, J. M., Bark, C., Hormuzdi, S. G., Helbig, I., Monyer, H., & Westbrook, G. L. (2005). Connexin36 mediates spike synchrony in olfactory bulb glomeruli. *Neuron*, *46*(5), 761–772. https://doi.org/10.1016/j.neuron.2005.04.030

Cohen, A. W., Hnasko, R., Schubert, W., & Lisanti, M. P. (2004). Role of caveolae and caveolins in health and disease. *Physiological Reviews*, *84*(4), 1341–1379.

https://doi.org/10.1152/physrev.00046.2003
Condorelli, D. F., Belluardo, N., Trovato-Salinaro, A., & Mudò, G. (2000). Expression of Cx36 in mammalian neurons. *Brain Research Reviews*, *32*(1), 72–85. https://doi.org/10.1016/S0165-0173(99)00068-5
Condorelli, D. F., Parenti, R., Spinella, F., Salinaro, A. T., Belluardo, N., Cardile, V., & Cicirata, F. (1998). Cloning of a new gap junction gene (Cx36) highly expressed in mammalian brain neurons. *European Journal of Neuroscience*, *10*(3), 1202–1208. https://doi.org/10.1046/j.1460-9568.1998.00163.x
Connors, B. W., & Long, M. A. (2004). ELECTRICAL SYNAPSES IN THE MAMMALIAN BRAIN %O Journal Article. *Annual Review of Neuroscience*, *27*(1), 393–418. https://doi.org/10.1146/annurev.neuro.26.041002.131128
Cook, J. E., & Becker, D. L. (1995). Gap junctions in the vertebrate retina. *Microscopy Research and Technique*, *31*(5), 408–419. https://doi.org/10.1002/jemt.1070310510
Cottrell, G. T., & Burt, J. M. (2001). Heterotypic gap junction channel formation between heteromeric and homomeric Cx40 and Cx43 connexons. *American Journal of Physiology - Cell Physiology*, *281*(5 50-5), 1559–1567. https://doi.org/10.1152/ajpcell.2001.281.5.c1559
Cottrell, G. T., & Burt, J. M. (2005). Functional consequences of heterogeneous gap junction channel formation and its influence in health and disease. *Biochimica et Biophysica Acta - Biomembranes*, *1711*(2 SPEC. ISS.), 126–141. https://doi.org/10.1016/j.bbamem.2004.11.013
Crow, D. S., Beyer, E. C., Paul, D. L., Kobe, S. S., & Lau, A. F. (1990). Phosphorylation of connexin43 gap junction protein in uninfected and Rous sarcoma virus-transformed mammalian fibroblasts. *Molecular and Cellular Biology*, *10*(4), 1754–1763. https://doi.org/10.1128/mcb.10.4.1754-1763.1990
Curti, S., Hoge, G., Nagy, J. I., & Pereda, A. E. (2012). Synergy between electrical coupling and membrane properties promotes strong synchronization of neurons of the mesencephalic trigeminal nucleus. *Journal of Neuroscience*, *32*(13), 4341–4359. https://doi.org/10.1523/JNEUROSCI.6216-11.2012
Daly, C., Sugimori, M., Moreira, J. E., Ziff, E. B., & Llina, R. (2000). Synaptophysin regulates clathrin-independent endocytosis of synaptic vesicles. *PNAS*, *97*(11).
De Pina-Benabou, M. H., Srinivas, M., Spray, D. C., & Scemes, E. (2001). Calmodulin kinase pathway mediates the K+-induced increase in gap junctional communication between mouse spinal cord astrocytes. *Journal of Neuroscience*, *21*(17), 6635–6643. https://doi.org/10.1523/jneurosci.21-17-06635.2001
De Vuyst, E., Decrock, E., Cabooter, L., Dubyak, G. R., Naus, C. C., Evans, W. H., & Leybaert, L. (2006). Intracellular calcium changes trigger connexin 32 hemichannel opening. *EMBO Journal*, *25*(1), 34–44. https://doi.org/10.1038/sj.emboj.7600908
De Zeeuw, C. I., Chorev, E., Devor, A., Manor, Y., Van Der Giessen, R. S., De Jeu, M. T., Hoogenraad, C. C., Bijman, J., Ruigrok, T. J. H., French, P., Jaarsma, D., Kistler, W. M., Meier, C., Petrasch-Parwez, E., Dermietzel, R., Sohl, G., Gueldenagel, M., Willecke, K., & Yarom, Y. (2003). Deformation of network connectivity in the inferior olive of connexin 36-deficient mice is compensated by morphological and electrophysiological changes at the single neuron level. *Journal of Neuroscience*, *23*(11), 4700–4711. https://doi.org/10.1523/jneurosci.23-11-

04700.2003
Deans, M. R., Gibson, J. R., Sellitto, C., Connors, B. W., & Paul, D. L. (2001). Synchronous activity of inhibitory networks in neocortex requires electrical synapses containing connexin36. *Neuron*, *31*(3), 477–485. https://doi.org/10.1016/S0896-6273(01)00373-7
Deans, M. R., Volgyi, B., Goodenough, D. A., Bloomfield, S. A., & Paul, D. L. (2002). Connexin36 Is Essential for Transmission of Rod-Mediated Visual Signals in the Mammalian Retina Figure 1. Rod Pathways in the Mouse Retina Utilize Cone Circuitry. *Neuron*, *36*, 703–712.
Degen, J., Meier, C., Van Der Giessen, R. S., Söhl, G., Petrasch-Parwez, E., Urschel, S., Dermietzel, R., Schilling, K., De Zeeuw, C. I., & Willecke, K. (2004). Expression Pattern of lacZ Reporter Gene Representing Connexin36 in Transgenic Mice. *Journal of Comparative Neurology*, *473*(4), 511–525. https://doi.org/10.1002/cne.20085
Del Corsso, C., Iglesias, R., Zoidl, G., Dermietzel, R., & Spray, D. C. (2012). Calmodulin dependent protein kinase increases conductance at gap junctions formed by the neuronal gap junction protein connexin36. *Brain Research*, *1487*, 69–77. https://doi.org/10.1016/j.brainres.2012.06.058
Dermietzel, R., Kremer, M., Paputsoglu, G., Stang, A., Skerrett, I. M., Gomes, D., Srinivas, M., Janssen-Bienhold, U., Weiler, R., Nicholson, B. J., Bruzzone, R., & Spray, D. C. (2000). Molecular and functional diversity of neural connexins in the retina. *Journal of Neuroscience*, *20*(22), 8331–8343. https://doi.org/10.1523/jneurosci.20-22-08331.2000
Deveau, H., Garneau, J. E., & Moineau, S. (2010). CRISPR/Cas system and its role in phage-bacteria interactions. *Annual Review of Microbiology*, *64*, 475–493. https://doi.org/10.1146/annurev.micro.112408.134123
Di Guglielmo, G. M., Le Roy, C., Goodfellow, A. F., & Wrana, J. L. (2003). Distinct endocytic pathways regulate TGF-β receptor signalling and turnover. *Nature Cell Biology*, *5*(5), 410–421. https://doi.org/10.1038/ncb975
Diez, J. A., Ahmad, S., & Evans, W. H. (1999). Assembly of heteromeric connexons in guinea-pig liver en route to the Golgi apparatus, plasma membrane and gap junctions. *European Journal of Biochemistry*, *262*(1), 142–148. https://doi.org/10.1046/j.1432-1327.1999.00343.x
Ding, H., Smith, R. G., Poleg-Polsky, A., Diamond, J. S., & Briggman, K. L. (2016). Species-specific wiring for direction selectivity in the mammalian retina. *Nature*. https://doi.org/10.1038/nature18609
Doble, B. W., Ping, P., & Kardami, E. (2000). The ε Subtype of Protein Kinase C Is Required for Cardiomyocyte Connexin-43 Phosphorylation. *Circulation Research Is*, *86*, 293–301. https://doi.org/10.1038/182551a0
Dowling, J. E. (1987). *The Retina*. Harvard University Press.
Duffy, H. S., Delmar, M., & Spray, D. C. (2002). Formation of the gap junction nexus: Binding partners for connexins. *Journal of Physiology Paris*, *96*(3–4), 243–249. https://doi.org/10.1016/S0928-4257(02)00012-8
Easter Jr, S. S., & Nicola, G. N. (1996). The Development of Vision in the Zebrafish. *Developmental Biology*, *180*(2), 646–663. https://ac.els-cdn.com/S0012160696903358/1-s2.0-S0012160696903358-

main.pdf?_tid=5127746c-bbc2-4d6b-99ba-76814082f1d5&acdnat=1549017063_e3b9adb656fb244c4fe9fc5d7a0f7c72%0Ahttp://www.sciencedirect.com/science/article/pii/S0012160696903358
Eastman, S. D., Chen, T. H. P., Falk, M. M., Mendelson, T. C., & Iovine, M. K. (2006). Phylogenetic analysis of three complete gap junction gene families reveals lineage-specific duplications and highly supported gene classes. *Genomics*, *87*(2), 265–274. https://doi.org/10.1016/j.ygeno.2005.10.005
Elfgang, C., Eckert, R., Lichtenberg-Fraté, H., Butterweck, A., Traub, O., Klein, R. A., Hülser, D. F., & Willecke, K. (1995). Specific permeability and selective formation of gap junction channels in connexin-transfected HeLa cells. *Journal of Cell Biology*, *129*(3), 805–817. https://doi.org/10.1083/jcb.129.3.805
Emran, F., Rihel, J., & Dowling, J. E. (2008). A behavioral assay to measure responsiveness of Zebrafish to changes in light intensities. *Journal of Visualized Experiments*, *20*. https://doi.org/10.3791/923
Euler, T., Haverkamp, S., Schubert, T., & Baden, T. (2014). Retinal bipolar cells: Elementary building blocks of vision. *Nature Reviews Neuroscience*, *15*(8), 507–519. https://doi.org/10.1038/nrn3783
Evans, W. H., & Martin, P. E. M. (2002). Gap junctions: structure and function (Review). *Molecular Membrane Biology*, *19*(2), 121–136. https://doi.org/10.1080/09687680210139839
Falk, M. M., Baker, S. M., Gumpert, A. M., Segretain, D., & Buckheit, R. W. (2009). Gap Junction Turnover Is Achieved by the Internalization of Small Endocytic Double-Membrane Vesicles. *Molecular Biology of the Cell*, *20*(July), 3342–3352. https://doi.org/10.1091/mbc.E09
Fallon, R. F., & Goodenough, D. A. (1981). Five-hour half-life of mouse liver gap-junction protein. *The Journal of Cell Biology*, *90*(2), 521–526. https://doi.org/10.1083/jcb.90.2.521
Farnsworth, N. L., & Benninger, R. K. P. (2014). New insights into the role of connexins in pancreatic islet function and diabetes. *FEBS Letters*, *588*(8), 1278–1287. https://doi.org/10.1016/j.febslet.2014.02.035
Feigenspan, A., Janssen-Bienhold, U., Hormuzdi, S., Monyer, H., Degen, J., Söhl, G., Willecke, K., Ammermüller, J., & Weiler, R. (2004). Expression of Connexin36 in Cone Pedicles and OFF-Cone Bipolar Cells of the Mouse Retina. *Journal of Neuroscience*, *24*(13), 3325–3334. https://doi.org/10.1523/JNEUROSCI.5598-03.2004
Feigenspan, A., Teubner, B., Willecke, K., & Weiler, R. (2001). Expression of neuronal connexin36 in AII amacrine cells of the mammalian retina. *Journal of Neuroscience*, *21*(1), 230–239. https://doi.org/10.1523/jneurosci.21-01-00230.2001
Fernandes, A. M., Fero, K., Arrenberg, A. B., Bergeron, S. A., Driever, W., & Burgess, H. A. (2012). Deep brain photoreceptors control light-seeking behavior in zebrafish larvae. *Current Biology*. https://doi.org/10.1016/j.cub.2012.08.016
Fiorini, C., Gilleron, J., Carette, D., Valette, A., Tilloy, A., Chevalier, S., Segretain, D., & Pointis, G. (2008). Accelerated internalization of junctional membrane proteins (connexin 43, N-cadherin and ZO-1) within endocytic vacuoles: An early event of DDT carcinogenicity. *Biochimica et Biophysica Acta - Biomembranes*, *1778*(1), 56–67. https://doi.org/10.1016/j.bbamem.2007.08.032

Fujimoto, K., Nagafuchi, A., Tsukita, S., Kuraoka, A., Ohokuma, A., & Shibata, Y. (1997). Dynamics of connexins, E-cadherin and α-catenin on cell membranes during gap junction formation. *Journal of Cell Science*, *110*(3), 311–322. https://doi.org/10.1242/jcs.110.3.311

Gabriel, H. D., Jung, D., Bützler, C., Temme, A., Traub, O., Winterhager, E., & Willecke, K. (1998). Transplacental uptake of glucose is decreased in embryonic lethal connexin26-deficient mice. *Journal of Cell Biology*, *140*(6), 1453–1461. https://doi.org/10.1083/jcb.140.6.1453

Gaietta, G., Deerinck, T. J., Adams, S. R., Bouwer, J., Tour, O., Laird, D. W., Sosinsky, G. E., Tsien, R. Y., & Ellisman, M. H. (2002). Multicolor and electron microscopic imaging of connexin trafficking. *Science*, *296*(5567), 503–507. https://doi.org/10.1126/science.1068793

Gajda, Z., Szupera, Z., Blazsó, G., & Szente, M. (2005). Quinine, a blocker of neuronal Cx36 channels, suppresses seizure activity in rat neocortex in vivo. *Epilepsia*, *46*(10), 1581–1591. https://doi.org/10.1111/j.1528-1167.2005.00254.x

Galbiati, F., Volonté, D., Gil, O., Zanazzi, G., Salzer, J. L., Sargiacomo, M., Scherer, P. E., Engelman, J. A., Schlegel, A., Parenti, M., Okamoto, T., & Lisanti, M. P. (1998). Expression of caveolin-1 and -2 in differentiating PC 12 cells and dorsal root ganglion neurons: Caveolin-2 is up-regulated in response to cell injury. *Proceedings of the National Academy of Sciences of the United States of America*, *95*(17), 10257–10262. https://doi.org/10.1073/pnas.95.17.10257

Gamble, E., & Koch, C. (1987). The dynamics of free calcium in dendritic spines in response to repetitive synaptic input. *Science*, *236*(4806), 1311–1315. https://doi.org/10.1126/science.3495885

Gaudreault, S. B., Blain, J. F., Gratton, J. P., & Poirier, J. (2005). A role for caveolin-1 in post-injury reactive neuronal plasticity. *Journal of Neurochemistry*, *92*(4), 831–839. https://doi.org/10.1111/j.1471-4159.2004.02917.x

George, C. H., Kendall, J. M., & Evans, W. H. (1999). Intracellular trafficking pathways in the assembly of connexins into gap junctions. *Journal of Biological Chemistry*, *274*(13), 8678–8685. https://doi.org/10.1074/jbc.274.13.8678

Gibson, J. R., Beierlein, M., & Connors, B. W. (1999). *Two networks of electrically coupled inhibitory neurons in neocortex*. *402*(November), 75–79.

Giepmans, B. N. G., Hengeveld, T., Postma, F. R., & Moolenaar, W. H. (2001). Interaction of c-Src with gap junction protein connexin-43. Role in the regulation of cell-cell communication. *Journal of Biological Chemistry*, *276*(11), 8544–8549. https://doi.org/10.1074/jbc.M005847200

Giepmans, B. N. G., Verlaan, I., Hengeveld, T., Janssen, H., Calafat, J., Falk, M. M., & Moolenaar, W. H. (2001). Gap junction protein connexin-43 interacts directly with microtubules S-Met/Cys-labeled cell lysates con- observed in lysates from rat liver epithelial T51B cells. *Current Biology*, *11*, 1364–1368.

Giepmans, B. N. G., Verlaan, I., & Moolenaar, W. H. (2001). Connexin-43 interactions with ZO-1 and α- and β-tubulin. *Cell Communication and Adhesion*, *8*(4–6), 219–223. https://doi.org/10.3109/15419060109080727

Gilleron, J., Carette, D., Fiorini, C., Dompierre, J., Macla, E., Denizot, J. P., Segretain, D., & Pointis, G. (2011). The large GTPase dynamin2: A new player in connexin 43 gap junction endocytosis, recycling and degradation. *International Journal of*

Biochemistry and Cell Biology, *43*(8), 1208–1217. https://doi.org/10.1016/j.biocel.2011.04.014

Go, M., Kojima, T., Takano, K. ichi, Murata, M., Koizumi, J., Kurose, M., Kamekura, R., Osanai, M., Chiba, H., Spray, D. C., Himi, T., & Sawada, N. (2006). Connexin 26 expression prevents down-regulation of barrier and fence functions of tight junctions by Na+/K+-ATPase inhibitor ouabain in human airway epithelial cell line Calu-3. *Experimental Cell Research*, *312*(19), 3847–3856. https://doi.org/10.1016/j.yexcr.2006.08.014

González-Nieto, D., Gómez-Hernández, J. M., Larrosa, B., Gutiérrez, C., Muñoz, M. D., Fasciani, I., O'Brien, J., Zappalà, A., Cicirata, F., & Barrio, L. C. (2008). Regulation of neuronal connexin-36 channels by pH. *Proceedings of the National Academy of Sciences of the United States of America*, *105*(44), 17169–17174. https://doi.org/10.1073/pnas.0804189105

González, M. I., Krizman-Genda, E., & Robinson, M. B. (2007). Caveolin-1 regulates the delivery and endocytosis of the glutamate transporter, excitatory amino acid carrier. *Journal of Biological Chemistry*, *282*(41), 29855–29865. https://doi.org/10.1074/jbc.M704738200

Goodenough, D. A., & Paul, D. L. (2009). Gap Junctions. *Cold Spring Harb Perspect Biol 2009;1:A002576*. https://doi.org/10.1016/b978-0-12-802401-0.00011-9

Goodenough, D. A., & Revel, J. P. (1970). A fine structural analysis of intercellular junctions in the mouse liver. *Journal of Cell Biology*, *45*(2), 272–290. https://doi.org/10.1083/jcb.45.2.272

Gorodinsky, A., & Harris, D. A. (1995). Glycolipid-anchored proteins in neuroblastoma cells form detergent- resistant complexes without caveolin. *Journal of Cell Biology*, *129*(3), 619–627. https://doi.org/10.1083/jcb.129.3.619

Govindarajan, R., Zhao, S., Song, X. H., Guo, R. J., Wheelock, M., Johnson, K. R., & Mehta, P. P. (2002). Impaired trafficking of connexins in androgen-independent human prostate cancer cell lines and its mitigation by α-catenin. *Journal of Biological Chemistry*, *277*(51), 50087–50097. https://doi.org/10.1074/jbc.M202652200

Güldenagel, M., Ammermüller, J., Feigenspan, A., Teubner, B., Degen, J., Söhl, G., Willecke, K., & Weiler, R. (2001). Visual transmission deficits in mice with targeted disruption of the gap junction gene connexin36. *Journal of Neuroscience*, *21*(16), 6036–6044. https://doi.org/10.1523/jneurosci.21-16-06036.2001

Gumpert, A. M., Varco, J. S., Baker, S. M., Piehl, M., & Falk, M. M. (2008). Double-membrane gap junction internalization requires the clathrin-mediated endocytic machinery. *FEBS Letters*, *582*(19), 2887–2892. https://doi.org/10.1016/j.febslet.2008.07.024

Han, Y., & Massey, S. C. (2005). Electrical synapses in retinal ON cone bipolar cells : Subtype-specific expression of connexins. *PNAS*, *102*(37).

Haverkamp, S., & Wässle, H. (2000). Immunocytochemical analysis of the mouse retina. *Journal of Comparative Neurology*, *424*(1), 1–23. https://doi.org/10.1002/1096-9861(20000814)424:1<1::AID-CNE1>3.0.CO;2-V

Head, B. P., Hu, Y., Finley, J. C., Saldana, M. D., Bonds, J. A., Miyanohara, A., Niesman, I. R., Ali, S. S., Murray, F., Insel, P. A., Roth, D. M., Patel, H. H., & Patel, P. M. (2011). Neuron-targeted caveolin-1 protein enhances signaling and promotes

arborization of primary neurons. *Journal of Biological Chemistry*, *286*(38), 33310–33321. https://doi.org/10.1074/jbc.M111.255976
Head, B. P., & Insel, P. A. (2007). Do caveolins regulate cells by actions outside of caveolae? *Trends in Cell Biology*, *17*(2), 51–57. https://doi.org/10.1016/j.tcb.2006.11.008
Head, B. P., Patel, H. H., Tsutsumi, Y. M., Hu, Y., Mejia, T., Mora, R. C., Insel, P. A., Roth, D. M., Drummond, J. C., & Patel, P. M. (2008). Caveolin-1 expression is essential for N -methyl- D -aspartate receptor-mediated Src and extracellular signal-regulated kinase 1/2 activation and protection of primary neurons from ischemic cell death . *The FASEB Journal*, *22*(3), 828–840. https://doi.org/10.1096/fj.07-9299com
Hernández-Deviez, D. J., Howes, M. T., Laval, S. H., Bushby, K., Hancock, J. F., & Parton, R. G. (2008). Caveolin regulates endocytosis of the muscle repair protein, dysferlin. *Journal of Biological Chemistry*, *283*(10), 6476–6488. https://doi.org/10.1074/jbc.M708776200
Hernández-Deviez, D. J., Martin, S., Laval, S. H., Lo, H. P., Cooper, S. T., North, K. N., Bushby, K., & Parton, R. G. (2006). Aberrant dysferlin trafficking in cells lacking caveolin or expressing dystrophy mutants of caveolin-3. *Human Molecular Genetics*, *15*(1), 129–142. https://doi.org/10.1093/hmg/ddi434
Hervé, J. C., Derangeon, M., Bahbouhi, B., Mesnil, M., & Sarrouilhe, D. (2007). The connexin turnover, an important modulating factor of the level of cell-to-cell junctional communication: Comparison with other integral membrane proteins. *Journal of Membrane Biology*, *217*(1–3), 21–33. https://doi.org/10.1007/s00232-007-9054-8
Hidaka, S., Kato, T., & Miyachi, E. I. (2002). Expression of gap junction connexin36 in adult rat retinal ganglion cells. *Journal of Integrative Neuroscience*, *1*(1), 3–22. https://doi.org/10.1142/S0219635202000025
Hitchcock, P. F., & Raymond, P. A. (2004). The teleost retina as a model for developmental and regeneration biology. *Zebrafish*, *1*(3), 257–271.
Hormuzdi, S. G., Filippov, M. A., Mitropoulou, G., Monyer, H., & Bruzzone, R. (2004). Electrical synapses: A dynamic signaling system that shapes the activity of neuronal networks. *Biochimica et Biophysica Acta - Biomembranes*, *1662*(1–2), 113–137. https://doi.org/10.1016/j.bbamem.2003.10.023
Hoshi, H., & Mills, S. L. (2009). Components and properties of the G3 ganglion cell circuit in the rabbit retina. *Journal of Comparative Neurology*, *513*(1), 69–82. https://doi.org/10.1002/cne.21941
Hu, G., Zhang, L., Zhang, M., Yang, C., Nie, X., Xiang, F., Chen, L., Dong, Z., & Yu, S. (2019). Novel gap junction protein beta-1 gene mutation associated with a stroke-like syndrome and central nervous system involvement in patients with X-linked Charcot–Marie–Tooth Type 1: A case report and literature review. *Clinical Neurology and Neurosurgery*, *180*(April 2018), 68–73. https://doi.org/10.1016/j.clineuro.2019.03.018
Hwang, W. Y., Fu, Y., Reyon, D., Maeder, M. L., Tsai, S. Q., Sander, J. D., Peterson, R. T., Yeh, J. R. J., & Joung, J. K. (2013). Efficient genome editing in zebrafish using a CRISPR-Cas system. *Nature Biotechnology*, *31*(3), 227–229. https://doi.org/10.1038/nbt.2501

Jacobson, G. M., Voss, L. J., Melin, S. M., Mason, J. P., Cursons, R. T., Steyn-Ross, D. A., Steyn-Ross, M. L., & Sleigh, J. W. (2010). Connexin36 knockout mice display increased sensitivity to pentylenetetrazol-induced seizure-like behaviors. *Brain Research*, *1360*, 198–204. https://doi.org/10.1016/j.brainres.2010.09.006

Janssen, E. A. M., Kemp, S., Hensels, G. W., Sie, O. G., De Die-Smulders, C. E. M., Hoogendijk, J. E., De Visser, M., & Bolhuis, P. A. (1997). Connexin32 gene mutations in X-linked dominant Charcot-Marie-Tooth disease (CMTX1). *Human Genetics*, *99*(4), 501–505. https://doi.org/10.1007/s004390050396

Jongen, W. M. F., Fitzgerald, D. J., Asamoto, M., Piccoli, C., Slaga, T. J., Gros, D., Takeichi, M., & Yamasaki, H. (1991). Regulation of connexin 43-mediated gap junctional intercellular communication by Ca2+ in mouse epidermal cells is controlled by E-cadherin. *Journal of Cell Biology*, *114*(3), 545–555. https://doi.org/10.1083/jcb.114.3.545

Jordan, K., Chodock, R., Hand, A. R., & Laird, D. W. (2001). The origin of annular junctions: A mechanism of gap junction internalization. *Journal of Cell Science*, *114*(4), 763–773.

Katti, C., Butler, R., & Sekaran, S. (2013). Diurnal and circadian regulation of connexin 36 transcript and protein in the mammalian retina. *Investigative Ophthalmology and Visual Science*, *54*(1), 821–829. https://doi.org/10.1167/iovs.12-10375

Kimmel, C. B., Ballard, W. W., Kimmel, S. R., Ullmann, B., & Schilling, T. F. (1995). Stages of embryonic development of the zebrafish. *Developmental Dynamics*, *203*(3), 253–310. https://doi.org/10.1002/aja.1002030302

Kirchhausen, T., Macia, E., & Pelish, H. E. (2008). Use of Dynasore, the Small Molecule Inhibitor of Dynamin, in the Regulation of Endocytosis. *Methods in Enzymology*, *438*(07), 77–93. https://doi.org/10.1016/S0076-6879(07)38006-3

Kiss, A. L., & Botos, E. (2009). Endocytosis via caveolae: Alternative pathway with distinct cellular compartments to avoid lysosomal degradation? *Journal of Cellular and Molecular Medicine*, *13*(7), 1228–1237. https://doi.org/10.1111/j.1582-4934.2009.00754.x

Kist, A. M., & Portugues, R. (2019). Optomotor Swimming in Larval Zebrafish Is Driven by Global Whole-Field Visual Motion and Local Light-Dark Transitions. *Cell Reports*, *29*(3), 659-670.e3. https://doi.org/10.1016/j.celrep.2019.09.024

Kitson, N., Lennep, E. W. Van, & Y, J. A. (1978). *Cell and Tissue Gap Junctions in Human Sebaceous Glands*. *121*, 115–121.

Kojima, T., Kokai, Y., Chiba, H., Yamamoto, M., Mochizuki, Y., & Sawada, N. (2001). Cx32 but not Cx26 is associated with tight junctions in primary cultures of rat hepatocytes. *Experimental Cell Research*, *263*(2), 193–201. https://doi.org/10.1006/excr.2000.5103

Kojima, T., Spray, D. C., Kokai, Y., Chiba, H., Mochizuki, Y., & Sawada, N. (2002). Cx32 formation and/or Cx32-mediated intercellular communication induces expression and function of tight junctions in hepatocytic cell line. *Experimental Cell Research*, *276*(1), 40–51. https://doi.org/10.1006/excr.2002.5511

Kotova, A., Timonina, K., & Zoidl, G. R. (2020). Endocytosis of connexin 36 is mediated by interaction with caveolin-1. *International Journal of Molecular Sciences*, *21*(15), 1–16. https://doi.org/10.3390/ijms21155401

Kovács-Öller, T., Debertin, G., Balogh, M., Ganczer, A., Orbán, J., Nyitrai, M., Balogh,

L., Kántor, O., & Völgyi, B. (2017). Connexin36 expression in the mammalian retina: A multiple-species comparison. *Frontiers in Cellular Neuroscience*, *11*(March), 1–15. https://doi.org/10.3389/fncel.2017.00065

Koval, M. (2006). Pathways and control of connexin oligomerization. *Trends in Cell Biology*, *16*(3), 159–166. https://doi.org/10.1016/j.tcb.2006.01.006

Koval, M., Harley, J. E., Hick, E., & Steinberg, T. H. (1997). Connexin46 is retained as monomers in a trans-Golgi compartment of osteoblastic cells. *Journal of Cell Biology*, *137*(4), 847–857. https://doi.org/10.1083/jcb.137.4.847

Kumar, N. M., Friend, D. S., & Gilula, N. B. (1995). Synthesis and assembly of human β1 gap junctions in BHK cells by DNA transfection with the human β1 cDNA. *Journal of Cell Science*, *108*(12), 3725–3734. https://doi.org/10.1242/jcs.108.12.3725

Laing, J. G., Manley-Markowski, R. N., Koval, M., Civitelli, R., & Steinberg, T. H. (2001). Connexin45 Interacts with Zonula Occludens-1 and Connexin43 in Osteoblastic Cells. *Journal of Biological Chemistry*, *276*(25), 23051–23055. https://doi.org/10.1074/jbc.M100303200

Laing, J. G., Tadros, P. N., Westphale, E. M., & Beyer, E. C. (1997). Degradation of connexin43 gap junctions involves both the proteasome and the lysosome. *Experimental Cell Research*, *236*(2), 482–492. https://doi.org/10.1006/excr.1997.3747

Laird, D. W. (2005). Connexin phosphorylation as a regulatory event linked to gap junction channel assembly. *Biochimica et Biophysica Acta - Biomembranes*, *1711*(2 SPEC. ISS.), 154–163. https://doi.org/10.1016/j.bbamem.2004.09.013

Laird, D. W. (2010). The gap junction proteome and its relationship to disease. *Trends in Cell Biology*, *20*(2), 92–101. https://doi.org/10.1016/j.tcb.2009.11.001

Laird, D. W., Castillo, M., & Kasprzak, L. (1995). Gap junction turnover, intracellular trafficking, and phosphorylation of connexin43 in brefeldin A-treated rat mammary tumor cells. *Journal of Cell Biology*, *131*(5), 1193–1203. https://doi.org/10.1083/jcb.131.5.1193

Laird, D. W., Puranam, K. L., & Revel, J. (1991). Turnover and phosphorylation dynamics of connexin43 gap junction protein in cultured cardiac myocytes. *Biochemical Journal*, *273*, 67–72.

Lampe, P. D., & Lau, A. F. (2000). Regulation of gap junctions by phosphorylation of connexins. *Archives of Biochemistry and Biophysics*, *384*(2), 205–215. https://doi.org/10.1006/abbi.2000.2131

Lampe, P. D., & Lau, A. F. (2004). The effects of connexin phosphorylation on gap junctional communication. *International Journal of Biochemistry and Cell Biology*, *36*(7), 1171–1186. https://doi.org/10.1016/S1357-2725(03)00264-4

Langlois, S., Cowan, K. N., Shao, Q., Cowan, B. J., & Laird, D. W. (2008). Caveolin-1 and -2 Interact with Connexin43 and Regulate Gap Junctional Intercellular Communication in Keratinocytes. *Molecular Biology of the Cell*, *19*(March), 912–928. https://doi.org/10.1091/mbc.E07–06–0596

Largrée, V., Brunschwig, K., Lopez, P., Gilula, N. B., Richard, G., & Falk, M. M. (2003). Specific amino-acid residues in the N-terminus and TM3 implicated in channel function and oligomerization compatibility of connexin43. *Journal of Cell Science*, *116*(15), 3189–3201. https://doi.org/10.1242/jcs.00604

Larsen, W. J., & Hai-Nan. (1978). Origin and fate of cytoplasmic gap junctional vesicles in rabbit granulosa cells. *Tissue and Cell*, *10*(3), 585–598. https://doi.org/10.1016/s0040-8166(16)30351-2

Larsen, W. J., Tung, H., Murray, S. A., & Swenson, C. A. (1979). Evidence for the participation of actin microfilaments and bristle coats in the internalization of gap junction membrane. *Journal of Cell Biology*, *83*(3), 576–587. https://doi.org/10.1083/jcb.83.3.576

Lau, A. F., Kurata, W. E., Kanemitsu, M. Y., Loo, L. W. M., Warn-Cramer, B. J., Eckhart, W., & Lampe, P. D. (1996). Regulation of connexin43 function by activated tyrosine protein kinases. *Journal of Bioenergetics and Biomembranes*, *28*(4), 359–368. https://doi.org/10.1007/BF02110112

Lauf, U., Giepmans, B. N. G., Lopez, P., Braconnot, S., Chen, S. C., & Falk, M. M. (2002). Dynamic trafficking and delivery of connexons to the plasma membrane and accretion to gap junctions in living cells. *Proceedings of the National Academy of Sciences of the United States of America*, *99*(16), 10446–10451. https://doi.org/10.1073/pnas.162055899

Le, P. U., Guay, G., Altschuler, Y., & Nabi, I. R. (2002). Caveolin-1 is a negative regulator of caveolae-mediated endocytosis to the endoplasmic reticulum. *Journal of Biological Chemistry*, *277*(5), 3371–3379. https://doi.org/10.1074/jbc.M111240200

Lee, E. J., Han, J. W., Kim, H. J., Kim, I. B., Lee, M. Y., Oh, S. J., Chung, J. W., & Chun, M. H. (2003). The immunocytochemical localization of connexin 36 at rod and cone gap junctions in the guinea pig retina. *European Journal of Neuroscience*, *18*(11), 2925–2934. https://doi.org/10.1046/j.1460-9568.2003.03049.x

Lee, S. C., Cruikshank, S. J., & Connors, B. W. (2010). Electrical and chemical synapses between relay neurons in developing thalamus. *Journal of Physiology*, *588*(13), 2403–2415. https://doi.org/10.1113/jphysiol.2010.187096

Leithet, E., & Rivedal, E. (2004). Ubiquitination and down-regulation of gap junction protein connexin-43 in response to 12-O-tetradecanoylphorbol 13-acetate treatment. *Journal of Biological Chemistry*, *279*(48), 50089–50096. https://doi.org/10.1074/jbc.M402006200

Li, X., Lu, S., & Nagy, J. I. (2009). Direct association of connexin36 with zonula occludens-2 and zonula occludens-3. *Neurochemistry International*, *54*(5–6), 393–402. https://doi.org/10.1016/j.neuint.2009.01.003

Li, X., Lynn, B. D., & Nagy, J. I. (2012). The effector and scaffolding proteins AF6 and MUPP1 interact with connexin36 and localize at gap junctions that form electrical synapses in rodent brain. *European Journal of Neuroscience*, *35*(2), 166–181. https://doi.org/10.1111/j.1460-9568.2011.07947.x

Li, X., Olson, C., Lu, S., & Nagy, J. I. (2000). Association of connexin36 with zonula occludens-1 in HeLa cells, βtC-3 cells, pancreas, and adrenal gland. *Histochemistry and Cell Biology*, *122*(5), 485–498. https://doi.org/10.1007/s00418-004-0718-5

Lin, D., Boyle, D. L., & Takemoto, D. J. (2003). IGF-I - Induced phosphorylation of connexin 43 by PKCγ: Regulation of gap junctions in rabbit lens epithelial cells. *Investigative Ophthalmology and Visual Science*, *44*(3), 1160–1168. https://doi.org/10.1167/iovs.02-0737

Lin, R., Warn-Cramer, B. J., Kurata, W. E., & Lau, A. F. (2001). v-Src-mediated phosphorylation of connexin43 on tyrosine disrupts gap junctional communication in mammalian cells. *Cell Communication and Adhesion*, *8*(4–6), 265–269. https://doi.org/10.3109/15419060109080735

Lippincott-Schwartz, J., Yuan, L., Tipper, C., Amherdt, M., Orci, L., & Klausner, R. D. (1991). Brefeldin A's effects on endosomes, lysosomes, and the TGN suggest a general mechanism for regulating organelle structure and membrane traffic. *Cell*, *67*(3), 601–616. https://doi.org/10.1016/0092-8674(91)90534-6

Liu, J., Liang, M., Liu, L., Malhotra, D., Xie, Z., & Shapiro, J. I. (2005). Ouabain-induced endocytosis of the plasmalemmal Na/K-ATPase in LLC-PK1 cells requires caveolin-1. *Kidney International*, *67*(5), 1844–1854. https://doi.org/10.1111/j.1523-1755.2005.00283.x

Liu, L., Li, Y., Lin, J., Liang, Q., Sheng, X., Wu, J., Huang, R., Liu, S., & Li, Y. (2010). Connexin43 interacts with Caveolin-3 in the heart. *Molecular Biology Reports*, *37*(4), 1685–1691. https://doi.org/10.1007/s11033-009-9584-5

Locke, D., Liu, J., & Harris, A. L. (2005). Lipid rafts prepared by different methods contain different connexin channels, but gap junctions are not lipid rafts. *Biochemistry*, *44*(39), 13027–13042. https://doi.org/10.1021/bi050495a

Long, M. A., Deans, M. R., Paul, D. L., & Connors, B. W. (2002). Rhythmicity without synchrony in the electrically uncoupled inferior olive. *Journal of Neuroscience*, *22*(24), 10898–10905. https://doi.org/10.1523/jneurosci.22-24-10898.2002

Malicki, J. (2000). Harnessing the power of forward genetics - Analysis of neuronal diversity and patterning in the zebrafish retina. *Trends in Neurosciences*, *23*(11), 531–541. https://doi.org/10.1016/S0166-2236(00)01655-6

Marchiando, A. M., Shen, L., Vallen Graham, W., Weber, C. R., Schwarz, B. T., Austin, J. R., Raleigh, D. R., Guan, Y., Watson, A. J. M., Montrose, M. H., & Turner, J. R. (2010). Caveolin-1-dependent occludin endocytosis is required for TNF-induced tight junction regulation in vivo. *Journal of Cell Biology*, *189*(1), 111–126. https://doi.org/10.1083/jcb.200902153

Martin, A. O., Mathieu, M. N., Chevillard, C., & Guérineau, N. C. (2001). Gap junctions mediate electrical signaling and ensuing cytosolic Ca2+ increases between chromaffin cells in adrenal slices: A role in catecholamine release. *Journal of Neuroscience*, *21*(15), 5397–5405. https://doi.org/10.1523/jneurosci.21-15-05397.2001

Martin, P. E. M., Blundell, G., Ahmad, S., Errington, R. J., & Evans, W. H. (2001). Multiple pathways in the trafficking and assembly of connexin 26, 32 and 43 into gap junction intercellular communication channels. *Journal of Cell Science*, *114*(21), 3845–3855. https://doi.org/10.1242/jcs.114.21.3845

Massey, S. C. (1990). Chapter 11 Cell types using glutamate as a neurotransmitter in the vertebrate retina. *Progress in Retinal Research*, *9*(C), 399–425. https://doi.org/10.1016/0278-4327(90)90013-8

Massey, S. C., & Redburn, D. A. (1987). Transmitter circuits in the vertebrate retina. *Progress in Neurobiology*, *28*(1), 55–96. https://doi.org/10.1016/0301-0082(87)90005-0

Mastronarde, D. N. (1983). Interactions between ganglion cells in cat retina. *Journal of Neurophysiology*, *49*(2), 350–365. https://doi.org/10.1152/jn.1983.49.2.350

Matsuda, T., Fujio, Y., Nariai, T., Ito, T., Yamane, M., Takatani, T., Takahashi, K., & Azuma, J. (2006). N-cadherin signals through Rac1 determine the localization of connexin 43 in cardiac myocytes. *Journal of Molecular and Cellular Cardiology*, *40*(4), 495–502. https://doi.org/10.1016/j.yjmcc.2005.12.010

Mauch, D. H., Nägier, K., Schumacher, S., Göritz, C., Müller, E. C., Otto, A., & Pfrieger, F. W. (2001). CNS synaptogenesis promoted by glia-derived cholesterol. *Science*, *294*(5545), 1354–1357. https://doi.org/10.1126/science.294.5545.1354

Maza, J., Das Sarma, J., & Koval, M. (2005). Defining a minimal motif required to prevent connexin oligomerization in the endoplasmic reticulum. *Journal of Biological Chemistry*, *280*(22), 21115–21121. https://doi.org/10.1074/jbc.M412612200

McLachlan, E., White, T. W., Ugonabo, C., Olson, C., Nagy, J. I., & Valdimarsson, G. (2003). Zebrafish Cx35: Cloning and characterization of a gap junction gene highly expressed in the retina. *Journal of Neuroscience Research*, *73*(6), 753–764. https://doi.org/10.1002/jnr.10712

Mesnil, M., Crespin, S., Avanzo, J. L., & Zaidan-Dagli, M. L. (2005). Defective gap junctional intercellular communication in the carcinogenic process. *Biochimica et Biophysica Acta - Biomembranes*, *1719*(1–2), 125–145. https://doi.org/10.1016/j.bbamem.2005.11.004

Miller, A. C., Whitebirch, A. C., Shah, A. N., Marsden, K. C., Granato, M., O'Brien, J., & Moens, C. B. (2017). A genetic basis for molecular asymmetry at vertebrate electrical synapses. *ELife*, *6*. https://doi.org/10.7554/eLife.25364

Miller, J. C., Holmes, M. C., Wang, J., Guschin, D. Y., Lee, Y. L., Rupniewski, I., Beausejour, C. M., Waite, A. J., Wang, N. S., Kim, K. A., Gregory, P. D., Pabo, C. O., & Rebar, E. J. (2007). An improved zinc-finger nuclease architecture for highly specific genome editing. *Nature Biotechnology*, *25*(7), 778–785. https://doi.org/10.1038/nbt1319

Mills, S. L., O'Brien, J. J., Li, W., O'Brien, J., & Massey, S. C. (2001). Rod pathways in the mammalian retina use Connexin 36. *Journal of Comparative Neurology*, *436*(3), 336–350. https://doi.org/10.1002/cne.1071

Misumi, Y., Misumi, Y., Miki, K., Takatsuki, A., Tamura, G., & Ikehara, Y. (1986). Novel blockade by brefeldin A of intracellular transport of secretory proteins in cultured rat hepatocytes. *Journal of Biological Chemistry*, *261*(24), 11398–11403.

Morgan, A. J., & Jacob, R. (1994). Ionomycin enhances Ca2+ influx by stimulating store-regulated cation entry and not by a direct action at the plasma membrane. *Biochemical Journal*, *300*(3), 665–672. https://doi.org/10.1042/bj3000665

Müller, S. M., Galliardt, H., Schneider, J., Barisas, B. G., & Seidel, T. (2013). Quantification of Förster resonance energy transfer by monitoring sensitized emission in living plant cells. *Front Plant Sci*, *4*(413), 1–20. https://doi.org/10.3389/fpls.2013.00413

Murata, M., Peränen, J., Schreiner, R., Wieland, F., Kurzchalia, T. V., & Simons, K. (1995). VIP21/caveolin is a cholesterol-binding protein. *Proceedings of the National Academy of Sciences of the United States of America*, *92*(22), 10339–10343. https://doi.org/10.1073/pnas.92.22.10339

Murray, S. A., Larsen, W. J., Trout, J., & Donta, S. T. (1981). Gap junction assembly and endocytosis correlated with patterns of growth in a cultured adrenocortical

tumor cell (sw-13). *Cancer Research*, *41*(10), 4063–4074.
Musil, L. S., & Goodenough, D. A. (1993). Multisubunit assembly of an integral plasma membrane channel protein, gap junction connexin43, occurs after exit from the ER. *Cell*, *74*(6), 1065–1077. https://doi.org/10.1016/0092-8674(93)90728-9
Nabi, I. R., & Le, P. U. (2003). Caveolae/raft-dependent endocytosis. *Journal of Cell Biology*, *161*(4), 673–677. https://doi.org/10.1083/jcb.200302028
Nagy, J. I., Lynn, B. D., Senecal, J. M. M., & Stecina, K. (2018). Connexin36 Expression in Primary Afferent Neurons in Relation to the Axon Reflex and Modality Coding of Somatic Sensation. *Neuroscience*, *383*, 216–234. https://doi.org/10.1016/j.neuroscience.2018.04.038
Nagy, J. I., Pereda, A. E., & Rash, J. E. (2019). On the occurrence and enigmatic functions of mixed (chemical plus electrical) synapses in the mammalian CNS. *Neuroscience Letters*, *695*(September 2017), 53–64. https://doi.org/10.1016/j.neulet.2017.09.021
Nagy, J. I., & Rash, J. E. (2017). Cx36, Cx43 and Cx45 in mouse and rat cerebellar cortex: species-specific expression, compensation in Cx36 null mice and co-localization in neurons vs. glia. *European Journal of Neuroscience*, *46*(2), 1790–1804. https://doi.org/10.1111/ejn.13614
Naumann, E. A., Fitzgerald, J. E., Dunn, T. W., Rihel, J., Sompolinsky, H., & Engert, F. (2016). From Whole-Brain Data to Functional Circuit Models: The Zebrafish Optomotor Response. *Cell*, *167*(4), 947-960.e20. https://doi.org/10.1016/j.cell.2016.10.019
Neves, G., Gomis, A., & Lagnado, L. (2001). Calcium influx selects the fast mode of endocytosis in the synaptic terminal of retinal bipolar cells. *Proceedings of the National Academy of Sciences of the United States of America*, *98*(26), 15282–15287. https://doi.org/10.1073/pnas.261311698
Nickel, B. M., DeFranco, B. H., Gay, V. L., & Murray, S. A. (2008). Clathrin and Cx43 gap junction plaque endoexocytosis. *Biochemical and Biophysical Research Communications*, *374*(4), 679–682. https://doi.org/10.1016/j.bbrc.2008.07.108
Nusrat, A., Chen, J. A., Foley, C. S., Liang, T. W., Tom, J., Cromwell, M., Quan, C., & Mrsny, R. J. (2000). The coiled-coil domain of occludin can act to organize structural and functional elements of the epithelial tight junction. *Journal of Biological Chemistry*, *275*(38), 29816–29822. https://doi.org/10.1074/jbc.M002450200
O'Brien, J., & Bloomfield, S. A. (2018). Plasticity of retinal gap junctions: Roles in synaptic physiology and disease. *Annual Review of Vision Science*, *4*, 79–100. https://doi.org/10.1146/annurev-vision-091517-034133
O'Brien, J., Bruzzone, R., White, T. W., Al-Ubaidi, M. R., & Ripps, H. (1998). Cloning and expression of two related connexins from the perch retina define a distinct subgroup of the connexin family. *Journal of Neuroscience*, *18*(19), 7625–7637. https://doi.org/10.1523/jneurosci.18-19-07625.1998
O'Brien, J. J., Chen, X., Macleish, P. R., O'Brien, J., & Massey, S. C. (2012). Photoreceptor coupling mediated by connexin36 in the primate retina. *Journal of Neuroscience*, *32*(13), 4675–4687. https://doi.org/10.1523/JNEUROSCI.4749-11.2012
O'Brien, J., Nguyen, H. B., & Mills, S. L. (2004). Cone photoreceptors in bass retina use

two connexins to mediate electrical coupling. *Journal of Neuroscience*, *24*(24), 5632–5642. https://doi.org/10.1523/JNEUROSCI.1248-04.2004
Ouyang, X., Winbow, V. M., Patel, L. S., Burr, G. S., Mitchell, C. K., & O'Brien, J. (2005). Protein kinase A mediates regulation of gap junctions containing connexin35 through a complex pathway. *Molecular Brain Research*, *135*(1–2), 1–11. https://doi.org/10.1016/j.molbrainres.2004.10.045
Palacios-Prado, N., Hoge, G., Marandykina, A., Rimkute, L., Chapuis, S., Paulauskas, N., Skeberdis, V. A., O'Brien, J., Pereda, A. E., Bennett, M. V. L., & Bukauskas, F. F. (2013). Intracellular Magnesium-Dependent Modulation of Gap Junction Channels Formed by Neuronal Connexin36. *Journal of Neuroscience*, *33*(11), 4741–4753. https://doi.org/10.1523/JNEUROSCI.2825-12.2013
Patel, L. S., Mitchell, C. K., Dubinsky, W. P., & O'Brien, J. (2006). Regulation of gap junction coupling through the neuronal connexin Cx35 by nitric oxide and cGMP. *Cell Communication and Adhesion*, *13*(1–2), 41–54. https://doi.org/10.1080/15419060600631474
Paul, D. L., Ebihara, L., Takemoto, L. J., Swenson, K. I., & Goodenough, D. A. (1991). Connexin46, a novel lens gap junction protein, induces voltage-gated currents in nonjunctional plasma membrane of Xenopus oocytes. *Journal of Cell Biology*, *115*(4), 1077–1089. https://doi.org/10.1083/jcb.115.4.1077
Peracchia, C., Wang, X. G., & Peracchia, L. L. (2000). Slow gating of gap junction channels and calmodulin. *Journal of Membrane Biology*, *178*(1), 55–70. https://doi.org/10.1007/s002320010015
Pereda, A. E., Curti, S., Hoge, G., Cachope, R., Flores, C. E., & Rash, J. E. (2013). Gap junction-mediated electrical transmission: Regulatory mechanisms and plasticity. *Biochimica et Biophysica Acta - Biomembranes*, *1828*(1), 134–146. https://doi.org/10.1016/j.bbamem.2012.05.026
Pereda, A. E., Rash, J. E., Nagy, J. I., & Bennett, M. V. L. (2004). Dynamics of electrical transmission at club endings on the Mauthner cells. *Brain Research Reviews*, *47*(1–3), 227–244. https://doi.org/10.1016/j.brainresrev.2004.06.010
Perkins, G. A., Goodenough, D. A., & Sosinsky, G. E. (1998). Formation of the gap junction intercellular channel requires a 30°rotation for interdigitating two apposing connexons. *Journal of Molecular Biology*, *277*(2), 171–177. https://doi.org/10.1006/jmbi.1997.1580
Peyroche, A., Antonny, B., Robineau, S., Acker, J., Cherfils, J., & Jackson, C. L. (1999). Brefeldin A acts to stabilize an abortive ARF-GDP-Sec7 domain protein complex: Involvement of specific residues of the Sec7 domain. *Molecular Cell*, *3*(3), 275–285. https://doi.org/10.1016/S1097-2765(00)80455-4
Pfaffl, M., Horgan, G., & Dempfle, L. (2002). Relative expression software tool (REST©) for group-wise comparison and statistical analysis of relative expression results in real-time PCR. *Nucleic Acids Research*, *30*(9).
Piehl, M., Lehmann, C., Gumpert, A. M., Denizot, J.-P., Segretain, D., & Falk, M. M. (2007). Internalization of Large Double-Membrane Intercellular Vesicles by a Clathrin-dependent Endocytic Process. *Molecular Biology of the Cell*, *18*(February), 337–347. https://doi.org/10.1091/mbc.E06
Porteus, M. H., & Baltimore, D. (2003). Chimeric nucleases stimulate gene targeting in human cells. *Science*, *300*(5620), 763. https://doi.org/10.1126/science.1078395

Portugues, R., & Engert, F. (2011). Adaptive locomotor behavior in larval zebrafsh. *Frontiers in Systems Neuroscience*. https://doi.org/10.3389/fnsys.2011.00072

Qin, H., Shao, Q., Igdoura, S. A., Alaoui-Jamali, M. A., & Laird, D. W. (2003). Lysosomal and proteasomal degradation play distinct roles in the life cycle of Cx43 in gap junctional intercellular communication-deficient and -competent breast tumor cells. *Journal of Biological Chemistry*, *278*(32), 30005–30014. https://doi.org/10.1074/jbc.M300614200

Rainy, N., Etzion, T., Alon, S., Pomeranz, A., Nisgav, Y., Livnat, T., Bach, M., Gerstner, C. D., Baehr, W., Gothilf, Y., & Stiebel-Kalish, H. (2016). Knockdown of unc119c results in visual impairment and early-onset retinal dystrophy in zebrafish. *Biochemical and Biophysical Research Communications*. https://doi.org/10.1016/j.bbrc.2016.04.041

Revel, J. P., & Karnovsky, M. J. (1967). Hexagonal array of subunits in intercellular junctions of the mouse heart and liver. *The Journal of Cell Biology*, *33*(3). https://doi.org/10.1083/jcb.33.3.C7

Rice, D. S., & Curran, T. (2000). Disabled-1 is expressed in type AII amacrine cells in the mouse retina. *Journal of Comparative Neurology*, *424*(2), 327–338. https://doi.org/10.1002/1096-9861(20000821)424:2<327::AID-CNE10>3.0.CO;2-6

Risinger, M. A., & Larsen, W. J. (1983). Interaction of filipin with junctional membrane at different stages of the junction's life history. *Tissue and Cell*, *15*(1), 1–15. https://doi.org/10.1016/0040-8166(83)90029-0

Rodieck RW. (1973). *The Vertebrate Retina: Principles of Structure and Function*. W. H. Freeman & Co.

Sáez, J. C., Berthoud, V. M., Brañes, M. C., Martínez, A. D., & Beyer, E. C. (2003). Plasma membrane channels formed by connexins: Their regulation and functions. *Physiological Reviews*, *83*(4), 1359–1400. https://doi.org/10.1152/physrev.00007.2003

Sankaranarayanan, S., & Ryan, T. A. (2001). Calcium accelerates endocytosis of vSNAREs at hippocampal synapses. *Nature Neuroscience*, *4*(2), 129–136.

Saraga, F., Ng, L., & Skinner, F. K. (2006). Distal gap junctions and active dendrites can tune network dynamics. *Journal of Neurophysiology*, *95*(3), 1669–1682. https://doi.org/10.1152/jn.00662.2005

Sarma, J. Das, Wang, F., & Koval, M. (2002). Targeted gap junction protein constructs reveal connexin-specific differences in oligomerization. *Journal of Biological Chemistry*, *277*(23), 20911–20918. https://doi.org/10.1074/jbc.M111498200

Scherer, P. E., Lewis, Y., Volonte, D., Engelman, J. A., Galbiati, F., Couet, J., Kohtz, D. S., Donselaar, E. Van, Peters, P., & Lisanti, M. P. (1997). Cell-type and Tissue-specific Expression of Caveolin-2. *Journal of Biological Chemistry*, *272*(46), 29337–29346.

Schubert, A. L., Schubert, W., Spray, D. C., & Lisanti, M. P. (2002). Connexin family members target to lipid raft domains and interact with caveolin-1. *Biochemistry*, *41*(18), 5754–5764. https://doi.org/10.1021/bi0121656

Schubert, T., Degen, J., Willecke, K., Hormuzdi, S. G., Monyer, H., & Weiler, R. (2005). Connexin36 mediates gap junctional coupling of alpha-ganglion cells in mouse retina. *Journal of Comparative Neurology*, *485*(3), 191–201. https://doi.org/10.1002/cne.20510

Serre-Beinier, V., Le Gurun, S., Belluardo, N., Trovato-Salinaro, A., Charollais, A., Haefliger, J. A., Condorelli, D. F., & Meda, P. (2000). Cx36 preferentially connects β-cells within pancreatic islets. *Diabetes*, *49*(5), 727–734. https://doi.org/10.2337/diabetes.49.5.727

Severs, N. J., Shovel, K. S., Slade, A. M., Powell, T., Twist, V. W., & Green, C. R. (1989). Fate of gap junctions in isolated adult mammalian cardiomyocytes. *Circulation Research*, *65*(1), 22–42. https://doi.org/10.1161/01.RES.65.1.22

Shi, F., & Sottile, J. (2008). Caveolin-1-dependent β1 integrin endocytosis is a critical regulator of fibronectin turnover. *Journal of Cell Science*, *121*(14), 2360–2371. https://doi.org/10.1242/jcs.014977

Shigematsu, S., Watson, R. T., Khan, A. H., & Pessin, J. E. (2003). The adipocyte plasma membrane caveolin functional/structural organization is necessary for the efficient endocytosis of GLUT4. *Journal of Biological Chemistry*, *278*(12), 10683–10690. https://doi.org/10.1074/jbc.M208563200

Shimizu, K., & Stopfer, M. (2013). Gap junctions. *Current Biology*, *23*(23), 1026–1031. https://doi.org/10.1016/j.cub.2013.10.067

Shin, S. I. (2013). Connexin-36 Knock-Out Mice have Increased Threshold for Kindled Seizures: Role of GABA Inhibition. *Biochemistry & Pharmacology: Open Access*, *S*(1), 1–9. https://doi.org/10.4172/2167-0501.s1-006

Siu, R. C. F., Kotova, A., Timonina, K., Zoidl, C., & Zoidl, G. R. (2021). Convergent NMDA receptor—Pannexin1 signaling pathways regulate the interaction of CaMKII with Connexin-36. *Communications Biology*, *4*(1), 1–14. https://doi.org/10.1038/s42003-021-02230-x

Siu, R. C. F., Smirnova, E., Brown, C. A., Zoidl, C., Spray, D. C., Donaldson, L. W., & Zoidl, G. (2016). Structural and functional consequences of connexin 36 (Cx36) interaction with calmodulin. *Frontiers in Molecular Neuroscience*, *9*(NOV2016), 1–15. https://doi.org/10.3389/fnmol.2016.00120

Smith, T. D., Mohankumar, A., Minogue, P. J., Beyer, E. C., Berthoud, V. M., & Koval, M. (2012). Cytoplasmic amino acids within the membrane interface region influence connexin oligomerization. *Journal of Membrane Biology*, *245*(5–6), 221–230. https://doi.org/10.1007/s00232-012-9443-5

Söhl, G., Maxeiner, S., & Willecke, K. (2005). Expression and functions of neuronal gap junctions. *Nature Reviews. Neuroscience*, *6*(3), 191–200. https://doi.org/10.1038/nrn1627

Söhl, G., & Willecke, K. (2004). Gap junctions and the connexin protein family. *Cardiovascular Research*, *62*(2), 228–232. https://doi.org/10.1016/j.cardiores.2003.11.013

Sosinsky, G. E., & Nicholson, B. J. (2005). Structural organization of gap junction channels. *Biochimica et Biophysica Acta - Biomembranes*, *1711*(2 SPEC. ISS.), 99–125. https://doi.org/10.1016/j.bbamem.2005.04.001

Sotgia, F., Razani, B., Bonuccelli, G., Schubert, W., Battista, M., Lee, H., Capozza, F., Schubert, A. L., Minetti, C., Buckley, J. T., & Lisanti, M. P. (2002). Intracellular Retention of Glycosylphosphatidyl Inositol-Linked Proteins in Caveolin-Deficient Cells. *Molecular and Cellular Biology*, *22*(11), 3905–3926. https://doi.org/10.1128/mcb.22.11.3905-3926.2002

Springer, S., Spang, A., & Schekman, R. (1999). A primer on vesicle budding. In *Cell*

(Vol. 97, Issue 2, pp. 145–148). https://doi.org/10.1016/S0092-8674(00)80722-9
Srinivas, M., Rozental, R., Kojima, T., Dermietzel, R., Mehler, M., Condorelli, D. F., Kessler, J. A., & Spray, D. C. (1999). Functional properties of channels formed by the neuronal gap junction protein connexin36. *Journal of Neuroscience*, *19*(22), 9848–9855. https://doi.org/10.1523/jneurosci.19-22-09848.1999
Stauffer, K. A., & Unwin, N. (1992). Structure of gap junction channels. *Seminars in Cell Biology*, *3*(1), 17–20. https://doi.org/10.1016/S1043-4682(10)80004-2
Stiebel-Kalish, H., Reich, E., Rainy, N., Vatine, G., Nisgav, Y., Tovar, A., Gothilf, Y., & Bach, M. (2012). Gucy2f zebrafish knockdown-a model for Gucy2d-related leber congenital amaurosis. *European Journal of Human Genetics*. https://doi.org/10.1038/ejhg.2012.10
Štih, V., Petrucco, L., Kist, A. M., & Portugues, R. (2019). Stytra: An open-source, integrated system for stimulation, tracking and closed-loop behavioral experiments. *PLoS Computational Biology*, *15*(4), 1–19. https://doi.org/10.1371/journal.pcbi.1006699
Stojkovic, T., Latour, P., Vandenberghe, A., Hurtevent, J. F., & Vermersch, P. (1999). Sensorineural deafness in X-linked Charcot-Marie-Tooth disease with connexin 32 mutation (R142Q). *Neurology*, *52*(5), 1010 LP – 1010. https://doi.org/10.1212/WNL.52.5.1010
Sun, S. W., Zu, X. Y., Tuo, Q. H., Chen, L. X., Lei, X. Y., Li, K., Tang, C. K., & Liao, D. F. (2010). Caveolae and caveolin-1 mediate endocytosis and transcytosis of oxidized low density lipoprotein in endothelial cells. *Acta Pharmacologica Sinica*, *31*(10), 1336–1342. https://doi.org/10.1038/aps.2010.87
Swenson, K. I., Piwnica-Worms, H., McNamee, H., & Paul, D. L. (1990). Tyrosine phosphorylation of the gap junction protein connexin43 is required for the pp60v-src-induced inhibition of communication. *Molecular Biology of the Cell*, *1*(13), 989–1002. https://doi.org/10.1091/mbc.1.13.989
Talhouk, R. S., Mroue, R., Mokalled, M., Abi-Mosleh, L., Nehme, R., Ismail, A., Khalil, A., Zaatari, M., & El-Sabban, M. E. (2008). Heterocellular interaction enhances recruitment of α and β-catenins and ZO-2 into functional gap-junction complexes and induces gap junction-dependant differentiation of mammary epithelial cells. *Experimental Cell Research*, *314*(18), 3275–3291. https://doi.org/10.1016/j.yexcr.2008.07.030
Taylor, W. R., & Smith, R. G. (2012). The role of starburst amacrine cells in visual signal processing. *Visual Neuroscience*, *29*(1), 73–81. https://doi.org/10.1017/S0952523811000393
Taylor, W. R., & Vaney, D. I. (2002). Diverse synaptic mechanisms generate direction selectivity in the rabbit retina. *Journal of Neuroscience*. https://doi.org/10.1523/jneurosci.22-17-07712.2002
Tetenborg, S., Liss, V., Breitsprecher, L., & Timonina, K. (2022). Intralumenal docking of Cx36 channels in the ER isolates mis-trafficked protein. *BioRxiv*. https://doi.org/https://doi.org/10.1101/2022.07.15.500247
Teubner, B., Degen, J., Söhl, G., Güldenagel, M., Bukauskas, F. F., Trexler, E. B., Verselis, V. K., De Zeeuw, C. I., Lee, C. G., Kozak, C. A., Petrasch-Parwez, E., Dermietzel, R., & Willecke, K. (2000). Functional Expression of the Murine Connexin 36 Gene Coding for a Neuron-Specific Gap Junctional Protein. *The*

Journal of Membrane Biology, *176*(3), 249–262. https://doi.org/10.1007/s00232001094

Thévenin, A. F., Kowal, T. J., Fong, J. T., Kells, R. M., Fisher, C. G., & Falk, M. M. (2013). Proteins and mechanisms regulating gap-junction assembly, internalization, and degradation. *Physiology*, *28*(2), 93–116. https://doi.org/10.1152/physiol.00038.2012

Thomas, T., Jordan, K., Simek, J., Shao, Q., Jedeszko, C., Walton, P., & Laird, D. W. (2005). Mechanism of Cx43 and Cx26 transport to the plasma membrane and gap junction regeneration. *Journal of Cell Science*, *118*(19), 4451–4462. https://doi.org/10.1242/jcs.02569

Timonina, K., Kotova, A., & Zoidl, G. (2020). Role of an aromatic–aromatic interaction in the assembly and trafficking of the zebrafish panx1a membrane channel. *Biomolecules*, *10*(2), 1–18. https://doi.org/10.3390/biom10020272

Toselli, M., Biella, G., Taglietti, V., Cazzaniga, E., & Parenti, M. (2005). Caveolin-1 expression and membrane cholesterol content modulate N-type calcium channel activity in NG108-15 cells. *Biophysical Journal*, *89*(4), 2443–2457. https://doi.org/10.1529/biophysj.105.065623

Toyofuku, T., Akamatsu, Y., Zhang, H., Kuzuya, T., Tada, M., & Hori, M. (2001). c-Src regulates the interaction between connexin-43 and ZO-1 in cardiac myocytes. *Journal of Biological Chemistry*, *276*(3), 1780–1788. https://doi.org/10.1074/jbc.M005826200

Traub, O., Look, J., Dermietzel, R., Brummer, F., Hulser, D., & Willecke, K. (1989). Comparative characterization of the 21-kD and 26-kD gap junction proteins in murine liver and cultured hepatocytes. *Journal of Cell Biology*, *108*(3), 1039–1051. https://doi.org/10.1083/jcb.108.3.1039

Trouet, D., Hermans, D., Droogmans, G., Nilius, B., & Eggermont, J. (2001). Inhibition of volume-regulated anion channels by dominant-negative caveolin-1. *Biochemical and Biophysical Research Communications*, *284*(2), 461–465. https://doi.org/10.1006/bbrc.2001.4995

Trouet, D., Nilius, B., Jacobs, A., Remacle, C., Droogmans, G., & Eggermont, J. (1999). Caveolin-1 modulates the activity of the volume-regulated chloride channel. *Journal of Physiology*, *520*(1), 113–119. https://doi.org/10.1111/j.1469-7793.1999.t01-1-00113.x

Unger, V. M., Kumar, N. M., Gilula, N. B., & Yeager, M. (1999). Three-dimensional structure of a recombinant gap junction membrane channel. *Science*, *283*(5405), 1176–1180. https://doi.org/10.1126/science.283.5405.1176

Urschel, S., Höher, T., Schubert, T., Alev, C., Söhl, G., Wörsdörfer, P., Asahara, T., Dermietzel, R., Weiler, R., & Willecke, K. (2006). Protein kinase A-mediated phosphorylation of connexin36 in mouse retina results in decreased gap junctional communication between AII amacrine cells. *Journal of Biological Chemistry*, *281*(44), 33163–33171. https://doi.org/10.1074/jbc.M606396200

Valiunas, V., Mui, R., McLachlan, E., Valdimarsson, G., Brink, P. R., & White, T. W. (2004). Biophysical characterization of zebrafish connexin35 hemichannels. *American Journal of Physiology - Cell Physiology*, *287*(6 56-6), 1596–1604. https://doi.org/10.1152/ajpcell.00225.2004

VanSlyke, J. K., Deschenes, S. M., & Musil, L. S. (2000). Intracellular transport,

assembly, and degradation of wild-type and disease-linked mutant gap junction proteins. *Molecular Biology of the Cell*, *11*(6), 1933–1946. https://doi.org/10.1091/mbc.11.6.1933
VanSlyke, J. K., & Musil, L. S. (2005). Cytosolic Stress Reduces Degradation of Connexin43 Internalized from the Cell Surface and Enhances Gap Junction Formation and Function. *Molecular Biology of the Cell*, *16*(November), 5247–5257. https://doi.org/10.1091/mbc.E05
Verselis, V. K., & Srinivas, M. (2008). Divalent cations regulate connexin hemichannels by modulating intrinsic voltage-dependent gating. *Journal of General Physiology*, *132*(3), 315–327. https://doi.org/10.1085/jgp.200810029
Voss, L. J., Mutsaerts, N., & Sleigh, J. W. (2010). Connexin36 Gap Junction Blockade Is Ineffective at Reducing Seizure-Like Event Activity in Neocortical Mouse Slices. *Epilepsy Research and Treatment*, *2010*, 1–6. https://doi.org/10.1155/2010/310753
Wall, M. E., Otey, C., Qi, J., & Banes, A. J. (2007). Connexin 43 is localized with actin in tenocytes. *Cell Motility and the Cytoskeleton*, *64*(2), 121–130. https://doi.org/10.1002/cm.20170
Wang, H. Y., Lin, Y. P., Mitchell, C. K., Ram, S., & O'Brien, J. (2015). Two-color fluorescent analysis of connexin 36 turnover: Relationship to functional plasticity. *Journal of Cell Science*, *128*(21), 3888–3897. https://doi.org/10.1242/jcs.162586
Wang, Y., & Belousov, A. B. (2011). Deletion of neuronal gap junction protein connexin 36 impairs hippocampal LTP. *Neuroscience Letters*, *502*(1), 30–32. https://doi.org/10.1016/j.neulet.2011.07.018
Watanabe, A. (1958). The Interaction of Electrical Activity Among Neurons of Lobster Cardiac Ganglion. *The Japanese Journal of Physiology*, *8*, 305–318. https://doi.org/10.2170/jjphysiol.8.305
Watanabe, T., & Raff, M. C. (1988). Retinal astrocytes are immigrants from the optic nerve. *Nature*, *332*(6167), 834–837.
Wei, C. J., Francis, R., Xu, X., & Lo, C. W. (2005). Connexin43 associated with an N-cadherin-containing multiprotein complex is required for gap junction formation in NIH3T3 cells. *Journal of Biological Chemistry*, *280*(20), 19925–19936. https://doi.org/10.1074/jbc.M412921200
Wen, Q., Cao, L., Yang, C., & Xie, Y. (2018). The Electrophysiological features in X-linked Charcot-Marie-Tooth disease with transient central nervous system deficits. *Frontiers in Neurology*, *9*(JUN), 1–7. https://doi.org/10.3389/fneur.2018.00461
Weng, S., Lauven, M., Schaefer, T., Polontchouk, L., Grover, R., & Dhein, S. (2002). Pharmacological modification of gap junction coupling by an antiarrhythmic peptide via protein kinase C activation. *The FASEB Journal : Official Publication of the Federation of American Societies for Experimental Biology*, *16*(9), 1114–1116. https://doi.org/10.1096/fj.01-0918fje
White, F. H., Thompson, D. A., & Gohari, K. (1984). Ultrastructural morphometry of gap junctions during differentiation of stratified squamous epithelium. *Journal of Cell Science*, *VOL. 69*, 67–85. https://doi.org/10.1242/jcs.69.1.67
White, T. W., Paul, D. L., Goodenough, D. A., & Bruzzone, R. (1995). Functional analysis of selective interactions among rodent connexins. *Molecular Biology of the Cell*, *6*(4), 459–470. https://doi.org/10.1091/mbc.6.4.459
Willmann, R., Pun, S., Stallmach, L., Sadasivam, G., Santos, A. F., Caroni, P., &

Fuhrer, C. (2006). Cholesterol and lipid microdomains stabilize the postsynapse at the neuromuscular junction. *EMBO Journal*, *25*(17), 4050–4060. https://doi.org/10.1038/sj.emboj.7601288

Windoffer, R., Beile, B., Leibold, A., Thomas, S., Wilhelm, U., & Leube, R. E. (2000). Visualization of gap junction mobility in living cells. *Cell and Tissue Research*, *299*(3), 347–362. https://doi.org/10.1007/s004410050033

Wood, A. J., Lo, T. W., Zeitler, B., Pickle, C. S., Ralston, E. J., Lee, A. H., Amora, R., Miller, J. C., Leung, E., Meng, X., Zhang, L., Rebar, E. J., Gregory, P. D., Urnov, F. D., & Meyer, B. J. (2011). Targeted genome editing across species using ZFNs and TALENs. *Science*, *333*(6040), 307. https://doi.org/10.1126/science.1207773

Wyse, B. D., Prior, I. A., Qian, H., Morrow, I. C., Nixon, S., Muncke, C., Kurzchalia, T. V., Thomas, W. G., Parton, R. G., & Hancock, J. F. (2003). Caveolin interacts with the angiotensin II type I receptor during exocytic transport but not at the plasma membrane. *Journal of Biological Chemistry*, *278*(26), 23738–23746. https://doi.org/10.1074/jbc.M212892200

Xu, X., Li, W. E. I., Huang, G. Y., Meyer, R., Chen, T., Luo, Y., Thomas, M. P., Radice, G. L., & Lo, C. W. (2000). N-cadherin and Cx43α1 gap junctions modulates mouse neural crest cell motility via distinct pathways. *Cell Adhesion and Communication*, *8*(4–6), 321–324. https://doi.org/10.3109/15419060109080746

Yeo, J. Y., Lee, E. S., & Jeon, C. J. (2009). Parvalbumin-immunoreactive neurons in the inner nuclear layer of zebrafish retina. *Experimental Eye Research*, *88*(3), 553–560. https://doi.org/10.1016/j.exer.2008.11.014

Yoshizaki, G., & Patiño, R. (1995). Molecular cloning, tissue distribution, and hormonal control in the ovary of Cx41 mRNA, a novel Xenopus connexin gene transcript. *Molecular Reproduction and Development*, *42*(1), 7–18. https://doi.org/10.1002/mrd.1080420103

Zhang, J. T., Chen, M., Foote, C. I., & Nicholson, B. J. (1996). Membrane integration of in vitro-translated gap junctional proteins: Co- and post-translational mechanisms. *Molecular Biology of the Cell*, *7*(3), 471–482. https://doi.org/10.1091/mbc.7.3.471

Zhang, J., & Wu, S. M. (2004). Connexin35/36 Gap Junction Proteins Are Expressed in Photoreceptors of the Tiger Salamander Retina. *Journal of Comparative Neurology*, *470*(1), 1–12. https://doi.org/10.1002/cne.10967

Zhang, L., Xiang, L., Liu, Y., Venkatraman, P., Chong, L., Cho, J., Bonilla, S., Jin, Z. B., Pang, C. P., Ko, K. M., Ma, P., Zhang, M., & Leung, Y. F. (2016). A naturally-derived compound schisandrin B enhanced light sensation in the pde6c zebrafish model of retinal degeneration. *PLoS ONE*, *11*(3), 1–19. https://doi.org/10.1371/journal.pone.0149663

Zoidl, G., Kremer, M., Zoidl, C., Bunse, S., & Dermietzel, R. (2008). Molecular diversity of connexin and pannexin genes in the retina of the zebrafish danio rerioc. *Cell Communication and Adhesion*, *15*(1–2), 169–183. https://doi.org/10.1080/15419060802014081

Zoidl, G., Meier, C., Petrasch-Parwez, E., Zoidl, C., Habbes, H. W., Kremer, M., Srinivas, M., Spray, D. C., & Dermietzel, R. (2002). Evidence for a role of the N-terminal domain in subcellular localization of the neuronal connexin36 (Cx36). *Journal of Neuroscience Research*, *69*(4), 448–465. https://doi.org/10.1002/jnr.10284

APPENDIX A - Plasmid Maps

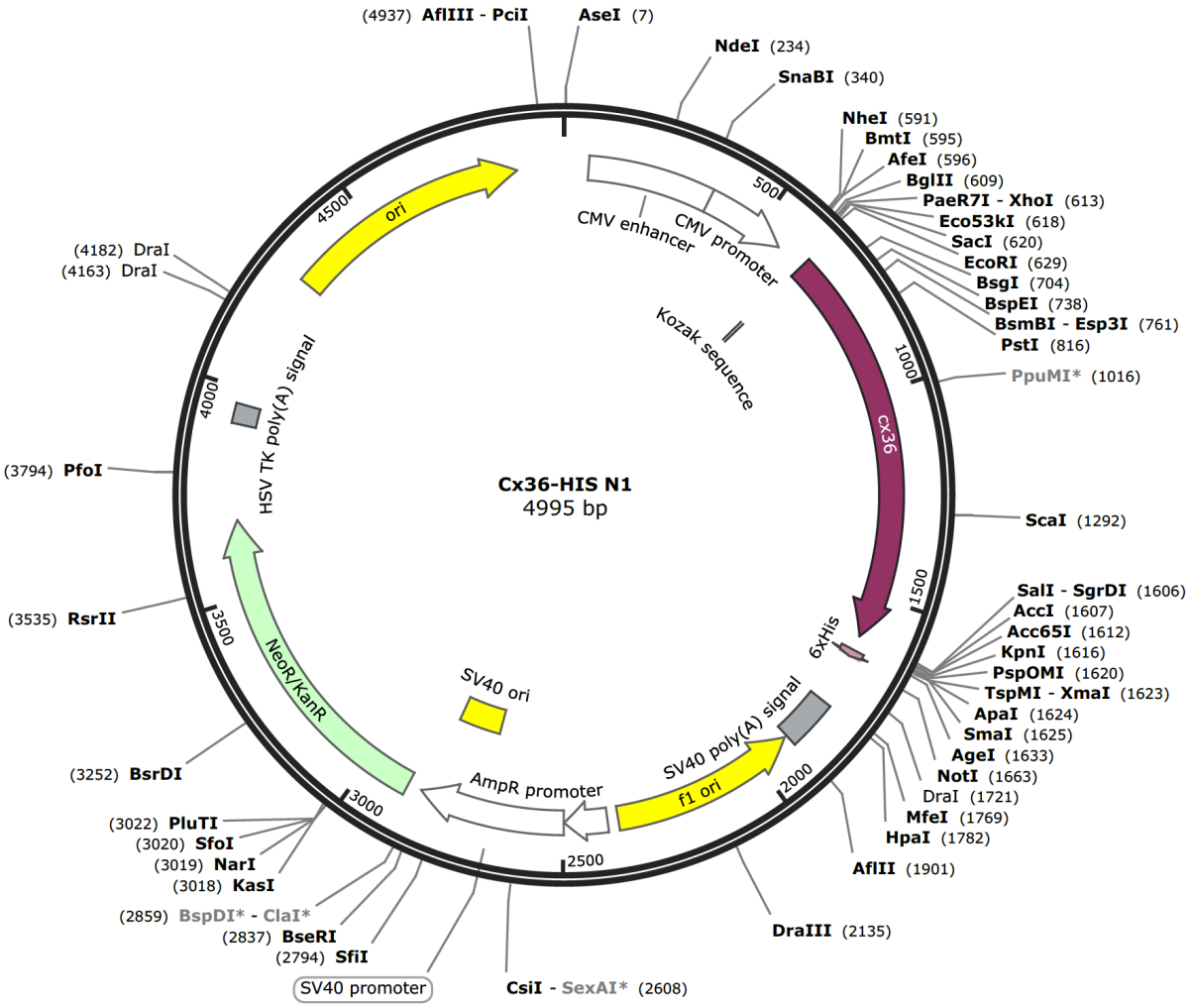

Figure A.1.1: Gene map of HIS-N1-Connexin36 (Cx36) indicating insert and various regions of expressions. Cx36 was cloned using EcoRI and SalI restriction sites.

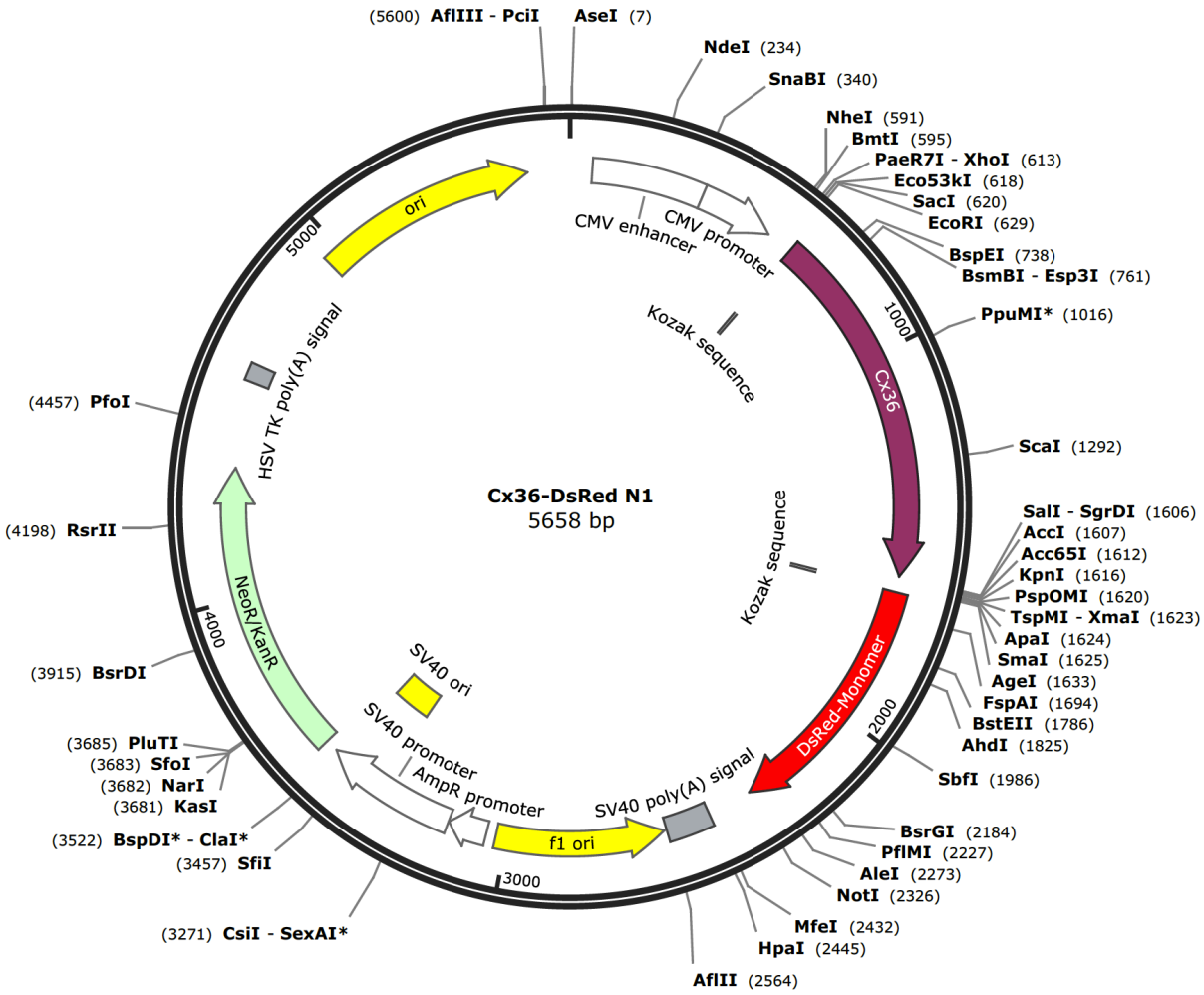

Figure A.1.2: Gene map of DsRed-N1-Connexin36 (Cx36) indicating insert and various regions of expressions. Cx36 was cloned using EcoRI and SalI restriction sites.

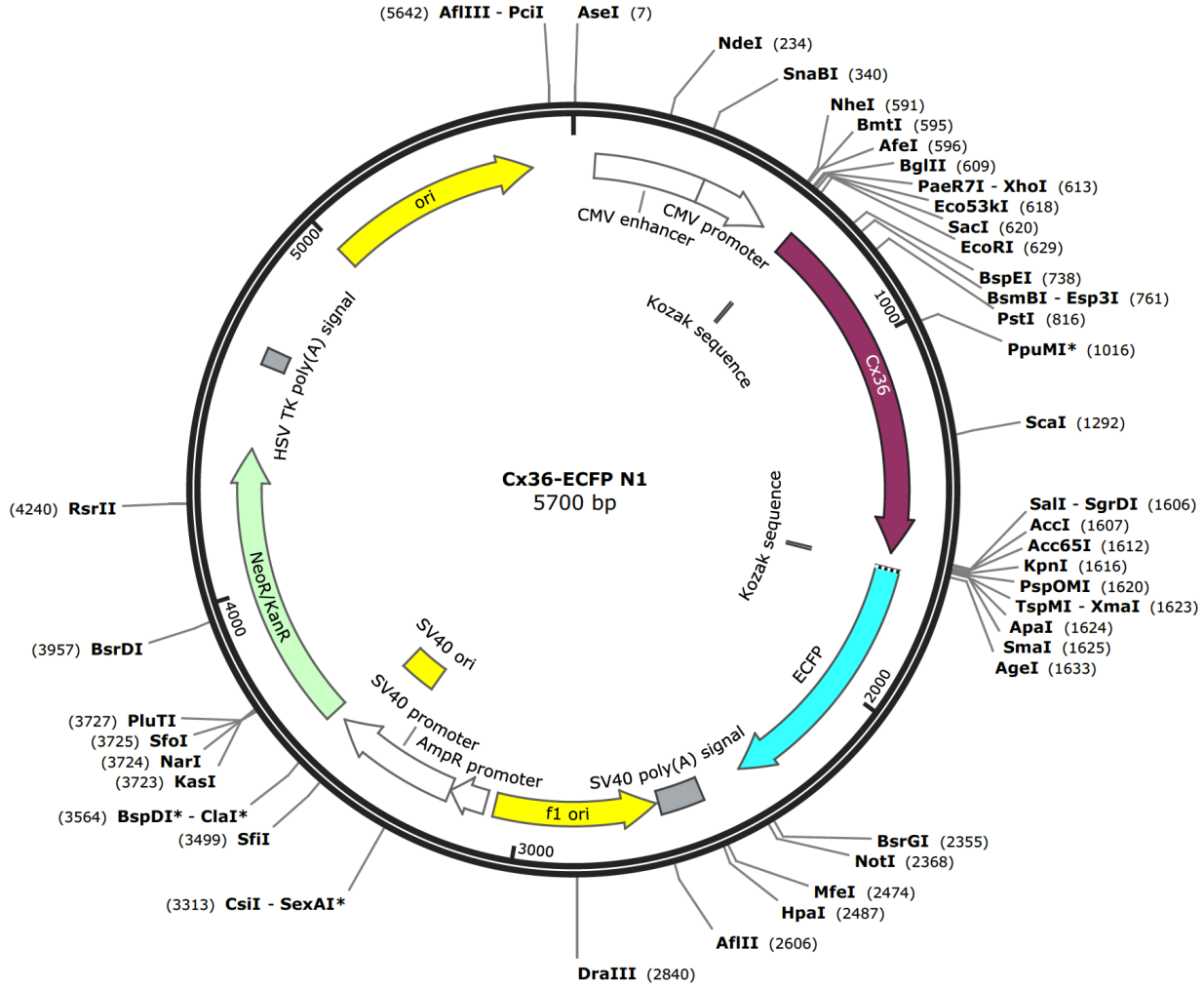

Figure A.1.3: Gene map of ECFP-N1-Connexin36 (Cx36) indicating insert and various regions of expressions. Cx36 was cloned using EcoRI and SalI restriction sites.

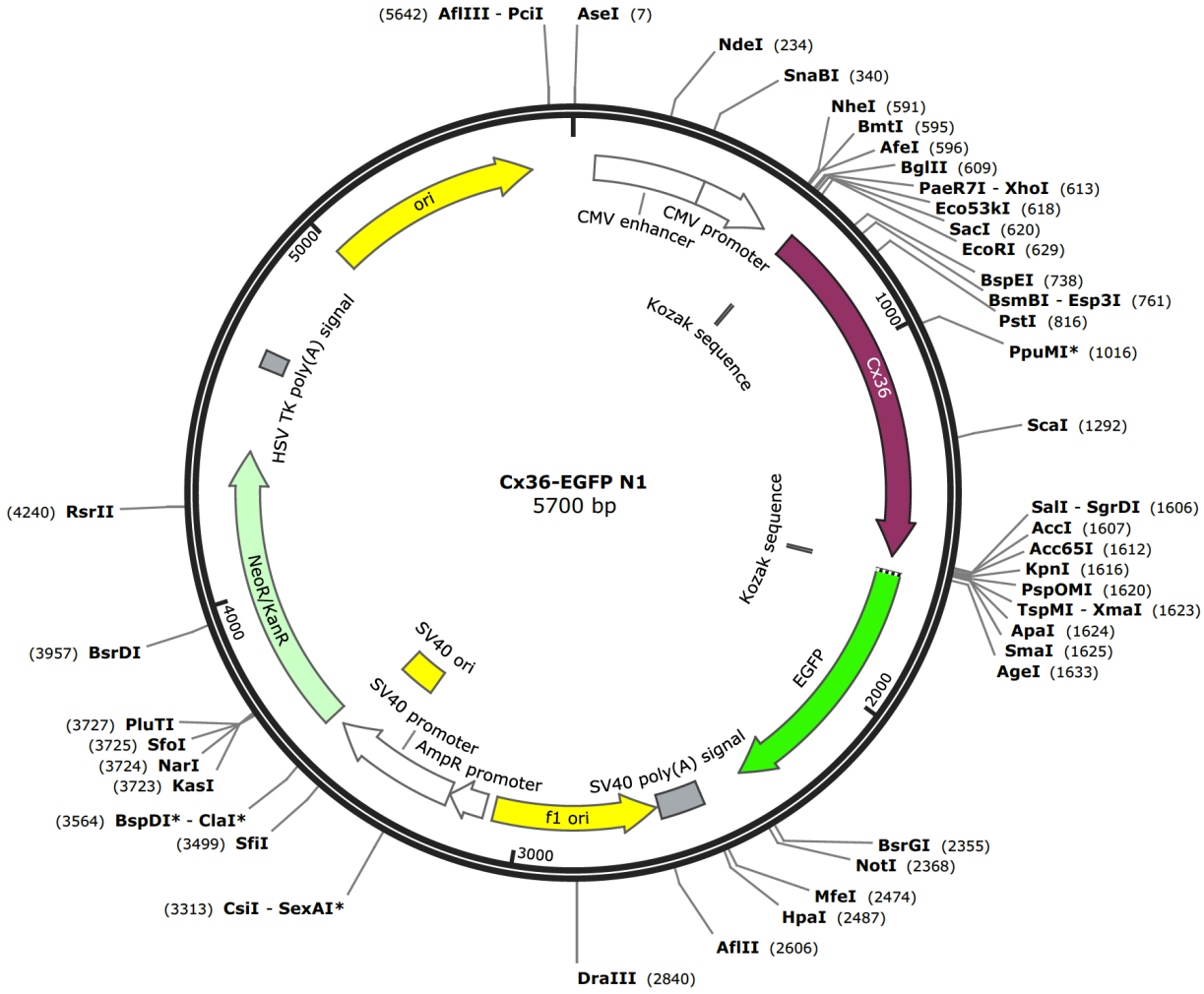

Figure A.1.4: Gene map of EGFP-N1-Connexin36 (Cx36) indicating insert and various regions of expressions. Cx36 was cloned using EcoRI and SalI restriction sites.

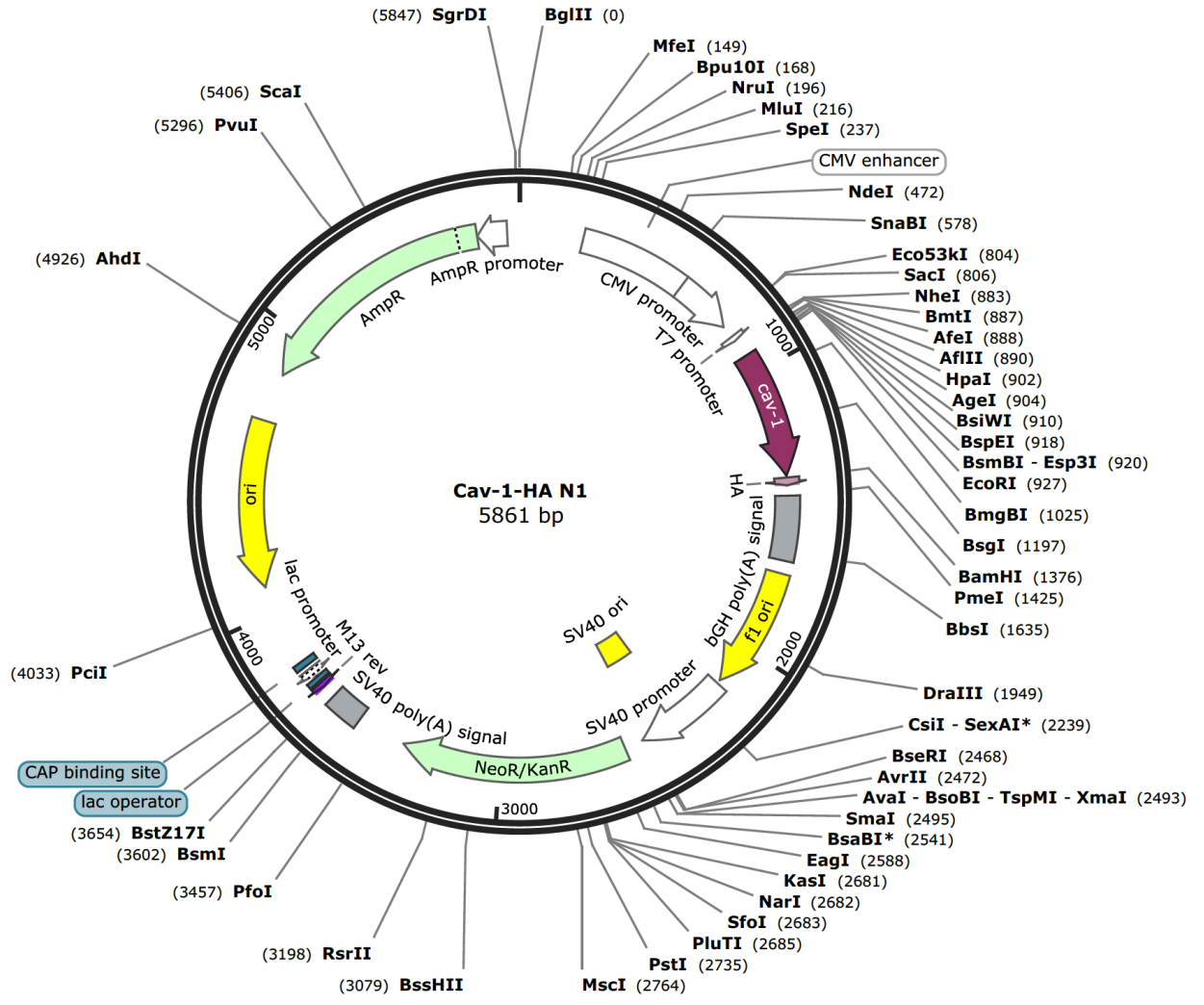

Figure A.1.5: Gene map of HA-N1-Caveolin-1 (Cav-1) indicating insert and various regions of expressions. Cav-1 was cloned using EcoRI and BamHI restriction sites.

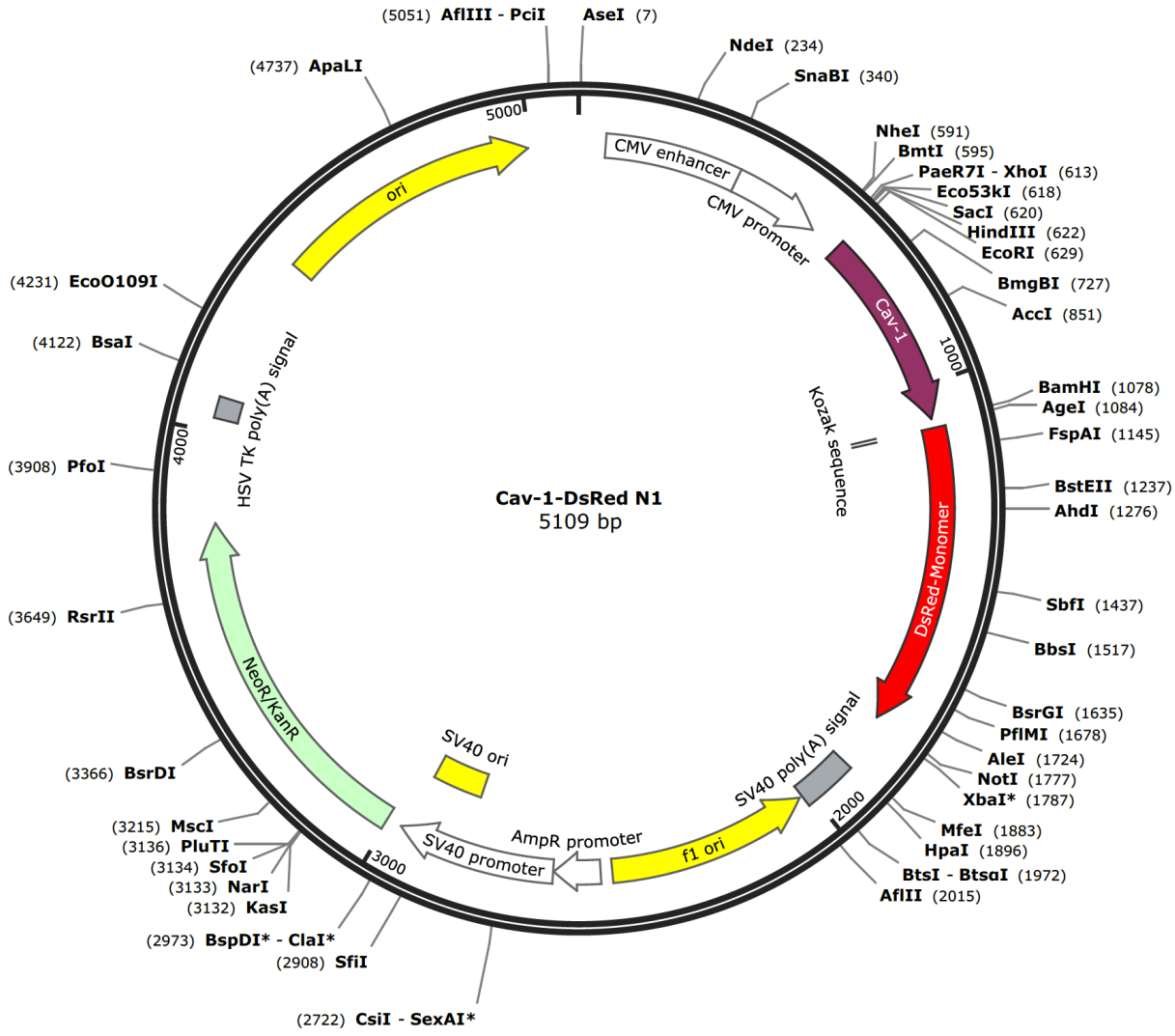

Figure A.1.6: Gene map of DsRed-N1-Caveolin-1 (Cav-1) indicating insert and various regions of expressions. Cav-1 was cloned using EcoRI and BamHI restriction sites.

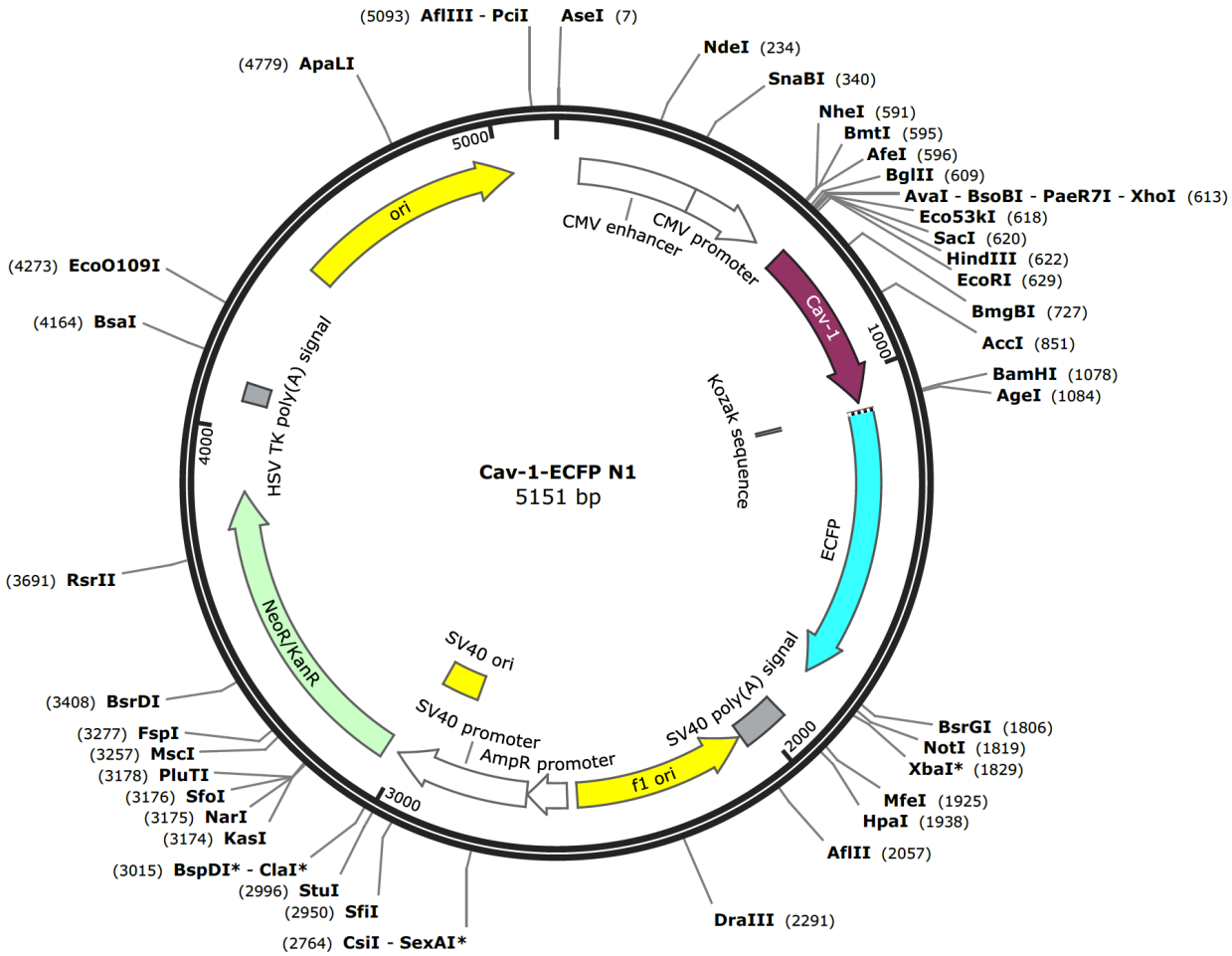

Figure A.1.7: Gene map of ECFP-N1-Caveolin-1 (Cav-1) indicating insert and various regions of expressions. Cav-1 was cloned using EcoRI and BamHI restriction sites.

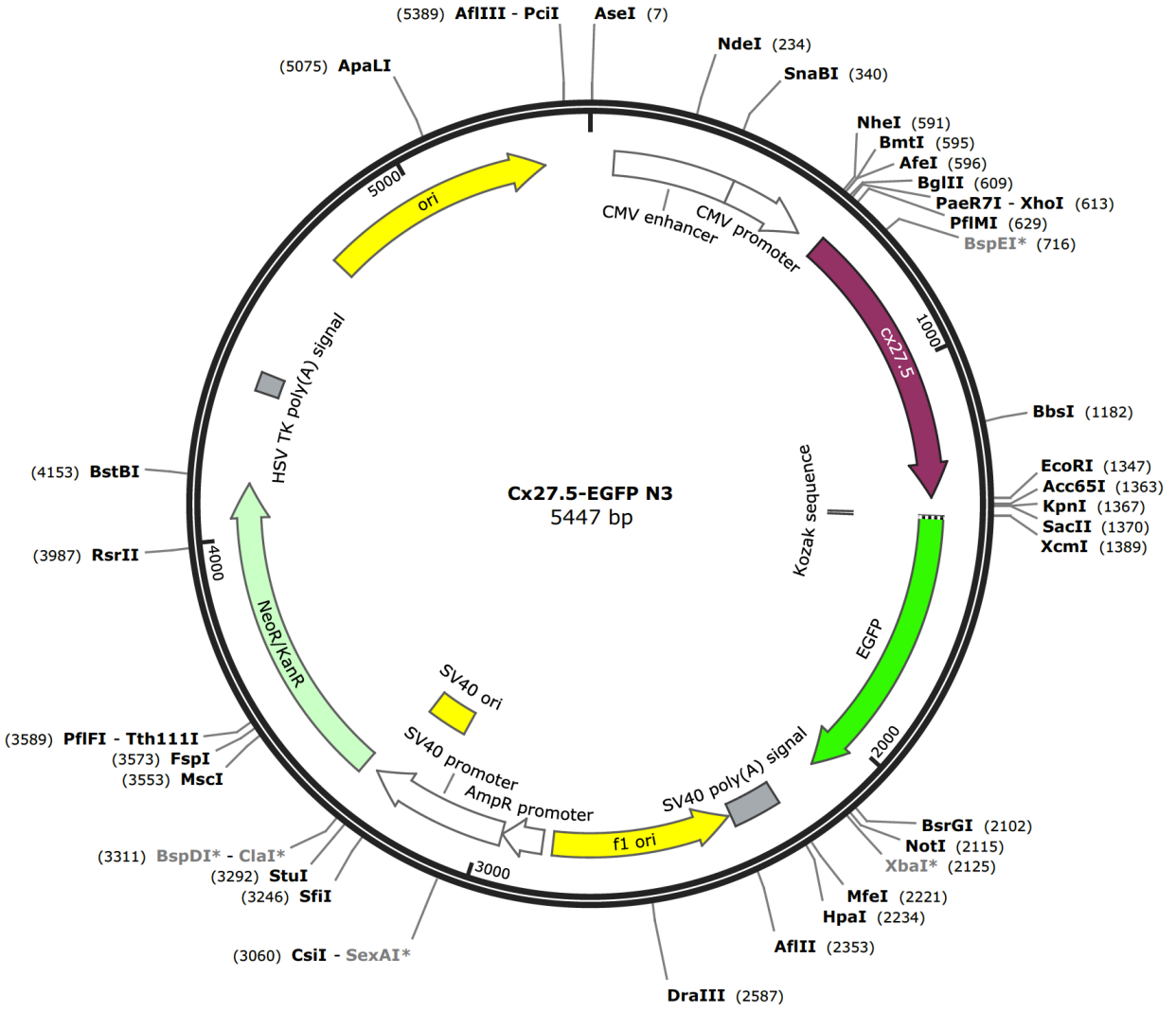

Figure A.1.8: Gene map of EGFP-N1-Connexin 27.5 (Cx27.5) indicating insert and various regions of expressions. Cx27.5 was cloned using XhoI and EcoRI restriction sites.

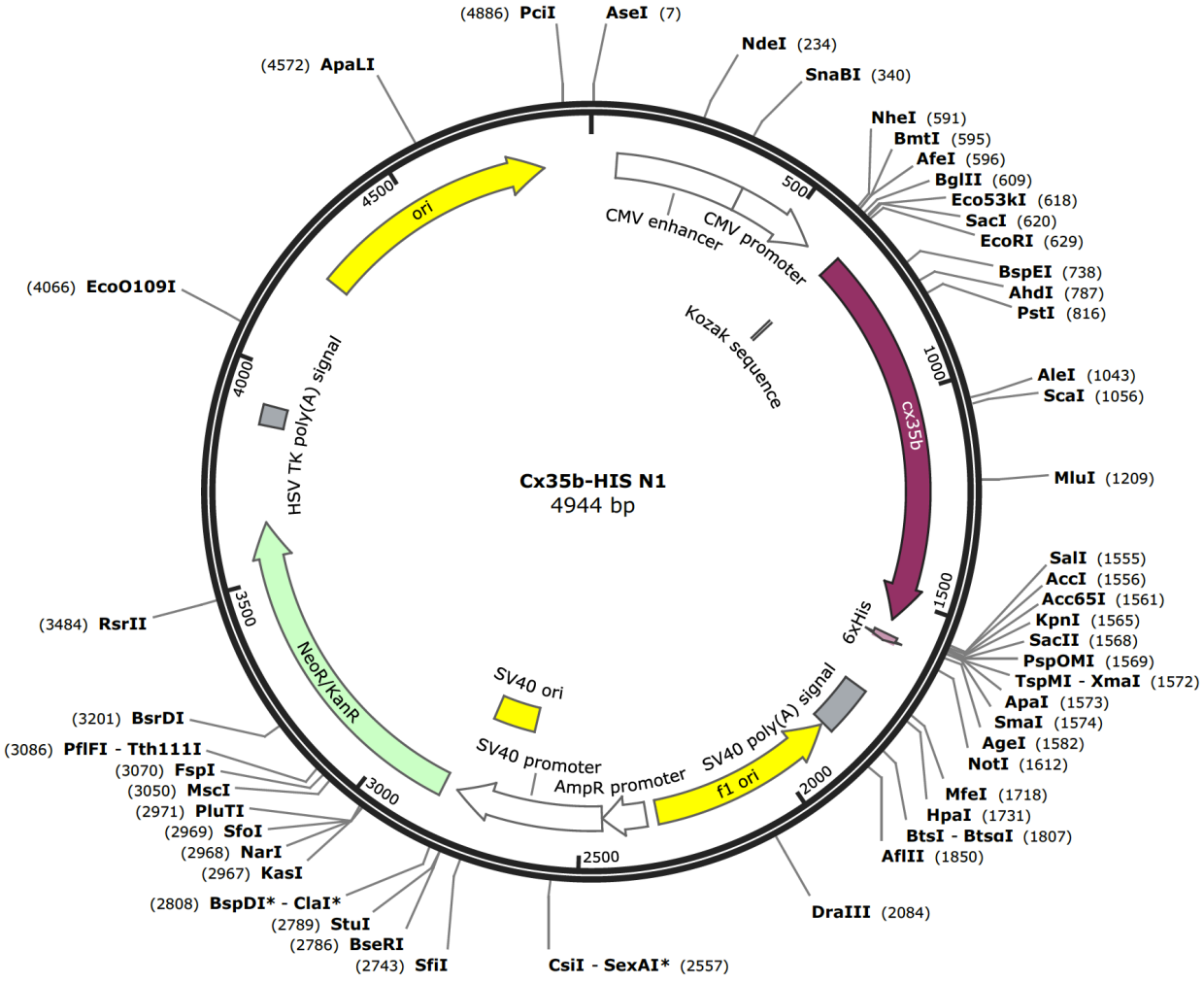

Figure A.1.9: Gene map of HIS-N1-Connexin35b (Cx35b) indicating insert and various regions of expressions. Cx35b was cloned using EcoRI and SalI restriction sites.

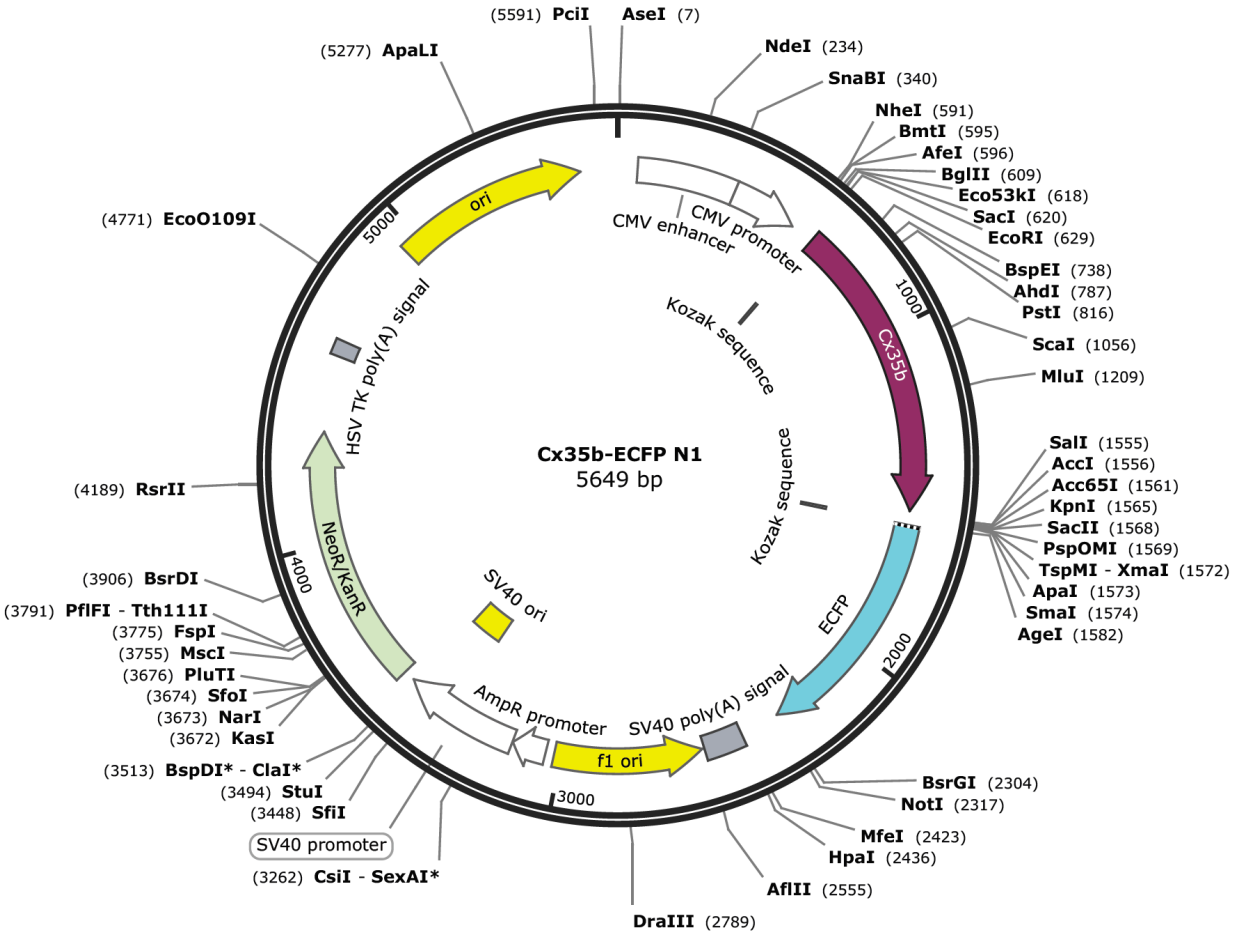

Figure A.1.10: Gene map of ECFP-N1-Connexin35b (Cx35b) indicating insert and various regions of expressions. Cx35b was cloned using EcoRI and SalI restriction sites.

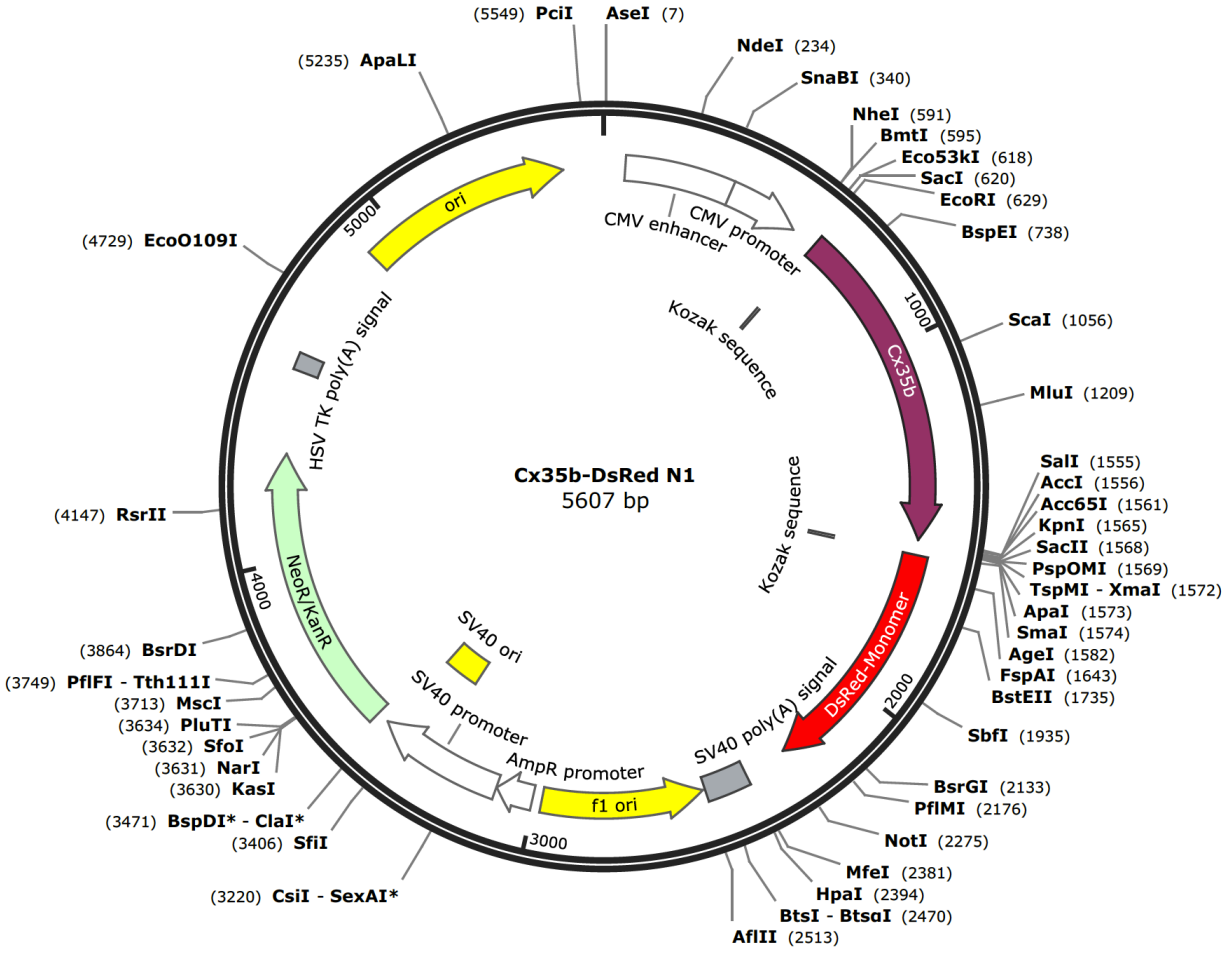

Figure A.1.11: Gene map of DsRed-N1-Connexin35b (Cx35b) indicating insert and various regions of expressions. Cx35b was cloned using EcoRI and SalI restriction sites.